Copyright

by

Kenneth David Clevenger

2014

The Dissertation Committee for Kenneth David Clevenger Certifies that this is the approved version of the following dissertation:

Investigation and engineering of PvdQ, a *Pseudomonas aeruginosa* enzyme at the nexus of quorum sensing and iron uptake pathways

Committee:

Walter L. Fast, Supervisor

Christian P. Whitman

Marvin Whiteley

Adrian T. Keatinge-Clay

Yan Jessie Zhang

Investigation and engineering of PvdQ, a *Pseudomonas aeruginosa* enzyme at the nexus of quorum sensing and iron uptake pathways

by

Kenneth David Clevenger, B.S.

Dissertation

Presented to the Faculty of the Graduate School of

The University of Texas at Austin

in Partial Fulfillment

of the Requirements

for the Degree of

Doctor of Philosophy

The University of Texas at Austin

December 2014

Dedication

This dissertation is dedicated to my beautiful wife, my loving parents, my talented brother, and the unfailing community of St. Elias Antiochian Orthodox Church in Austin, TX.

Acknowledgements

I first and foremost would acknowledge my adviser, Professor Walter Fast for his earnest support and patience over the years, among many other blessings he bestowed so freely. Everyone who has worked for Dr. Fast knows he is a "gem" and we can only hope to one day "pay forward" what he has given us, since we could never pay it back. I have been supported by a warm community of both faculty and student scientists at the University of Texas in Austin and am particularly indebted to members of the Fast lab, past and present, as well as the faculty and staff of the Medicinal Chemistry and Biochemistry divisions in general.

As I was bolstered from within UT Austin, I was also bolstered from without it. I have benefited tremendously from my collaboration with Professor Dali Liu and his PhD student Rui Wu at Loyola University Chicago. Their sharp expertise in X-ray crystallography has greatly enriched this story. On a more personal note, I am indebted to a long list of friends in Austin, TX and particularly to the loving and wise community of St. Elias Antiochian Orthodox Church, whose members have the courage to invest a little piece of themselves in student after student, only to have to say goodbye a few years later. Finally, I would acknowledge my wife for her loving support and the joy she makes in my life, as well as my parents and the rest of my family and friends from Indianapolis, for the years of lessons and continuous love, support, and prayers, which have enabled me to complete this dissertation and degree.

Investigation and engineering of PvdQ, a *Pseudomonas aeruginosa* enzyme at the nexus of quorum sensing and iron uptake pathways

Kenneth David Clevenger, PhD

The University of Texas at Austin, 2014

Supervisor: Walter L. Fast

The gram-negative human pathogen *Pseudomonas aeruginosa* is a widespread global health concern. Two key pathways of *P. aeruginosa* that are involved in its infection and/or survival within mammalian hosts are the pyoverdine biosynthetic pathway, which is necessary for iron acquisition, and the *N*-acyl-homoserine lactone (AHL) quorum sensing (QS) system, which is necessary for *P. aeruginosa* virulence and infection. The *P. aeruginosa* enzyme PvdQ is unique in that it is proposed to play roles in both these pathways. To investigate the role of PvdQ in *P. aeruginosa*, the enzyme's *in vitro* substrate profile was characterized and found to favor substrates with unsubstituted myristic acyl groups, supporting a role for PvdQ in pyoverdine biosynthesis, but challenging its proposed role in regulating *P. aeruginosa* QS. Knowledge of PvdQ's substrate preference and mechanism enabled rational inhibitor design, leading to the discovery of long chain (≥ 10 carbons) *n*-alkylboronic acids as highly potent transition state analog inhibitors of PvdQ, with 1-tridecylboronic acid having a K_i of 200 ± 40 pM and having the ability to recapitulate the growth phenotype of a *pvdQ* transposon insertion strain of *P. aeruginosa*

under certain experimental conditions. Investigation of PvdQ inhibition by alkylboronic acids was extended to short- and medium-chain alkylboronic acids and revealed an eight order of magnitude span of affinity that is linearly related to alkyl chain length. Through structural studies, short-chain alkylboronic acids (≤ 4 carbons) were found to adopt an alternate binding conformation relative to other alkylboronic acids, which suggests a mechanism by which PvdQ excludes short substrates such as *P. aeruginosa* QS molecule *N*-butyroyl-homoserine lactone. Finally, a circular permutation of PvdQ (cpPvdQ) was designed and constructed in order to uncouple the catalytic and self-processing activities of PvdQ and to facilitate the production of mutants that affect catalysis and specificity. The cpPvdQ monomer recapitulates the catalytic and structural features of PvdQ. A catalytically impaired cpPvdQ mutant that is shown to maintain affinity for PvdQ's native substrate, the pyoverdine precursor, but does not hydrolyze the substrate, has been produced and will be a valuable tool for future efforts to trap a PvdQ derivative in complex with the pyoverdine precursor.

Table of Contents

List of Tables

List of Figures

Chapter I: Background and Significance

Pseudomonas aeruginosa is a major clinical threat

The gram-negative human pathogen *Pseudomonas aeruginosa* has emerged as a major clinical threat in the last century and is among the three top causes of human infection worldwide.[1] *P. aeruginosa* is described as ubiquitous due to its ability to grow in almost any environment, such as in distilled water [2] and has a highly complex genome of 6.3 mega bases,[1] leading to its complex biology. The number of predicted ORFs in *P. aeruginosa* (5,570) approaches that of the simple eukaryote, *Saccharomyces cerivisiae* (6,200).[1] *P. aeruginosa* is a significant contributor to the pathologies of cystic fibrosis (CF), urinary tract infections, and burn wound infections,[3] among others, and is generally a serious threat in hospital settings to immuncompromised individuals.[4] In the lungs of CF patients, *P. aeruginosa* is thought to exist predominately as a biofilm, an antibiotic-refractory, exopolymeric-matrix-encased collection of microbial cells.[5] *P. aeruginosa* infections can persist for up to 30 years in such patients, with most CF patients being colonized by the age of 8.[6] *P. aeruginosa's* significance as a clinical pathogen is further enhanced by its resistance to disinfectants, as well as a complement of strategies for resisting antibiotics which include degradation through β-lactamase enzymes, reduction of cellular permeability to antibiotics through mutation of porins, and upregulation of multidrug efflux pumps. Multidrug resistant (MDR, defined as resistance to three or more classes of antibiotics) strains of *P. aeruginosa* are widespread. A study from 1994 to 2002 found an exponential increase in MDR *P. aeruginosa* cases at one hospital in the U.S.A. from 1%

of *P. aeruginosa* infections in 1994 to 16% of *P. aeruginosa* infections in 2002.[7] The challenge of *P. aeruginosa* antibiotic resistance fits within the broader global health crisis of widespread antibiotic resistance, and has prompted some experts beginning to ask whether we might already be living in a post-antibiotic world of untreatable infections.[8] To develop novel therapeutics that address this crisis, new antimicrobial targets have been proposed, including pathways that facilitate iron acquisition and those that regulate quorum-sensing.[9,10] The protein PvdQ (EC 3.5.1.97)[11,12] is an unusual example found at the nexus of these two pathways because its enzymatic function has been proposed to play roles both in production of the siderophore pyoverdine (Pvd) and in degradation of some *N*-acyl-homoserine lactone (AHL) signaling molecules.[13,14]

PvdQ is an NTN-hydrolase

PvdQ is a member of the structurally diverse and widespread [15] *N*-terminal nucleophile aminohydrolase (NTN-hydrolase) superfamily of enzymes.[16] The NTN-hydrolase superfamily was first described in 1995 [17] as having "single amino acid" catalytic centers [17–19] because their catalytic nucleophile (a Ser, Thr, or Cys side chain) is deprotonated by that same amino acid's *N*-α-amine.[17] For this to be possible, the catalytic amino acid must be on the *N*-terminus of the peptide, or else it cannot serve as a general acid or base in the reaction. Despite this, like all known NTN-hydrolases, the *pvdQ* gene is translated as a propeptide where the eventual *N*-terminal nucleophile is in the middle of the primary sequence. Thus, NTN-hydrolases must undergo posttranslational cleavage (generally through a self-processing reaction) to free the *N*-terminal amine and become

catalytically active (Figure 1.1). It has been speculated that NTN-hydrolase post translational modification may serve to temporally regulate activity, [17] somewhat analogous to how digestive serine proteases are initially expressed as inactive zymogens.[20]

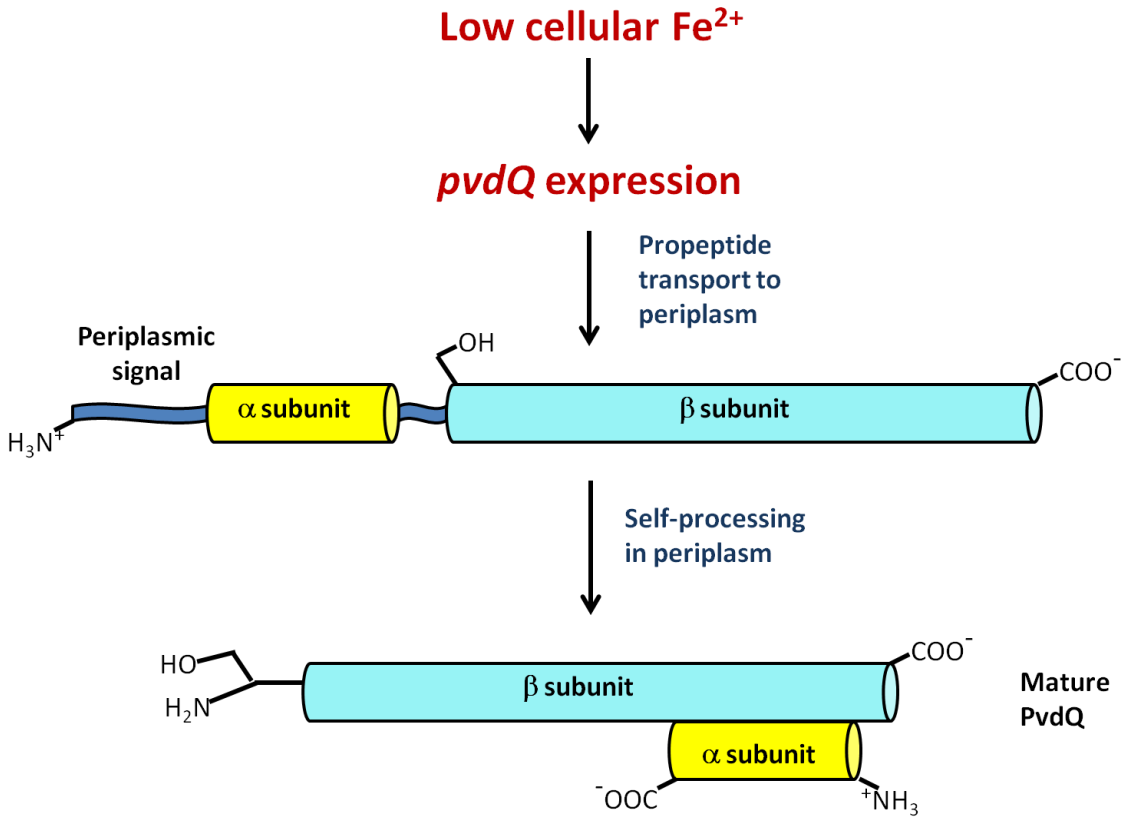

Figure 1.1 Expression, transport, and processing of PvdQ

Expression of the *pvdQ* gene is activated by iron scarcity. The PvdQ propeptide is exported to the periplasmic space, where the periplasmic signal sequence is thought to be removed by cellular machinery and the remaining peptide undergoes a self-processing reaction, removing a 20 amino acid spacer between the α and β subunits and yielding catalytically active enzyme comprised of a heterodimer of the α and β subunits. The catalytic nucleophile, Serβ1, is on the *N*-terminus of the mature β subunit.

The catalytic mechanism of NTN-hydrolases resembles that of serine proteases (see attacks the carbonyl carbon of an amide bond to form a covalent ester intermediate that is

subsequently hydrolyzed to release the reaction products.[16] The primary difference is that there is no catalytic triad; instead the *N*-terminal amino acid's amine group acts as the catalytic base. For this reason, NTN-hydrolases are often described as having single amino acid catalytic centers, though the semantics of this term could be debated [21] since they still require support from other amino acids, for example in providing an oxyanion hole to stabilize tetrahedral adducts during the reaction.

The NTN-hydrolases have a wide biological distribution. For example, the first three NTN-hydrolase X-ray crystal structures to be solved, which served as the basis for the superfamily's naming, were a purine biosynthetic regulatory enzyme from *Bacillus subtilis*, [22] penicillin acylase from *Escherichia coli*, [18] and the 20S proteasome subunit from the *archae*, *Thermoplasma acidophilum.* [23] NTN-hydrolases are present in species from all domains of life, including in humans.[24]

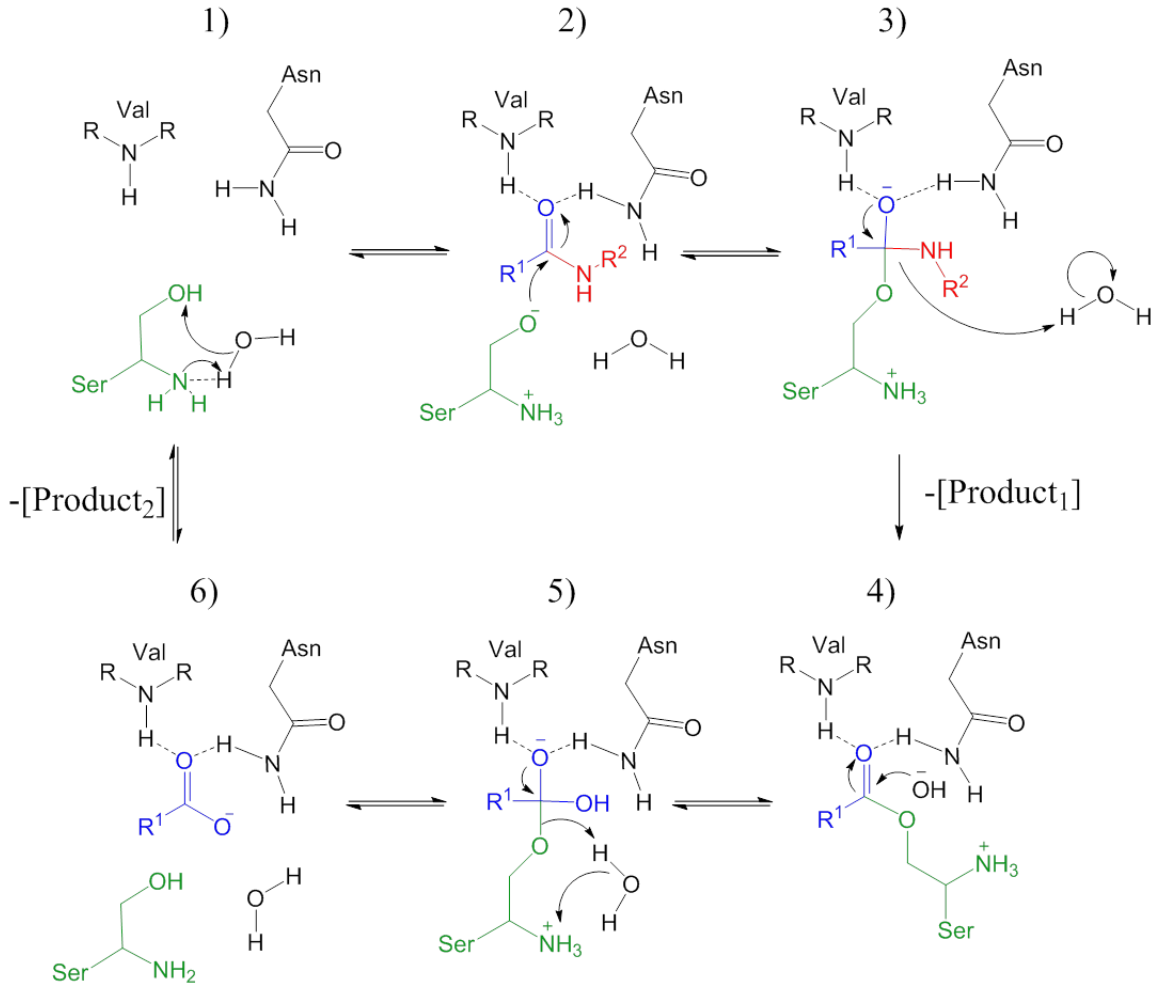

Figure 1.2 Proposed mechanism for PvdQ hydrolysis of an amide substrate[16]

Clockwise from the top left. 1) The *N*-terminal amino group deprotonates the seryl oxygen of Ser β1 through a bridging water, activating it for nucleophilic attack. 2) Following formation of the Michaelis complex, nucleophilic attack on the substrate's carbonyl carbon occurs. 3) The tetrahedral reaction transition state is formed and breaks down through departure of the amide leaving group, also called the "head group." 4) Attack at the carbonyl carbon of the acyl intermediate by a hydroxyl. 5) The second tetrahedral reaction transition state is formed and breaks down through departure of the alcohol leaving group on the serine side chain. 6) Non-covalent complex between enzyme and product is shown, which is followed by product release to complete the cycle. Note the presence of oxyanion stabilizing amino acids, which are described as forming an "oxyanion hole" (Val β70 and Asn β269),[16] as well as the absence of a catalytic triad.

Structure of PvdQ

The X-ray crystal structure of PvdQ was independently solved by two groups (Figure 1.3).[16,25] Apo-PvdQ is a heterodimer possessing the classic NTN-hydrolase α-β-β-α sandwich fold.[17,18,26] The protein is heart shaped, with a long hydrophobic pocket that extends into its interior on one side of the catalytic machinery, and a large solvent exposed cleft on the other side of the catalytic machinery. In addition to apo enzyme, a structure of PvdQ covalently acylated with lauric (C12) acid derived from *N* -dodecanoyl-HSL (C12-HSL) substrate was determined,[16] as well as a structure of PvdQ covalently acylated with myristic (C14) acid derived from the Pvd precursor substrate produced by a *pvdQ* transposon insertion strain of *P. aeruginosa*.[25] In both cases, these covalently acylated structures were obtained by soaking PvdQ at pH 5 with the respective substrates in order to slow catalysis, presumably by hindering activation of the seryl nucleophile in the first half reaction or by hindering hydroxide formation the second half reaction (Figure 1.2). These structures revealed the catalytic machinery of PvdQ by showing a covalent bond between the substrate acyl chain and the seryl oxygen of the β subunit's *N*-terminal serine (Ser β1), forming an ester intermediate (Figure 1.3 *Bottom*). The carbonyl oxygen of the ester intermediate is coordinated by the backbone amide of Val β70 and the sidechain of Asn β269, which form the enzyme's oxyanion hole. The hydrophobic acyl group was buried in the long hydrophobic pocket (the "acyl group binding site"). The enzyme also features a large solvent exposed cleft (the "head group binding site") (Figure 1.4), which is thought to accommodate the siderophore precursor's large, cyclic non-ribosomal peptide during processing by PvdQ and would also be

expected to accommodate the homoserine lactone moiety during turnover of AHL substrates. Notably, no structures were found to have electron density corresponding to either the homoserine lactone or pyoverdine head groups in the putative head group binding site.[6,25]

Bioinformatic comparison of PvdQ's structure to other known NTN-hydrolase structures [16] showed that PvdQ is most structurally related to cephalosporin acylase (CA),[27] followed by penicillin G acylase, [28] penicillin V [26] acylase, and more remotely, the 20S proteasome subunit. [29] Alignment of myristoylated PvdQ with CA (Figure 1.5) reveals conservation of the catalytic machinery: the PvdQ catalytic nucleophile Ser β1, and the oxyanion stabilizing residues Val β70, and Asn β269 (Figure 1.5, *Bottom*). Among other conserved PvdQ amino acids are His β23, and Arg β297. Specific roles for the His β23 and Arg β297 side chains in catalysis by either PvdQ or CA have not been proposed,[27,30] however the γ amino group of the His β23 sidechain and guanidino group of the Arg β269 sidechain are within 2.9 and 3.6 Å respectively of the *N*-terminal amino group of Ser β1, thus it is possible that these side chains play a role in depressing the pK_a of the *N*-α amino group of Ser β1, so that it can act as a proton acceptor during catalysis. Notable differences between PvdQ and CA near the active site seem to be related to substrate binding. Phe β24 of PvdQ has been proposed to serve as a "gate", swinging out of the way to allow substrate binding, but closing off a portion of the substrate binding pocket in apo-enzyme. In CA, this amino acid is replaced by a Leu residue. Asn β57 of PvdQ, which plays no notable role in catalysis other than contributing to the surface of the acyl group binding pocket, is replaced with an Arg residue in CA, which would

sharply cut off the substrate binding pocket in PvdQ (Figure 1.5, *Bottom*). Differences in features related to substrate binding between PvdQ and CA are not surprising, considering that PvdQ prefers long, unsubstituted *n*-alkyl substituents (see Chapter 2 and Table 2.1), while CA binds relatively short, and sometimes bulky, highly functionalized substituents.[27]

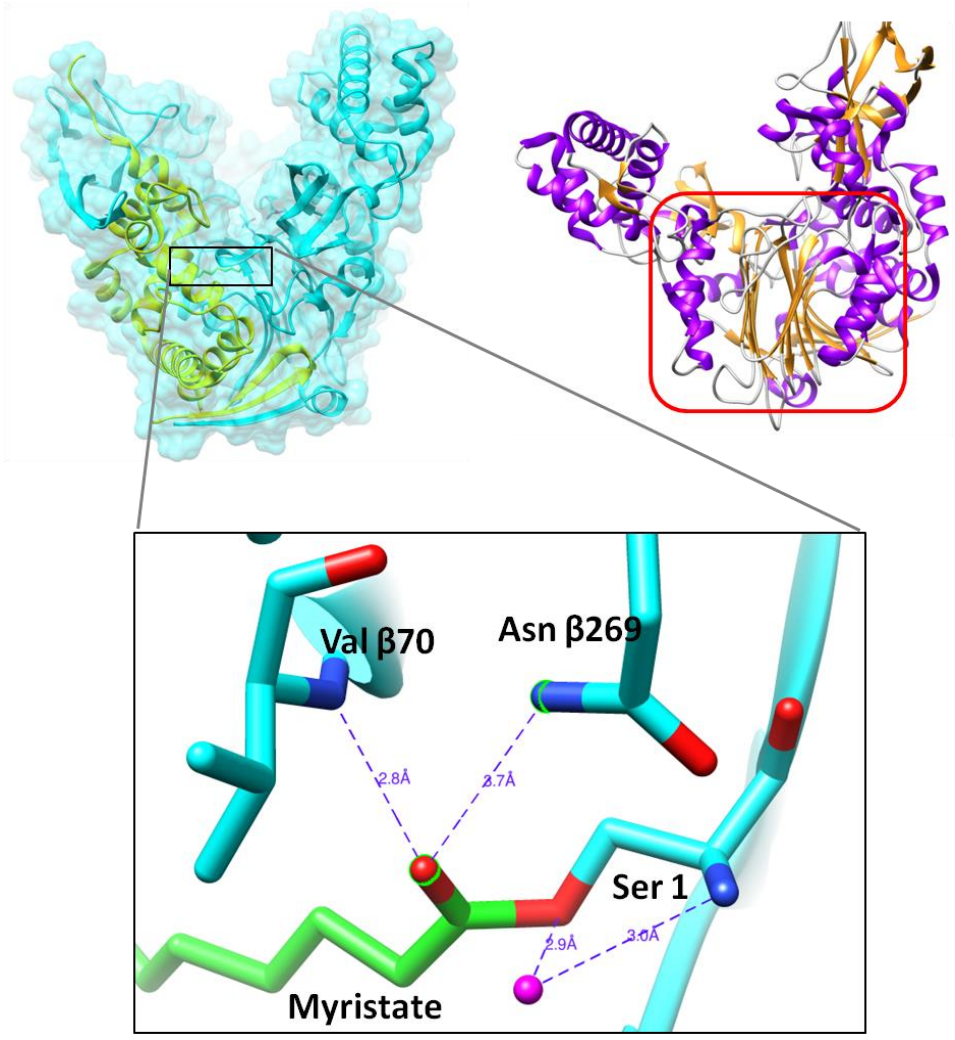

Figure 1.3 X-ray crystal structures of PvdQ

Top left, PvdQ is shown covalently myristoylated on its catalytic nucleophile Ser β1 (PDB: 3L94).[25] The α subunit is shown in yellow and the β subunit is shown in turquoise. The enzyme's "heart" or "chalice" shape is apparent. *Bottom*, an expanded view of the enzyme's catalytic machinery is given, showing the covalent bond between the myristate and the seryl oxygen of Ser β1, coordination of a water molecule between the seryl oxygen and the terminal amino group, as well as coordination of the acyl group's oxygen in the enzyme's oxyanion hole. *Top right*, apo-PvdQ (PDB: 2WYE)[16] is colored by secondary structure, α-helices in purple and β-sheets in orange. The classic NTN-hydrolase α-β-β-α fold is highlighted by the red box.

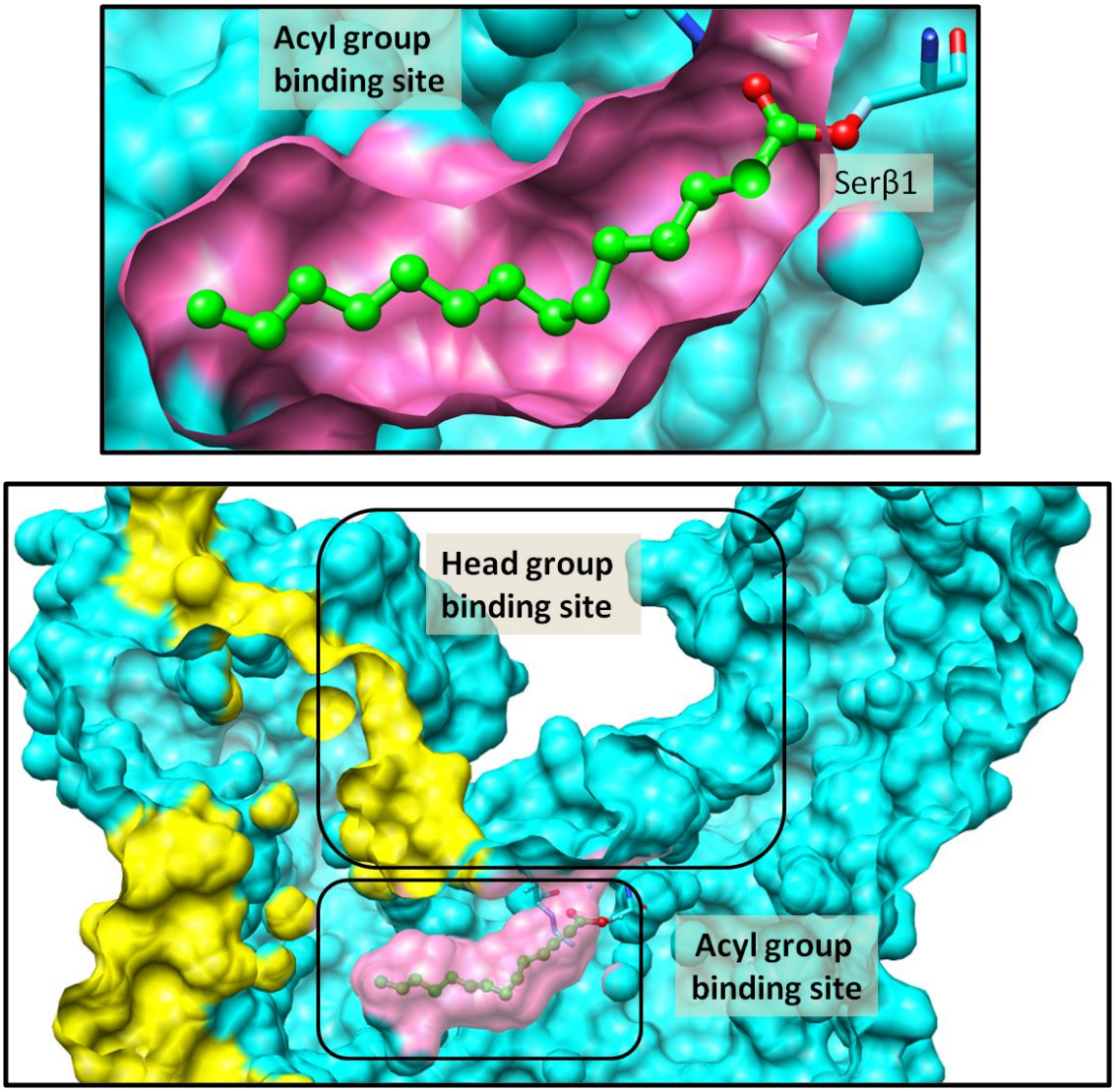

Figure 1.4 Acyl and putative head group binding sites of PvdQ

PvdQ (PDB: 3L94) appears to be equipped to bind large substrates with an acyl chain and a polar head group. The β subunit is colored turquoise, the α subunit is colored yellow, and the acyl group binding site is colored pink. *Top,* the covalently bound myristic acyl group is shown buried in the hydrophobic pocket of PvdQ, the "acyl group binding site". *Bottom*, the acyl group binding site and putative "head group binding site" can be seen. It has been proposed that the solvent exposed head group binding site is large enough to accommodate the pyoverdine precursor.[25,31] See figure 3.4 for a more detailed representation of the atomic surface composition of the acyl group binding site.

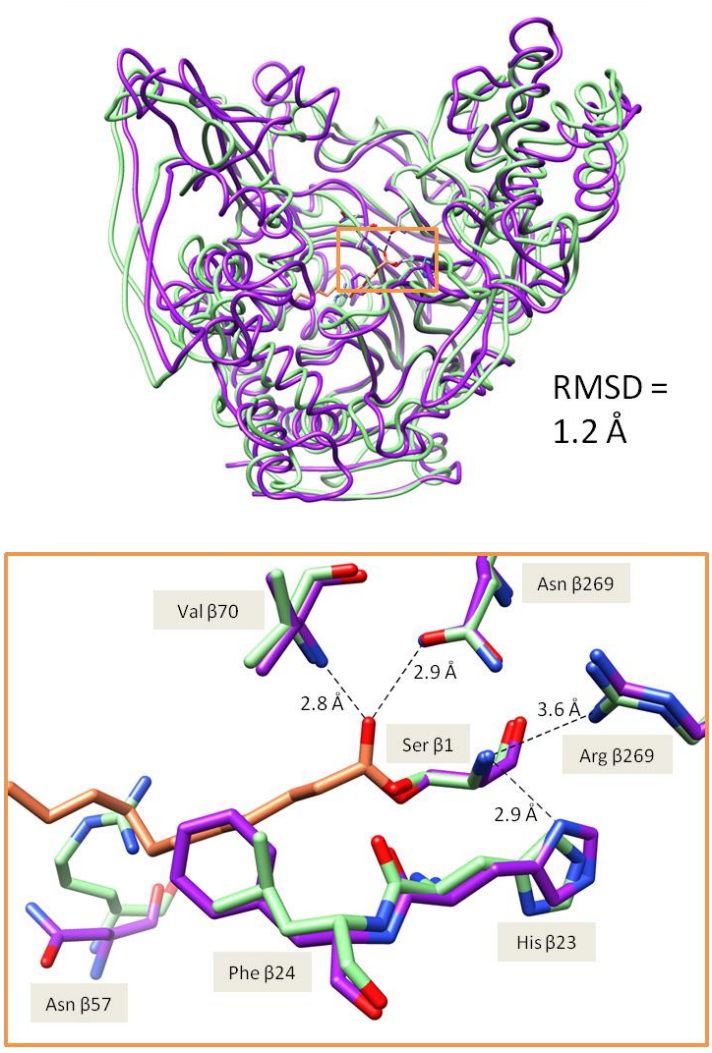

Figure 1.5 Alignment of PvdQ with Cephalosporin Acylase

Covalently acylated PvdQ (purple, PDB: 3L94) is shown aligned with its closest known structural relative, CA (sea green, PDB: 1FM2). *Top*, the overall similarity in shape and chain topology is apparent. *Bottom*, key PvdQ active site amino acids are labeled. The catalytic nucleophile and oxyanion hole are both conserved and well aligned. A significant difference near the active site is the replacement of Phe β24 from PvdQ with Leu in CA; Phe β24 is believed to serve as a gate for substrate during catalysis by PvdQ.[16] The other noticeable difference is the replacement of Asn β57 from PvdQ, with an Arg residue in CA that would serve to sterically occlude long alkyl chains, such as the C14 acyl chain shown here. The conserved Arg β269 and His β23 sidechains have not been reported to have a role in catalysis, but may help depress the *N*-terminal amino group's pK_a, based on their close proximity and conservation.

Role of PvdQ in Pyoverdine Biosynthesis

Iron is a unique nutrient for pathogenic bacteria in that it is not readily available from the host, either in serum or within cells, despite being the fourth most abundant element on the planet.[32,33] In an oxidizing environment at neutral pH, soluble Fe^{2+} is rapidly converted to Fe^{3+}, which has a solubility of $\approx 10^{-9}$ M in neutral aqueous solution.[32] This limited pool of soluble iron is tightly bound by mammalian host factors such as the iron transport and storage proteins, transferrin and ferritin respectively,[32,34,35] thus the resulting concentration of free Fe^{3+} in mammalian serum is actually around 10^{-24} M.[34,36] To overcome this challenge to microbial survival and proliferation, one strategy evolved by many bacteria, including *P. aeruginosa*, has been iron-regulated biosynthetic pathways that produce siderophores: potent small molecule Fe^{3+} chelators that are secreted and imported back into the cell in complex with Fe^{3+}(Figure 1.7).[37] *P. aeruginosa* is widely held to produce two primary siderophores, pyoverdine (Pvd) and pyochelin, that are released into the surrounding environment to scavenge iron and to shuttle it back into *P. aeruginosa*.[31,32,35,36]

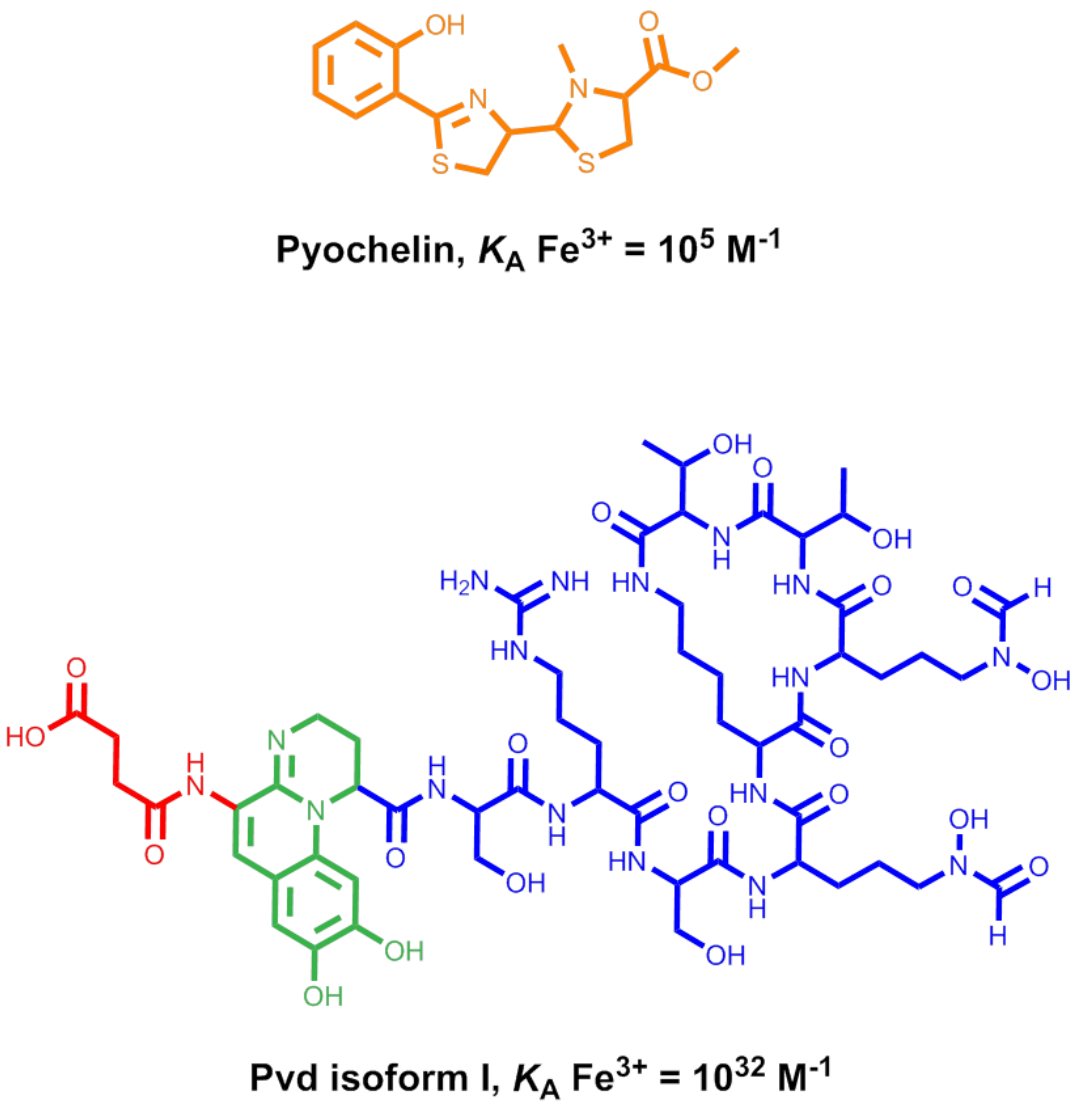

Figure 1.6 Pyochelin and pyoverdine, siderophores of *P. aeruginosa*

Top, pyochelin is in orange and has a K_a of 10^5 M^{-1} for Fe^{3+}.[36] *Bottom*, Pvd isoform I is shown with sidechain in red, chromophore in green, and variable peptide region in blue and has a K_a of 10^{32} M^{-1} for Fe^{3+}.[38]

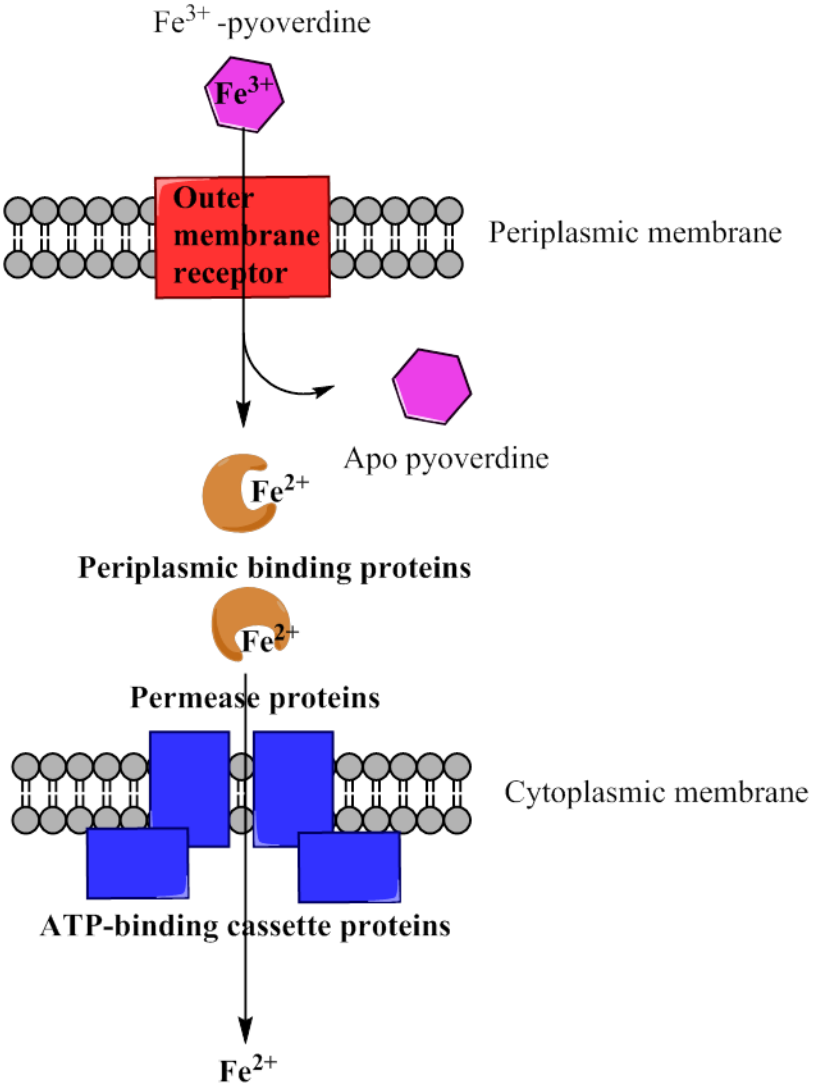

Figure 1.7 Pyoverdine-mediated import of iron by *P. aeruginosa*

Pyoverdine in complex with Fe^{3+} is transported into the periplasm through selective outer membrane receptor FpvA, and then is released from the siderophore through reduction by the periplasmic binding protein FpvCF. Fe^{2+} is then transported into the cytoplasm by the ATP dependent ABC transporter, FpvED.[37,39]

Pvd and pyochelin are distinct from each other in structure, biosynthesis, iron affinity, and regulation. Pyochelin, which features two thiazolidine rings, is thought to biosynthetically derive from salicylic acid and two cyclized cysteine residues.[32,35] Pyochelin does not appear to be expressed under severe iron limitation,[36] has little or no effect on mammalian infection,[40] and has an affinity of only $\approx 10^5$ M^{-1} for Fe^{3+},[36] making it a poor competitor for pulling iron away from mammalian host factors that have affinities in excess of 10^{20} M^{-1}.[32] Pyoverdine, synthesized by non-ribosomal peptide synthetases (NRPS) is a far stronger chelator than pyochelin, with an affinity of 10^{32} M^{-1} for Fe^{3+}.[38] However, Pvd is also much more structurally complex and "expensive" for the cell to produce and is thus only expressed under severe iron limitation.[36] Pvd consists of three parts: 1) an invariable hydroxoquinoline chromophore bearing a chatecholate group that contributes to iron chelation and the distinctive coloring of fluorescent pseudomonads, 2) a modified, cyclic peptide region which varies between strains and species and confers selectivity for the FpvA transporter proteins that import the Fe-Pvd complex into the periplasm and 3) a side chain, attached to the C3 position of the chromophore group (Figure 1.6). In addition to contributing to the uptake of iron, Pvd is also proposed to play a role in the homeostasis of other metal ions such as Mn^{2+}, Zn^{2+}, and Cu^{2+} by coordinating them in the periplasmic space and carrying them out of the cell through the PvdRT-OmPQ efflux pump, which also transports apo-Pvd out of the cell.[38] Consistent with its importance to iron uptake and divalent metal homeostasis, Pvd has been shown to be essential for *P. aeruginosa* growth and infection in mammalian hosts and is considered to be a virulence factor.[3,40,41]

Pvd is synthesized by non-ribosomal peptide synthetases in the cytoplasm, near the cell's old pole.[42] A myristoyl (C14) acyl group, which is installed by the first NRPS module, PvdL,[25] is thought to help localize the siderophore precursor near the cell's old pole, in proximity to the periplasmic membrane. It is thought that this localization of the pyoverdine biosynthetic machinery serves to prevent the undesirable complexation of cytoplasmic iron by the precursor, as well as to enhance biosynthetic efficiency.[38,42] Following synthesis of the pyoverdine backbone by the NRPS, the precursor is exported to the periplasm, where its acyl chain is removed by PvdQ, and further biosynthetic transformations occur to produce the mature siderophore, which is secreted by the PvdRT-OmPQ transporter.[14,38] The PvdQ propeptide is translated with an *N*-terminal periplasmic localization tag [13,16,31] and PvdQ has been experimentally confirmed to be localized in the periplasmic space,[42] consistent with its proposed role in removing the C14 acyl group from the pyoverdine precursor. The mature siderophore is exported into the surrounding medium by an efflux pump and imported back into the periplasm by FpvA, which is selective for the macrocyclic peptide produced by the given strain.[38] Periplasmic release of iron from the siderophore is not well understood, but is thought to rely on its reduction from Fe^{3+} to Fe^{2+} and its sequestration by a periplasmic iron binding protein. An Fe^{2+} selective ABC transporter protein is then responsible for transferring iron from the periplasm into the cytoplasm.[39]

Siderophore biosynthetic enzymes have been suggested as novel antibiotic targets since inhibitors would block iron acquisition and severely limit bacterial growth in host tissues.[9,25,43–45] This effect has been demonstrated as an effective strategy in both

Mycobacterium tuberculosis [43] and *Yersinia pestis*.[46] Moreover, the approved antimycotic drug flucytosine was found to suppress *P. aeruginosa* pathogenicity in a mouse lung infection model by targeting the iron starvation sigma factor PvdS, which regulates the iron uptake machinery of *P. aeruginosa.* [47]

As mentioned earlier, PvdQ is thought to remove the C14 acyl chain from the pyoverdine precursor, after its export into the periplasmic space. In support of this hypothesis, periplasmic fractionation of *P. aeruginosa* under iron limited conditions reveals that the pyoverdine precursor in the cytoplasm is myristoylated, while precursor in the periplasm is not.[48] Moreover, a genetic knockout of *pvd*Q results in a bacterial strain that does not produce pyoverdine, but instead secretes an immature, myristoylated precursor of pyoverdine at an eight-fold reduced level.[25] The lower yield may be due to sequestration of the acylated precursor at the periplasmic membrane. Regardless, *P. aeruginosa* strains with disrupted or knocked out *pvdQ* are growth inhibited in iron-limited medium, but not in rich medium, [30,31] and have reduced virulence in plant and animal models of infection. [30] For this reason, PvdQ has been proposed by our lab and others as a target for therapeutic intervention.[30,31,45]

PvdQ and Quorum Sensing

A second notable feature of PvdQ is its ability to modulate the native quorum sensing of *P. aeruginosa* through hydrolysis of the signal molecule *N*-3-oxo-dodecanoyl-homoserine lactone (3-oxo-C12-HSL).[13,49] Quorum sensing is the process by which bacteria "sense" their neighbors through the synthesis, diffusion, and detection of cell

permeable small molecule signals, enabling a population of bacteria to act communally. Quorum sensing in *P. aeruginosa* is known to utilize three distinct small molecule signals: 3-oxo-C12-HSL, *N*-butyroyl-homoserine lactone (C4-HSL), and 2-heptyl-3-hydroxy-4-quinolone, called *Pseudomonas* Quinolone Signal (PQS). Quorum sensing in *P. aeruginosa* is hierarchically organized, such that 3-oxo-C12-HSL stimulates production of C4-HSL, and both AHL signals regulate production of PQS (Figure 1.8).[6] Thus, 3-oxo-C12-HSL serves as the master regulator of this system. Altogether, about 500 genes [6] are controlled by QS in *P. aeruginosa*, including activation of virulence factors.[50]

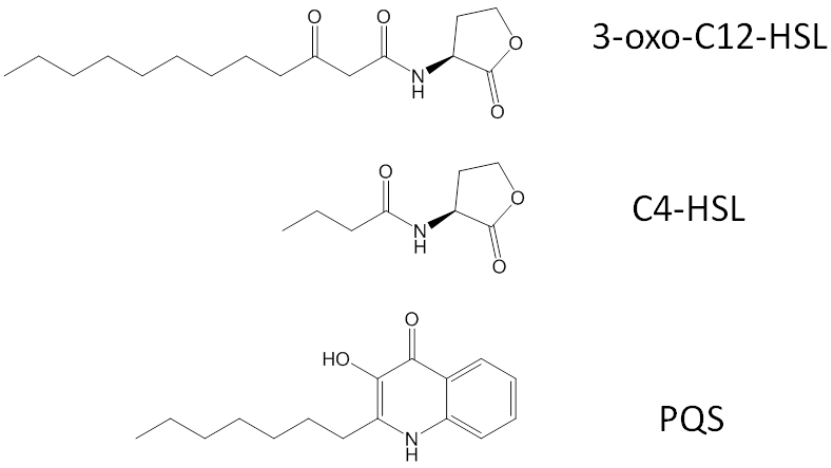

Figure 1.8 Quorum sensing signals of *P. aeruginosa*

The three QS signals of *P. aeruginosa* are shown. 3-oxo-C12-HSL serves to activate expression of both C4-HSL and PQS. C4-HSL suppresses PQS.[6,50]

Artificial constitutive expression of PvdQ in *P. aeruginosa*, or addition of exogenous purified PvdQ, reduces accumulation of 3-oxo-C12-HSL and reduces production of the quorum sensing regulated virulence factors pyocyanin and elastase.[13,51] Qualitative *in vitro* bioassays have shown that PvdQ hydrolyzes both 3-oxo-C12-HSL and other AHL molecules, such as *N*-octanoyl-homoserine lactone and *N*-dodecanoyl-homoserine lactone (C8-HSL and C12-HSL respectively). Significantly, the second AHL quorum sensing autoinducer of *P. aeruginosa*, C4-HSL, is not hydrolyzed by PvdQ.[13] Enzymes that disrupt quorum sensing (a process called "quorum quenching") are known, however all known examples are thought to act on non-host, exogenous quorum sensing signals.[16] Thus, it would be significant if PvdQ was evolved to attenuate the endogenous quorum sensing pathways of *P. aeruginosa.*

Known quorum quenching enzymes of AHL signals are generally not very selective toward ligand chain length.[52–54] In contrast, the fact that PvdQ does not appear to hydrolyze short chain AHLs such as C4-HSL, suggests that it may be useful for selectively targeting specific AHL signals. AHL signaling is widely used by gram-negative bacteria,[50] and thus PvdQ may be useful for selectively blocking the quorum-sensing dependent behavior of specific species or groups of species within polymicrobial systems, either *in vitro* or in mammalian infections. In pursuit of this goal, PvdQ has been engineered to target the C8-HSL signal of *Burkholderia,* though its utility in polymicrobial systems was not demonstrated, and this particular engineering effort resulted in an enzyme of overall reduced activity.[55] Another potential quorum quenching use of PvdQ might be in the treatment of *P. aeruginosa* infections, such as the recalcitrant lung infections that are characteristic of CF pathology, through attenuation of *P. aeruginosa* QS behaviors and thus virulence. Towards this end, PvdQ has been successfully developed into a stable, freeze-dried, inhalable powder, with the goal of applying this to CF lung infection models as a therapeutic protein.[56]

Biological function of PvdQ

The earliest report of PvdQ comes from gene chip studies, which found it to be upregulated under iron limited conditions.[57] Subsequent studies found PvdQ to have a conserved role in iron limited growth among fluorescent pseudomonads.[58] It was after the initial implication of PvdQ in *P. aeruginosa* iron limited growth that PvdQ was found to hydrolyze AHL molecules, including 3-oxo-C12-HSL, and was thus proposed to have a

role in quorum sensing regulation.[13] This discovery touched off more specific research into PvdQ. Since then, papers independently emphasizing both proposed roles of PvdQ have been published, with some labs emphasizing one role in one paper, and the other role in a different paper.[16,30,49] At the time I began this project, most studies supported a biological role in iron uptake for PvdQ, however it was less clear whether PvdQ was truly evolved to serve a function in endogenous quorum quenching. The lack of clarity about the biological role of PvdQ creates a challenge for anyone interested in its pharmacological significance (Figure 1.9). On the one hand, its clear participation in iron uptake suggests that PvdQ might serve as a drug target. On the other hand, if PvdQ acts as an endogenous quorum quencher, inhibiting PvdQ may actually lead to upregulation of virulence factors and be undesirable. In this model however, PvdQ might itself be useful as a therapeutic protein, to be applied to entrenched *P. aeruginosa* infections on skin, or in the lungs, in order to suppress quorum sensing related behaviors.

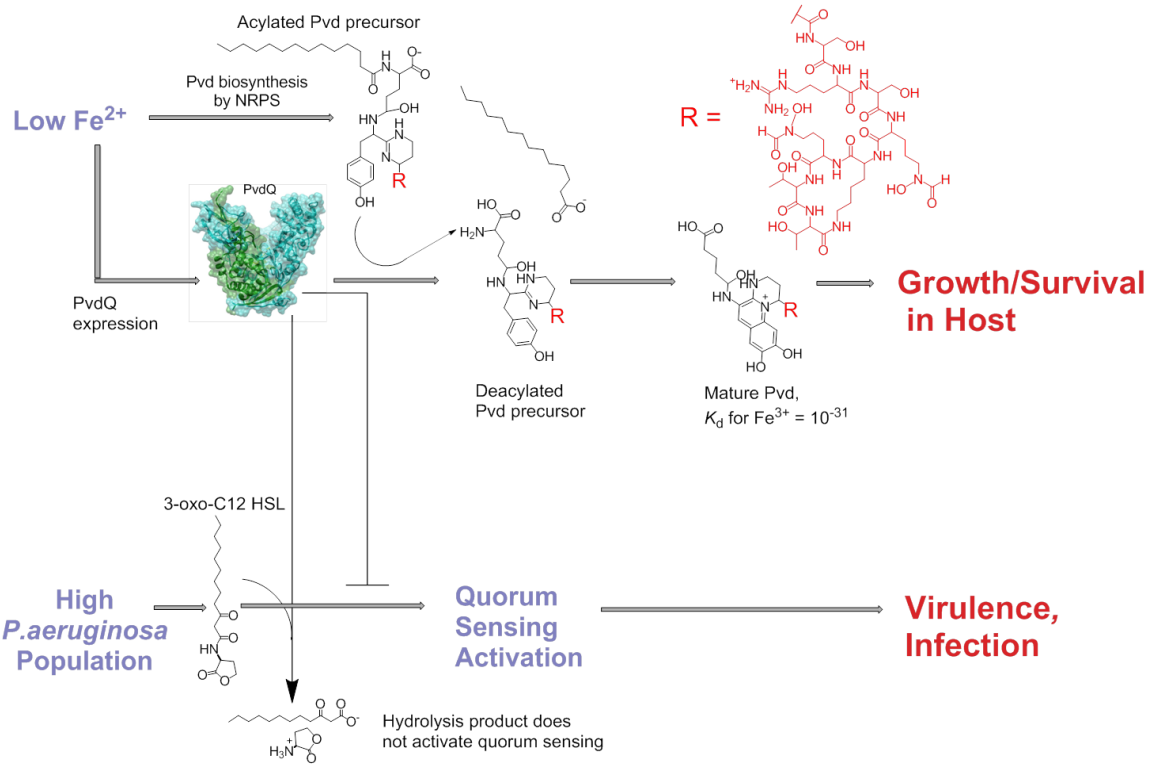

Figure 1.9 Tension between proposed biological roles of PvdQ

In the top pathway, PvdQ's iron regulated expression and role in Pvd biosynthesis are illustrated, resulting in the production of Pvd and growth within an iron-limited host environment, suggesting that inhibition of PvdQ may be a useful therapeutic strategy. In the bottom pathway, PvdQ's potential role in QS attenuation is demonstrated, which would lead to reduced virulence, suggesting that exogenous application of PvdQ or otherwise enhancing its activity would be a useful therapeutic strategy. These conflicting models create a challenge in determining the pharmacological significance of PvdQ.

Specific Aims of Research

To help clarify the role of PvdQ, I undertook a series of *in vitro* enzymology studies. In Chapter 2, I describe work that determines the enzyme's *in vitro* substrate selectivity, the discovery and characterization of potent long chain alkylboronic acid inhibitors of PvdQ, and the *in vitro* application of those inhibitors to iron-limited *P. aeruginosa* growth. In chapter 3, I describe my work characterizing a related class of inhibitors, short chain alkylboronic acids, and their use to probe the mechanism of PvdQ substrate selectivity and exclusion. In chapter 4, I describe the creation of a circular permutation of PvdQ in order to uncouple its self-processing and enzymatic activities, thus facilitating site-directed mutagenesis and protein engineering, laying the groundwork for future mechanistic, structural, and engineering studies.

Chapter II: Rational design of a transition state analog with picomolar affinity for *Pseudomonas aeruginosa* PvdQ, a siderophore biosynthetic enzyme [1]

INTRODUCTION

Roles for PvdQ in *N*-acyl homoserine lactone (AHL) degradation, quorum sensing regulation, and pyoverdine (Pvd) biosynthesis were originally proposed on the basis of genetic and cell-based studies.[13,30,42,48,49,51,59] Specifically, the gene encoding PvdQ was found to be located in the same operon as known Pvd biosynthetic enzymes,[57] knockout of *pvdQ* was shown by liquid chromatography-electrospray ionization-Fourier transform-mass spectrometry to cause production of an immature form of Pvd carrying a myristic (C14) acyl group,[14] and *pvdQ* transcription was found to be upregulated by iron starvation through GeneChip® studies.[57] Iron regulation of *pvdQ* homologues was found to be conserved in *Pseudomonas putida* and *Pseudomonas syringae*.[58] PvdQ's role in Pvd biosynthesis was further supported by the discovery that the C14 acyl group is removed by an enzymatic activity in the periplasm.[48] PvdQ was shown to be localized in the periplasm by fluorescence microscopy of *P. aeruginosa* expressing PvdQ fused to the fluorescent protein mCHERRY.[60,42]

[1] Clevenger, K. D., Wu, R., Er, J. A. V., Liu, D., and Fast, W. (2013) Rational Design of a Transition State Analogue with Picomolar Affinity for Pseudomonas aeruginosaPvdQ, a Siderophore Biosynthetic Enzyme. ACS Chem. Biol. 8, 2192–2200. Clevenger designed and carried out protein purification, enzyme assay, steady state kinetics, inhibitor screening, and cell growth assays and helped wrote those portions of the manuscript. Wu designed and carried out X-ray crystallization experiments and helped write that portion of the manuscript. Fast and Liu assisted in general experiment design and helped write the manuscript.

While this body of evidence strongly suggests a biological role for PvdQ in Pvd biosynthesis, evidence also exists that PvdQ is involved in degradation of AHL molecules through hydrolysis of their amide linkage (Figure 1.9), and particularly the degradation of 3-oxo-C12-HSL, an autoinducer of *P. aeruginosa*. Heterologous expression of PvdQ in *Escherichia coli* in the presence of 3-oxo-C12-HSL lead to degradation of 3-oxo-C12-HSL.[13] Meanwhile, constitutive expression of PvdQ in *P. aeruginosa* grown in rich medium prevented the accumulation of 3-oxo-C12-HSL that would normally be observed in the absence of constitutively expressed PvdQ, while having little effect on cell density.[13] Constitutive *P. aeruginosa* overexpression of PvdQ in *C. elegans* killing assays was found to increase *P. aeruginosa*-treated-*C. elegans* survival rates to that of *C. elegans* treated with non-virulent *E. coli*, and addition of purified exogenous PvdQ similarly protected *C. elegans* and reduced overall levels of 3-oxo-C12-HSL.[49]

Due to the body of evidence supporting PvdQ roles in both Pvd biosynthesis and AHL degradation, I undertook *in vitro* studies of purified PvdQ in order to determine its substrate preference, thus shedding light on its preferred substrate(s) and laying the ground work for the discovery of highly potent alkylboronic acid covalent inhibitors of PvdQ.[31] Much of the text in this chapter has been adapted with permission from my prior publication, where the experiments and results from this chapter were first reported.[31]

RESULTS AND DISCUSSION

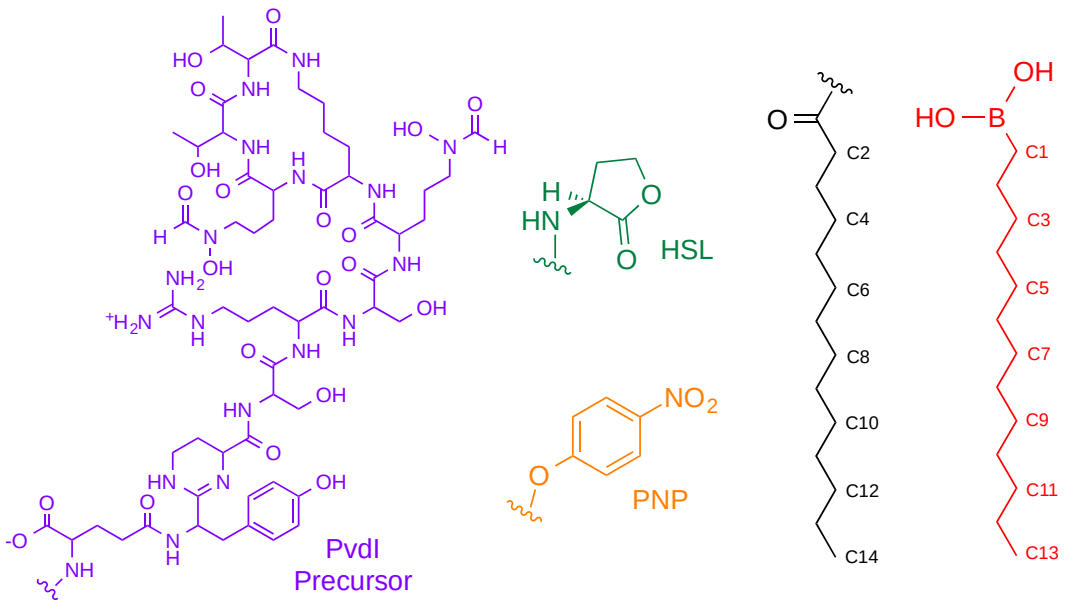

Figure 2.1 Selected PvdQ Ligands.

The C14 alkyl substitution (black) of a Pvd type I (PvdI) precursor (purple) is removed by PvdQ-catalyzed amide hydrolysis. The *N*-acyl substitutions of varying length (black) on *N*-acyl-L-homoserine lactones (HSL, green) are hydrolyzed by PvdQ, as are the corresponding *p*-nitrophenol (PNP, orange) esters. *N*-Acyl-HSLs with 3-oxo substitutions bear a carbonyl at C3 (not pictured). Alkylboronic acids (C_n-$B(OH)_2$, red) are inhibitors of PvdQ.

PvdQ *in vitro* substrate selectivity

To investigate the *in vitro* activity and substrate preference of PvdQ, I expressed and isolated PvdQ recombinantly to ≥ 95% purity with a C-terminal 6 × histidine tag. The *N*-terminal sequence of the SDS-PAGE band corresponding to the β subunit was found to be S-N-A-I-A, consistent with the expected sequence for the processed β subunit. To quantify the *in vitro* selectivity of PvdQ for different *N*-acyl-HSL substrates and thus probe its potential role in quorum sensing regulation, I developed a discontinuous assay, using *o*-

phthaldialdehyde (OPA) derivatization followed by HPLC detection, for the detection of free homoserine lactone through reaction with its primary amine which is released by PvdQ hydrolysis of *N*-acyl-HSL substrates. Steady-state kinetic parameters for a series of AHL substrates were determined (Figure 2.1, Table 2.1). C12-HSL was found to be a good substrate (k_{cat}/K_M = 2.2 × 10^5 $M^{-1}s^{-1}$), but shorter acyl chains were poorly hydrolyzed ($k_{cat}/K_M \leq 10^3$ $M^{-1}s^{-1}$) (Figure 2.1, Table 2.1). Notably, 3-oxo-C12-HSL was a poor substrate. Thus, PvdQ does not appear to be evolutionarily optimized for hydrolysis of either C4-HSL[51] or 3-oxo-C12-HSL, the two endogenously produced *N*-acyl-HSLs of *P. aeruginosa.* This suggests PvdQ is not tuned for a role in regulation of the endogenous quorum sensing of *P. aeruginosa*, though moonlighting[61] roles cannot be ruled out, nor can potential roles in modulating the quorum sensing of other species. My quantitative steady state kinetics results are consistent with qualitative bioassay studies by another group which showed PvdQ to have a preference for substrates with linear acyl chains at least 8 carbons in length.[13]

Although these results suggest that PvdQ was not evolutionarily optimized to regulate endogenous *P. aeruginosa* signaling, this activity of PvdQ may still be a useful tool for degrading certain *N*-acyl-HSLs. For example, the specificity constants of PvdQ for selected substrates compare favorably with quorum-quenching enzymes from different superfamilies such as the homoserine lactonase AiiA from *Bacillus thuringiensis* (dizinc metalloform k_{cat}/K_M values ≈ 10^4 $M^{-1}s^{-1}$; dicobalt metalloform k_{cat}/K_M ≈ 10^6 $M^{-1}s^{-1}$)[53] and an engineered version of the homoserine lactonase PLL from *Mycobacterium avium*

($k_{cat}/K_M \approx 10^4$ $M^{-1}s^{-1}$), indicating that PvdQ might serve equally well to degrade certain *N*-acyl-HSLs.[52]

Substrate	K_M (μM)	k_{cat} (min^{-1})	k_{cat}/K_M ($M^{-1}s^{-1}$)
C8-HSL	ND[a]	ND	2.2×10^{2} [b]
C10-HSL	ND	ND	2.2×10^{3} [b]
C12-HSL	11 ± 2	148 ± 7	2.2×10^{5}
3-oxo-C12-HSL	ND	ND	2.3×10^{3} [b]
C10-PNP	61 ± 13	49 ± 5	1.3×10^{4}
C12-PNP	0.8 ± 0.1	52 ± 3	1.1×10^{6}
C14-PNP	0.60 ± 0.06	86 ± 3	2.4×10^{6}
C16-PNP	4 ± 1	1.9 ± 0.1	8×10^{3}

[a]ND: not determined because limited substrate solubility prevents determination of V_{max}
[b] Fitting error is ≤ 8 %.

Table 2.1 Steady-state rate constants for PvdQ catalyzed hydrolysis of selected substrates.

In contrast to other quorum-quenching enzymes that have limited selectivity for AHL chain length and substitution, but are selective for the homoserine lactone moiety, [53,54] PvdQ appears to tolerate different ring substitutions, but is more selective for chain length. To define the selectivity of PvdQ more precisely, I compared steady-state kinetic constants for *p*-nitrophenyl fatty acid ester reporter substrates (Figure 2.1, Table 2.1). Notably, the k_{cat}/K_M values measured here are significantly larger than previously reported by another group,[25] due mostly to lower K_M values. This difference may reflect increased substrate solubility under my assay conditions (See Methods).

PvdQ was shown to preferentially hydrolyze PNP substrates with linear 12 – 14 carbon alkyl chains, with shorter or longer chains showing ≥ 2 orders of magnitude decrease in k_{cat}/K_M (Table 2.1). Hydrolysis of PNP substrates even further removed from this optimal range (≤ C8, ≥ C18) could not be reliably quantified. Taken together, these

findings suggest that PvdQ has evolved in response to a need for processing myristoylated substrates and has not been optimized for the endogenous quorum-sensing signals of *P. aeruginosa* (although moonlighting roles are possible). This conclusion is consistent with the proposed primary role of PvdQ in processing myristoylated precursors of the siderophore pyoverdine (Figure 2.1).[14,30]

Inhibitor Design

Two previous reports of high-throughput screening for PvdQ inhibitors describe the discovery of structurally diverse inhibitors. Two compounds of moderate potency, NS2028 (8-bromo-4H-[1,2,4]oxadiazolo[3,4-c][1,4]benzoxazin-1-one: IC_{50} = 130 μM) and SMER28 (6-bromo-N-(prop-2-en-1-yl)quinazolin-4-amine: IC_{50} = 65 μM) were identified from a 1280-compound library of bioactive compounds (LOPAC) and determined by X-ray crystallography to bind in the acyl group binding site, predominantly through hydrophobic interactions, each making only one hydrogen bond with the enzyme (Figure 2.2A-B).[25] The characterization of a more potent lead from HTS has also been reported, a fluoro-substituted biaryl nitrile, designated ML318 ([*p*-(fluoromethyl)phenyl][*m*-(trifluoromethyl)phenyl]acetonitrile: IC_{50} = 20 nM) from screening the NIH molecular libraries probe production centers network compound library.[25] The structure of ML318 in complex with PvdQ revealed that ML318 also binds in the acyl group binding site and makes only one hydrogen bond with PvdQ (Figure 2.2C). Alignment of all three inhibitors, along with a covalently bound myristoyl group (Figure

2.3) reveals their similar positioning in the acyl group binding site of PvdQ, removed from the catalytic machinery of the enzyme.

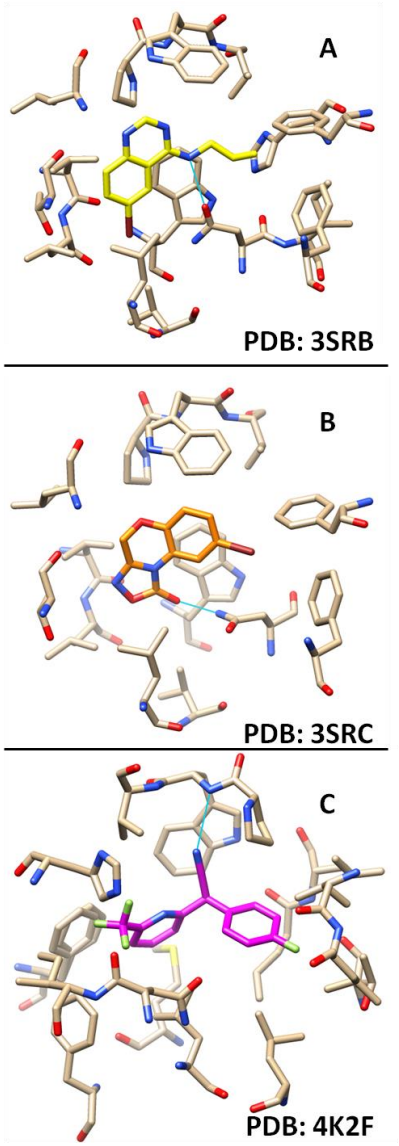

Figure 2.2 Reported inhibitors of PvdQ discovered by HTS

The inhibitors SMER28 (6-bromo-N-(prop-2-en-1-yl)quinazolin-4-amine) (A, yellow), NS2028 (8-bromo-4H-[1,2,4]oxadiazolo[3,4-c][1,4]benzoxazin-1-one) (B, orange), and ML318 ([*p*-(fluoromethyl)phenyl][*m*-(trifluoromethyl)phenyl]acetonitrile) (C, magenta) are shown bound in the hydrophobic pocket of PvdQ (tan). Hydrogen bonds are shown as teal lines. Atoms are colored by heteroatom: red = oxygen, blue = nitrogen, and green = fluorine.

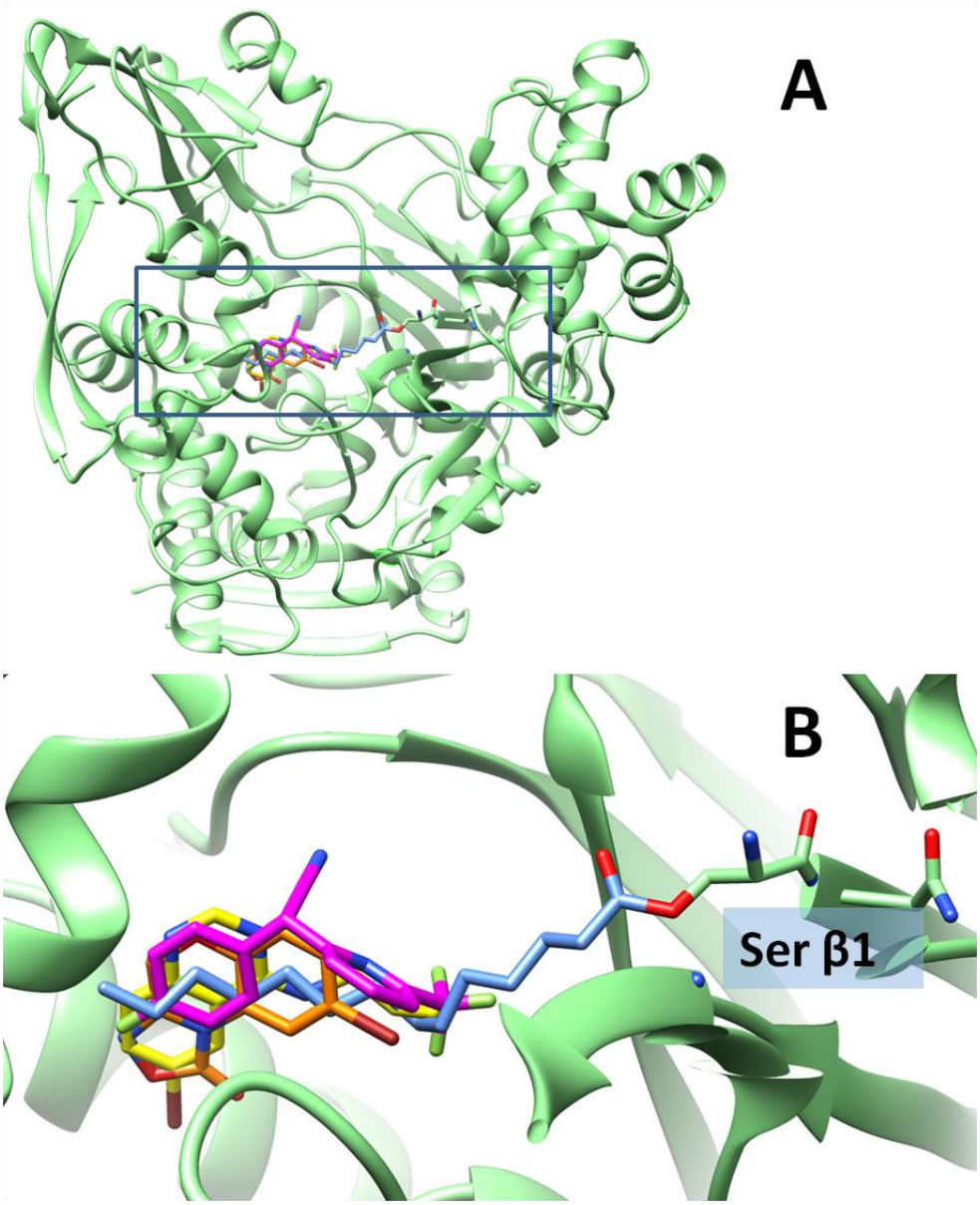

Figure 2.3 Alignment of reported PvdQ inhibitors discovered by HTS

Inhibitors are colored as in Figure 2.2A-C, with the addition of a myristoyl group (light blue) covalently bound to Ser β1 of PvdQ. The inhibitors derived from HTS bind at the back of the acyl group binding site in roughly the same location, do not make direct contact with the enyzme's catalytic machinery, and each make only one hydrogen bond with PvdQ, as shown in Figure 2.2.

Given the very hydrophobic nature of the pocket in PvdQ that makes up the tail group binding site, it is not surprising that an HTS approach has mostly yielded very hydrophobic molecules which inhibit PvdQ by interacting with this region, but lack significant hydrogen bonding. It seems likely that such compounds will lack chemical selectivity *in vivo.* Taking an alternative rational design approach, I tested using a boronate moiety as a warhead, since boronates are known to interact directly with the catalytic machinery of other Ser/Thr-dependent hydrolases,[62,63] and then interrogated the potency of a series of alkyl substitutions that mimic the observed substrate preference of PvdQ. An initial screen of alkylboronic acids and fatty acids at single inhibitor and substrate concentrations was carried out to assess the overall affinity of alkylboronic acids relative to the structurally related fatty acids, which represent reaction products for various AHL and acyl-PNP substrates (Figure 2.5). Alkylboronic acid potency was found to vary with chain length, with C12-$B(OH)_2$ and C13-$B(OH)_2$ apparently having very high potencies; 50 nM of C12-$B(OH)_2$ and C13-$B(OH)_2$ was sufficient to inhibit 97% of substrate turnover. The alkylboronic acids in general were much more potent than the related fatty acids; a 900-fold greater concentration of the related fatty acids (40 μM) still could not match the extent of inhibition achieved with the alkylboronic acids at 50 nM (Figure 2.5). It should be noted that the C13-$B(OH)_2$ inhibitor is the closest structural match to myristoylated (C14) substrates, because the boron takes the position of the initial carbon in the corresponding substrate (Figure 2.1).

To determine the true potencies of alkylboronic acids for PvdQ, I determined their K_i values in the presence of C12-PNP substrate. Initial measurement of the IC_{50} values for

C12-$B(OH)_2$ and C13-$B(OH)_2$ however were found to approach half of the total enzyme concentration in the inhibition assay (≈ 5 nM), suggesting that IC_{50} cannot be used to directly calculate the apparent K_i value for the inhibitors, since it is likely much smaller than the enzyme concentration.[64] To overcome this technical challenge, multiple IC_{50} values for both C12-$B(OH)_2$ and C13-$B(OH)_2$ were determined at different substrate concentrations, followed by a replot of IC_{50} values against substrate concentrations (Figure 2.4A). The linear shape of the resulting plots indicates a competitive mode of inhibition, while apparent K_i values for each compound can be determined from the plot's positive slope.[64] Assuming a competitive mode of inhibition, the true K_i values for C12-$B(OH)_2$ and C13-$B(OH)_2$ were then calculated to be ≈ 200 pM (Table 2.2). Interestingly, inhibition had a rapid onset with no observed time-dependence, unlike many other tight binding inhibitors.[64] Some PvdQ activity was restored upon dialysis (not shown), consistent with a rapid equilibrium reversible mode of inhibition. The K_i values for the other linear alkylboronic acid compounds (with 8, 10, 14, and 15 carbon alkyl substituents) were determined by standard methods, deriving an apparent K_i from a single IC_{50} plot and calculating the true K_i based on an assumed competitive mode of inhibition, like that determined for the C12 and C13 alkylboronic acids (Table 2.2).[64]

Inhibitor	K_i (nM)
C8-B(OH)$_2$	161 ± 3
C10-B(OH)$_2$	1.1 ± 0.4
C12-B(OH)$_2$	0.19 ± 0.02
C13-B(OH)$_2$	0.20 ± 0.04
C14-B(OH)$_2$	1.0 ± 0.3
C15-B(OH)$_2$	8.3 ± 0.9
C12-COOH	6000 ± 200

Table 2.2 K_i values for alkylboronic and fatty acid inhibitors of PvdQ

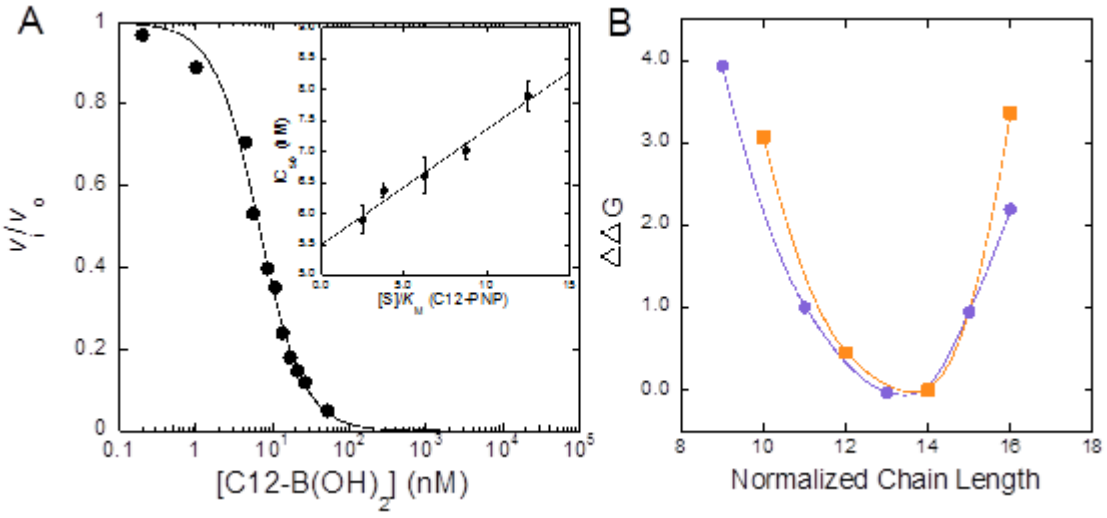

Figure 2.4 Competitive tight-binding inhibition of PvdQ by C12-B(OH)$_2$.

A) IC_{50} values were determined for the inhibitor using varying concentrations of C12-PNP substrate. Main panel shows a representative plot with 5 μM substrate. Inset shows a linear dependence of IC_{50} on [S] / K_M, indicating competitive inhibition. B) Free energy correlation between K_i and k_{cat}/K_M for a structurally related set of inhibitors and substrates. Inhibitors are designated using their chain length +1 to account for boron at the initial position (Figure 2.1). The $\Delta\Delta G_{bind}$ for inhibitor K_i values (**purple circles**) relative to that of the normalized C14 length are plotted along with $\Delta\Delta G^{\ddagger}$ values for k_{cat}/K_M of PNP substrates (**orange squares**) relative to C14-PNP.

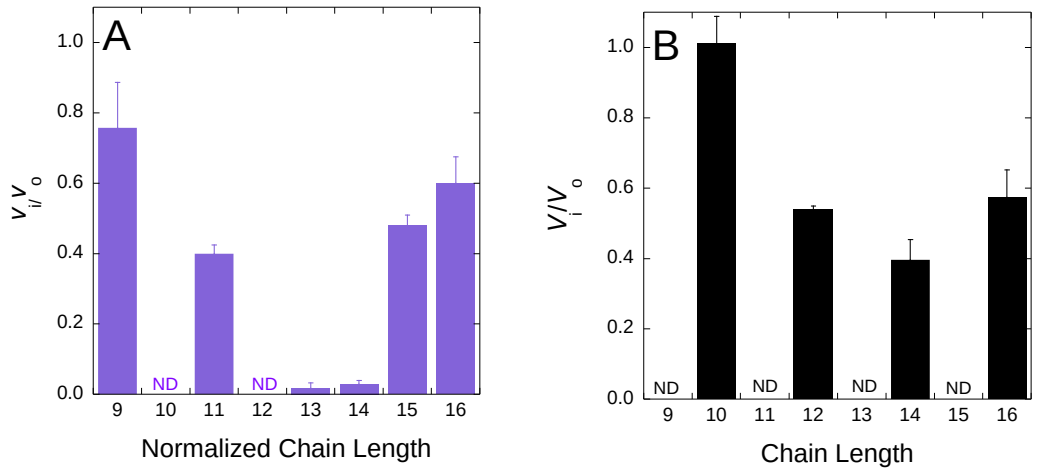

Figure 2.5 Inhibition of PvdQ by fatty acids and alkylboronates.

A) Inhibition of PvdQ at one concentration each (50 nM) of various length alkylboronates (purple). Normalized chain length for alkylboronates is the number of alkyl carbons +1, to allow direct comparison with fatty acid chain length (Figure 1). B) Inhibition of PvdQ at one concentration each (40 μM) of various length fatty acids (black). ND: not determined.

Due to the potency of the alkylboronic acid inhibitors and the previously demonstrated ability of boronates to form reversible tetrahedral adducts with Ser/Thr dependent enzymes, I suspected that alkylboronic acids act as transition state mimics. In general, the free energy of binding transition state analogs is expected to parallel the free energy of transition state stabilization for a structurally similar series of substrates.[64] However, the structural offset of the inhibitors and substrates described here (Figure 2.1) prevents traditional linear comparison plots between the compounds tested. Instead, I sought to determine whether the ΔG_{bind} (calculated from K_i values) for changes in inhibitor chain length correlated with $\Delta G^{\ddagger}$ (calculated from k_{cat}/K_M values) for a similar series of substrates. When these ΔG values are plotted against normalized chain length (Figure 2.4),

they clearly overlap, a result that is consistent with transition state mimicry. ΔΔG values were used in the plot to enable a more clear comparison between K_i and k_{cat}/K_M derived values, by normalizing the lowest value on each curve to zero.

Structural Characterization

Though the above covariance of ΔΔG curves, along with the very high potency of C12-$B(OH)_2$ and C13-$B(OH)_2$, strongly suggested transition state mimicry by alkylboronic acids, to more fully investigate this matter I worked with Professor Dali Liu's laboratory (Loyola University Chicago) to acquire an X-ray crystal structure of PvdQ in complex with C13-$B(OH)_2$. It has been reported that boron-containing inhibitors can bind non-covalently or bind through reversible di-, or tricovalent bonds with nitrogen or oxygen nucleophiles. Planar, sp^2 hybridization of covalent boron inhibitors has also been reported. [63,65–68] These different possible binding mechanisms made *a priori* predictions problematic, underscoring the potential value of structural characterization.

Co-crystals of C13-$B(OH)_2$ inhibited PvdQ at pH 7.5 were grown and an X-ray crystal structure at 1.8 Å resolution was determined by molecular replacement, as described previously (Table 2.3, Figures 2.3, 2.5, 2.6). The final model was built as a heterodimer and comprises an α subunit (residues 28-192) and a β subunit (residues 217-907) as a result of self-processing, as anticipated. In general, the final model aligns very closely to previously reported X-ray crystal structures of apo PvdQ (PDB: 2WYE) with an RMSD of 0.3 Å.[16]

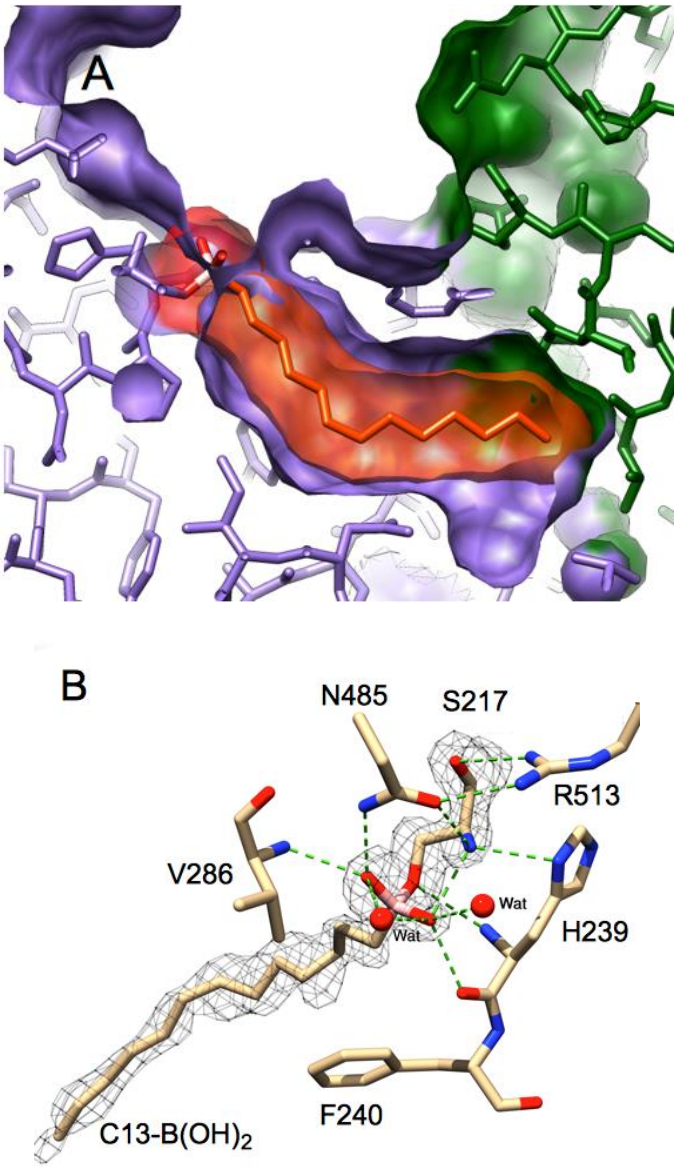

Figure 2.6 A 1.8 Å structure of PvdQ inhibited by C13-B(OH)$_2$.

A) Cutaway surface view showing the alkyl chain of the inhibitor (orange) bound to the myristoyl-binding site of PvdQ, with the α subunit in green and the β subunit in purple. See Figure 2.7 for a wider perspective. B) A simulated annealing composite omit map at 1.1 σ showing a monocovalent adduct between the inhibitor's boron (pink) and the side chain of Ser217 (the *N*-terminal residue of the β-chain, numbered relative to the PvdQ propeptide here, but elsewhere as Ser β1), with H-bonds and water molecules included. Figure 2.6B was prepared by and used with permission of Professor Dali Liu (Loyola University Chicago).

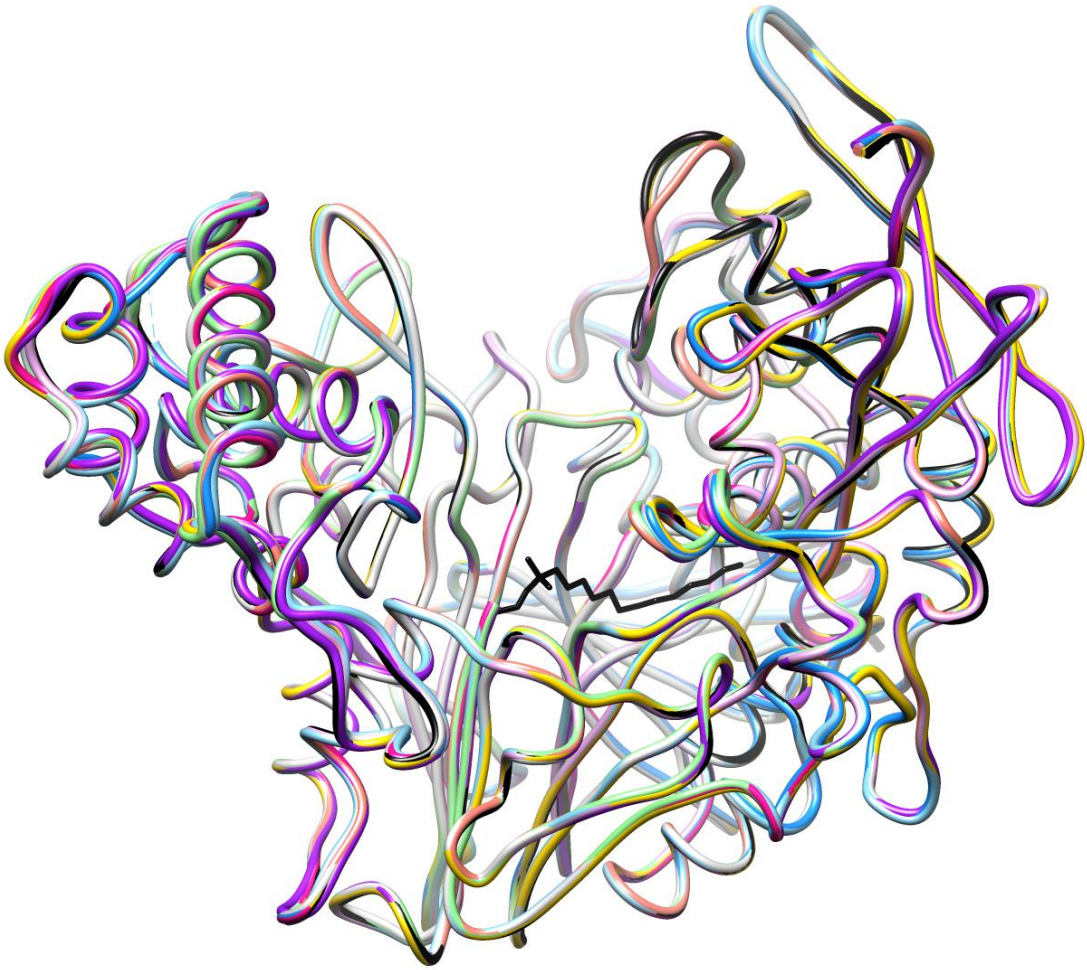

Figure 2.7 Structural overlay of PvdQ structures.

The backbone trace of the PvdQ-C13-$B(OH)_2$ complex is superimposed with that of the other reported PvdQ structures and shows only minor rearrangements in loop regions. Except for C13-$B(OH)_2$, all ligands and ordered water molecules are omitted. Color coding is a follows: PvdQ-C13-$B(OH)_2$ (black), 3L94 (light blue), 3L91 (pink), 3SRB (light green), 3SRC (salmon), 3SRA (grey), 2WYD (dark pink), 2WYB (yellow), 2WYC (blue), 2WYE (purple). Figure was prepared using UCSF Chimera.[69]

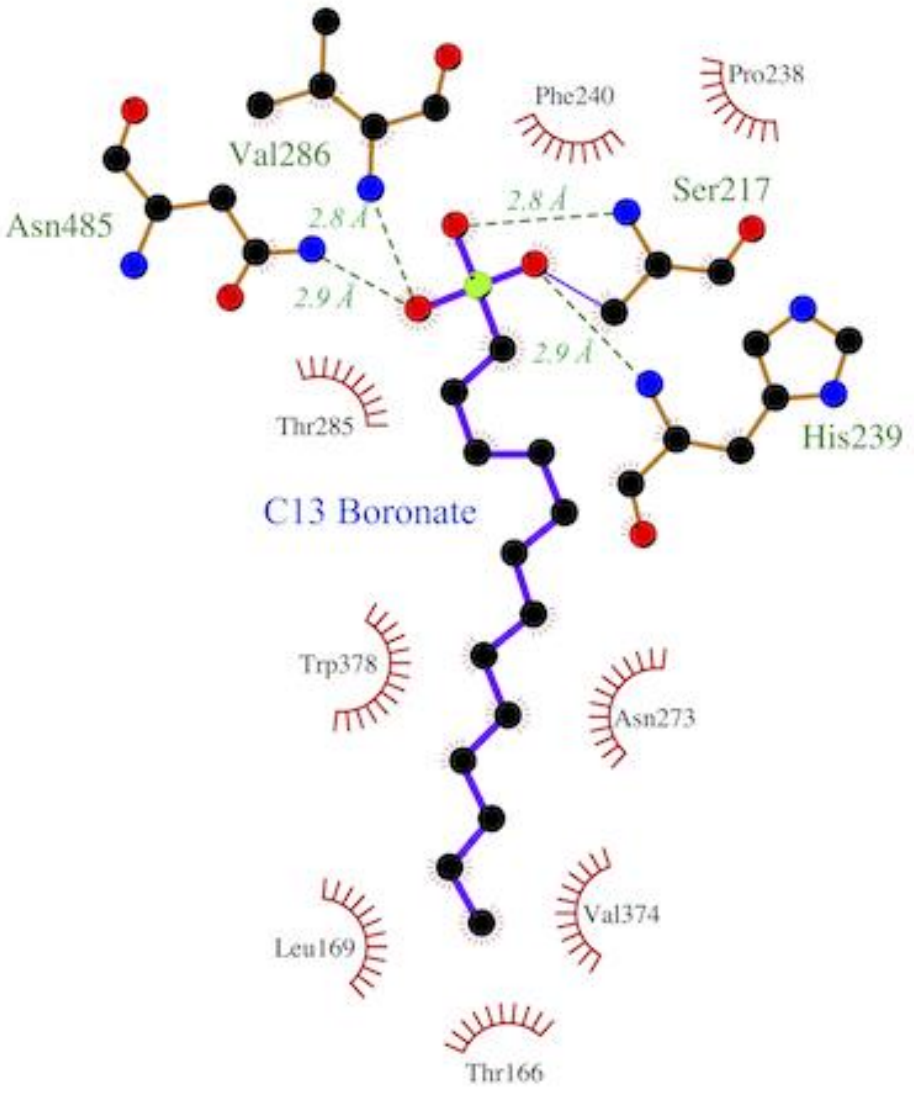

Figure 2.8. Interactions between C13-$B(OH)_2$ and PvdQ.

Distances between selected atoms are indicated. Atoms are colored by identity: boron (green), carbon (black), oxygen (red), nitrogen (blue), with bonds of the protein in tan, bonds of the inhibitor in purple and hydrophobic interactions in red hash marks. Figure was prepared using LigPlot. [70]

The one exception to the similarity between our structure and 2WYE is in the electron density around the active site serine and in the acyl group binding site for the alkyl chain of the substrate. A simulated annealing composite omit map to remove phase bias reveals extra electron density at the active site (Figure 2.6) that is well fit by a monocovalent Ser217 - C13-$B(OH)_2$ adduct, with an unambiguous sp^3 tetrahedral geometry (Figure 2.6, 2.6). Our model therefore strongly supports C13-$B(OH)_2$ as a transition state mimic for PvdQ. The tight packing of the alkyl chain into the myristoyl-binding site also helps explain the observed substrate preference (Table 2.1) because substrates longer than C14 would be disfavored by steric occlusion. The side chains of several residues, including Phe240, Thr285, Val286, Val403 and Pro238, are found in close proximity (≤ 5 Å) to C2 of the inhibitor, which corresponds to the position bearing the disfavored 3-oxo-substitutent in *N*-acyl-HSL substrates. These residues may therefore contribute to the substrate preference of PvdQ for unsubstituted *N*-acyl-HSLs. It is less clear however, either from these results or from the models reported by other groups,[16,25] how PvdQ disfavors substrates shorter than C12, such as the native quorum sensing signal of *P. aeruginosa*, C4-HSL. Such selectivity may be important because C4-HSL is responsible for triggering a variety of cellular processes, including the production of some virulence factors.[50] Further studies investigating this critical aspect of the substrate selectivity of PvdQ will be reported in Chapter 3.

Data Processing	
Space group	$C222_1$
Cell dimensions	
α, β, γ (°)	90.0; 90.0; 90.0
a, b, c (Å)	121.0; 166.4; 94.2
Resolution (Å)	41.0 - 1.8
Mosaicity (°)	0.33
[a]R_{merge} (%)	0.124 (0.603)[b]
I/σ	9.6 (2.1)
Completeness (%)	99.7 (100)
Multiplicity	6.3 (6.3)
No. Reflections	488124
No. Unique Reflections	86070
Refinement	
[c]R_{work}/[d]R_{free} (%)	16.23 / 18.78
No. of Atoms	
Protein	6304
Ligand	22
Water	598
B-factors (Å^2)	29.5
Overall Average	
Protein Average	23.68
Ligand B-factor Range	18.45/44.97
[e]RMSD	
Bond length (Å)	0.007
Bond angle (°)	1.126
Ramachandran Statistics (%)	
Most Favored	96.07
Allowed	3.37
Outliers	0.56

[a] $Rmerge = \Sigma|I_{obs}-I_{avg}|/ \Sigma I_{avg}$

[b] The values for the highest resolution bind are in parentheses.

[c] $R_{work} = \Sigma|F_{obs}-F_{calc}|/ \Sigma F_{obs}$.

[d] Five percent of the reflection data were selected at random as a test set and only these data were used to calculate R_{free}.

[e] RMSD, root mean square deviation.

Table 2.3. Crystallographic Statistics for C13-$B(OH)_2$ inhibited PvdQ.

Cultured Cell Growth Assays.

Previously, it has been show that inhibition of siderophore biosynthetic enzymes in *Mycobacteria* and *Yersinia* cells is a useful strategy for suppressing iron-limited growth of bacteria.[43,46,71] To test alkylboronic acids for inhibition of iron limited growth and siderophore biosynthesis, I applied C13-B(OH)$_2$ to iron limited cell culture of *P. aeruginosa* (Figure 2.9). Wild type *P. aeruginosa* can grow in iron-limited minimal media, but the transposon-disrupted *pvdQ* mutant strain only shows very limited growth. Wild type *P. aeruginosa* cultures given an initial dose of 1 μM inhibitor (5000 × K_i) are growth inhibited. Similar growth inhibition is observed down to 10 nM inhibitor (data not shown). However, after 30 h, growth of the inhibitor-treated culture recovers and then parallels that of the untreated wild-type strain (Figure 2.9A). To test if inhibitor degradation was responsible for the loss of potency after 30 hours, repeated dosing of the inhibitor at 6 hour intervals over 30 h was undertaken, but had the same effect on growth as only one initial dosing at t_0 (not shown). This suggested that degradation of C13-B(OH)$_2$ is not the cause of growth recovery.

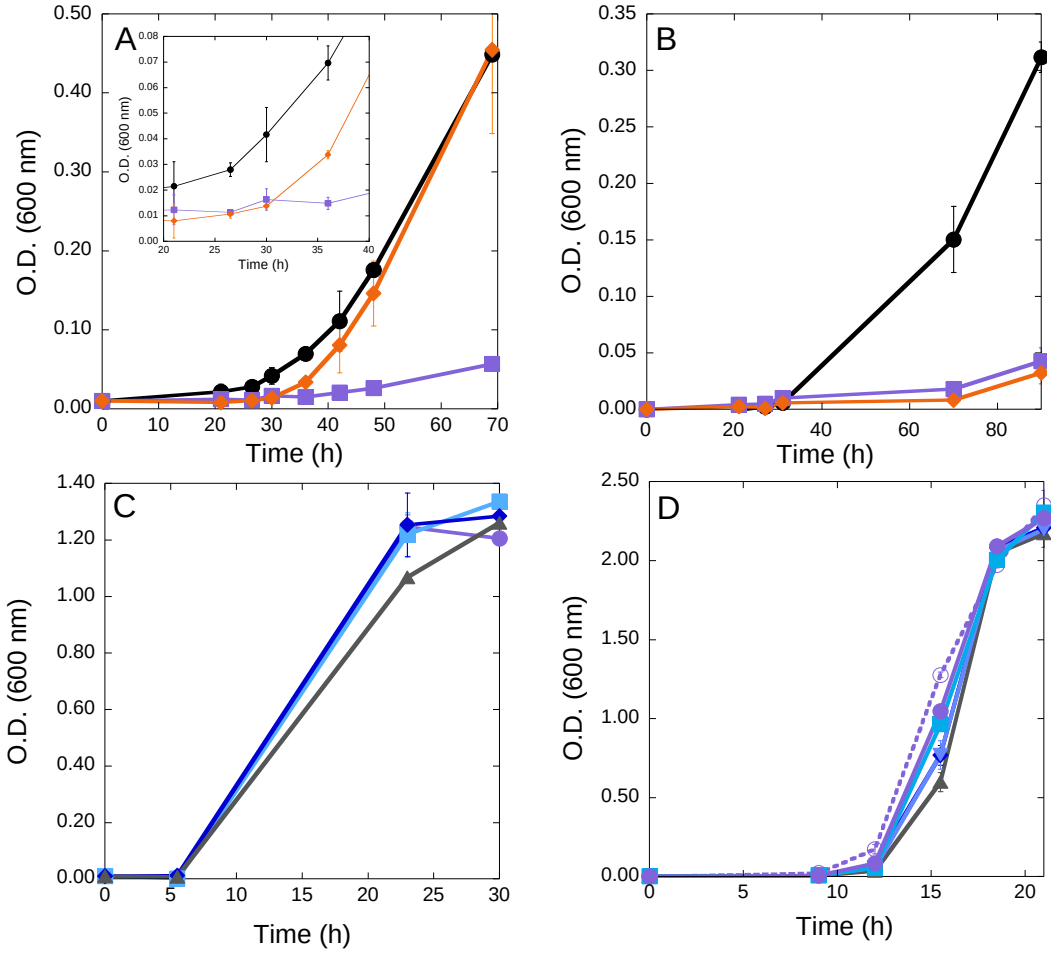

Figure 2.9. *P. aeruginosa* growth studies with C13-B(OH)$_2$ inhibitor.

A) In iron-limited minimal media, the growth of wild-type *P. aeruginosa* in the absence of C13-B(OH)$_2$ (inhibitor) (**black circle**), or after initial treatment with 1 μM inhibitor (**orange diamond**), is shown in comparison to the untreated transposon *pvdQ* transposon insertion mutant *P. aeruginosa* strain (**purple square**). O.D. is optical density. Inset shows 20 – 40 h in more detail. B) Same experiment as in A, except all incubations also contain 40 μM PAβN. C) In minimal media containing trace iron, the growth of the transposon *pvdQ* insertion mutant *P. aeruginosa* strain is shown in the presence of 0 (**purple diamonds**), 0.1 (**teal squares**), 10 (**navy diamonds**), and 100 (**black triangles**) μM inhibitor. D) Same experiment as in C, with an additional concentration of inhibitor (1 μM, **light blue inverse triangles**), except each incubation also contains 40 μM PAβN, and one incubation (**purple open circle, dashed line**) contains neither inhibitor nor PAβN.

Based on the above results, I hypothesized that the recovery of growth by cells treated with C13-B$(OH)_2$ may be a result of a cellular adaptation to the inhibitor. It has been reported that compounds structurally similar to C13-B$(OH)_2$ including *N*-acyl-HSLs and sodium dodecyl sulfate are exported by the MexAB-OprM efflux pump.[72–74] To test this, I repeated these experiments in the presence of phenylalainine-arginine-β-naphthylamide (PAβN; CAS: 100929-99-5), a wide-spectrum competitive inhibitor of multidrug-resistance efflux pumps.[75] Co-administration of both C13-B$(OH)_2$ and PAβN severely inhibits growth of wild-type *P. aeruginosa* under iron-limited conditions, and growth does not recover like it did in the absence of PAβN (Figure 2.9B). These studies indicate that the PvdQ inhibitor C13-B$(OH)_2$ can inhibit the growth of *P. aeruginosa* in iron-limited conditions, but that the efficacy of this particular compound in cell culture is likely limited by poor access to the target due to outer membrane impermeability or a multidrug efflux pump.

As predicted, when iron is not limiting, control experiments using the same concentrations of inhibitors to treat the transposon-disrupted *pvdQ* strain do not result in a similar growth inhibition (Figures 2.9C and D). This result is consistent with our proposal that C13-B$(OH)_2$ targets iron acquisition, most likely through inhibition of PvdQ. Higher concentrations of C13-B$(OH)_2$ do result in minor growth inhibition (Figure 2.9C), which suggests that this particular inhibitor may have deleterious off-target effects when used at elevated concentrations. This result is not surprising due to the hydrophobicity of the unsubstituted *n*-alkyl substituent. However, to the best of my knowledge, this is the first

rationally-designed inhibitor of siderophore biosynthesis that blocks the growth of *P. aeruginosa* in iron-limited conditions, and serves as a proof of principle.

In summary, PvdQ is revealed to have high specificity constants for myristoylated substrates, yet it discriminates against *N*-acyl-HSLs produced endogenously by *P. aeruginosa*. This finding supports the conclusion that PvdQ has not primarily evolved to regulate quorum-sensing endogenous to *P. aeruginosa*. However, the quorum-quenching ability of PvdQ makes it a useful biochemical tool for depleting quorum-sensing signals, particularly if combined with protein engineering approaches to tune substrate specificity.[55] To counteract the primary role of PvdQ in siderophore production, I identified *n*-alkylboronic acids as extremely potent PvdQ inhibitors, due, in part, to the similarity of their monocovalent tetrahedral adducts to the reaction transition state. One of the most potent compounds, 1-tridecylboronic acid (C13-$B(OH)_2$), inhibits growth of *P. aeruginosa* in iron-limited media, and serves as a proof of principle for targeting siderophore biosynthetic pathways in *P. aeruginosa*. The efficacy of this particular compound is limited by poor target access and likely by limited selectivity due to its unsubstituted *n*-alkyl moiety. However, since boron-based inhibitors are used clinically[62] and have proven useful in cultured *P. aeruginosa*,[74] I suggest that this moiety may be a productive chemotype to retain in the design of more biologically effective PvdQ inhibitors.

METHODS

Materials

Unless otherwise noted, all chemicals were obtained from Sigma-Aldrich Chemical Co. (St. Louis, MO, USA) and all restriction enzymes from New England BioLabs (Beverly, MA, USA). 1-Octylboronic acid (C8-$B(OH)_2$), 1-decylboronic acid (C10-$B(OH)_2$), 1-dodecylboronic acid (C12-$B(OH)_2$), and 1-tetradecylboronic acid (C14-$B(OH)_2$) were from Alfa Aesar (Ward Hill, MA, USA). *p*-Nitrophenyl esters of capric (C10-PNP), lauric (C12-PNP), myristic (C14-PNP) and palmitic (C16-PNP) acids were from Research Organics (Cleveland, OH). Syringe filters are MillexGP filter units (0.22 μm, PES membrane, Millipore). PAβN was from Bachem (Torrance, California).

3-Oxo-dodecanoyl-homoserine lactone (3-oxo-C12-HSL) is known to undergo non-enzymic rearrangement.[76] To verify the stock solutions of this compound had not rearranged from the lactone (which is susceptible to AiiA mediated hydrolysis) to the tetramic acid (which is not), LC-ESI-MS (+ ionization) was used to show an 18 Da increase between untreated (298.2 Da) and AiiA[77] -treated (316.2) samples, consistent with maintaining an intact lactone, 3-oxo-C12-HSL, in the stock solution.

1-Tridecylboronic acid (C13-$B(OH)_2$) was synthesized by Ms. Joyce Er (Fast Lab, University of Texas, Austin) in two steps using a published route for butylboronic acid (*36*), but substituting tridecylic acid for butyric acid. The product was recrystallized from hexanes as white needles (57% yield). ^{1}H NMR (DMSO): δ 7.28 (s, 2H), 1.26 (m, 22H), 0.84 (t, J = 6.5 Hz, 3H), 0.55 (t, J = 7.5 Hz, 2H). ^{13}C NMR (DMSO): δ 32.1, 31.3, 29.1,

29.0, 28.7, 24.2, 22.1, 15.4, 13.9. ^{11}B NMR (DMSO): δ 32.4. HRMS: $[M-H]^-$ calcd. for $C_{13}H_{28}BO_2$: 227.2190; found: 227.2190.

Cloning, Expression and Purification

The coding sequence, including that for the periplasmic sorting signal sequence of PvdQ from PAO1 was amplified via PCR from a previously reported expression vector (*4*) using the following primers: 5'-TCCGAATTCATGGGGATGCGTACCGTACTGACCGGCCTGG-3' and 5'-GTGCGGCCGCTTCGCGAATGCTTAGCCGTTGCAGTTGCGGG-3'. The resulting product (≈ 2 Kb) was purified and cloned into the EcoRI and NotI sites in pET24a(+) to encode a His_6-affinity tag at the C-terminus. The insert and flanking regions in this expression vector, pET24-PvdQ, were verified by DNA sequencing (DNA Facility, University of Texas, Austin).

Tuner (DE3) pLysS *Escherichia coli* (*E. coli*) cells (EMD Millipore) were transformed with pET24-PvdQ and stored as a glycerol stock. Starter cultures in LB media (50 mL), supplemented with kanamycin (30 μg/mL) were grown overnight at 37 °C with shaking and used to inoculate 2 L of fresh LB media, supplemented with kanamycin. Expression cultures were grown at 37 °C with shaking to an $OD_{600} \approx 0.6$, cooled on ice for 1 h and induced with isopropyl β-D-1-thiogalactopyranoside (IPTG, 0.5 mM). After an additional incubation for 30 h with shaking at 25 °C, cells were harvested by centrifugation (7000 × *g*; Beckman Coulter Avanti JE Centrifuge (Brea, CA, USA)) and either used immediately or were frozen using $N_{2(l)}$ and transferred to -20 °C storage.

Cell pellets were resuspended in Lysis Buffer (30 mL, 1 mg / mL egg white lysozyme, 20 mM imidazole, 300 mM NaCl, and 50 mM Na_2HPO_4 at pH 8.0), incubated on ice for 30 min, and lysed by sonication (2 min) alternating 10 s bursts and 59 s rests (Thermo Fisher Sonic Dismembrator 500, 70% amplitude, microtip). Cell debris was removed by centrifugation at 31,000 × *g* for 1 h. Lysate was added to NiNTA affinity resin (Qiagen, Valencia, CA, USA) preequilibrated with Binding Buffer (Lysis Buffer omitting lysozyme) and incubated at 4 °C for 3 h with rocking. Resin was pelleted (20 s at 2000 × *g*), washed three times with Binding Buffer (50 mL) and eluted batchwise three times with Elution Buffer (Binding Buffer supplemented with 250 mM imidazole). Buffer was exchanged for Phosphate Buffer (50 mM Na_2HPO_4, pH 8.0) by dialysis (1 L × 3 at 4 °C) using 12-14 KDa molecular weight cut off (MWCO) tubing (Spectrum, Rancho Dominguez, CA). Dialysate was incubated batchwise with anion exchange resin (Q Sepharose Fast Flow, GE Healthcare, Little Chalfont, Buckinhamshire, UK) preequilibrated with Phosphate Buffer for 4 h at 4 °C, and the resin was pelleted by centrifugation (2000 × *g*) and washed with Phosphate Buffer (3 × 6 mL). PvdQ was present in the pooled unbound and wash fractions. If necessary, PvdQ was concentrated to approximately 50 μM using an Amicon Ultra Centrifugal Filter with a 10 KDa MWCO (EMD Millipore). Fractions from all purification steps were analyzed by sodium dodecyl sulfate polyacrylamide gel electrophoresis (SDS-PAGE) using a discontinuous gel with a 12% polyacrylamide resolving layer and stained using GelCode™ Blue Safe Protein Stain (Thermo Fisher). PvdQ from the pooled anion exchange fractions is > 90% homogenous by densitometry analysis and shows the expected two subunits (α and β at 17 and 60 kDa,

respectively). PvdQ concentration was determined by dilution into guanidine-HCl (6 M) and Na_2HPO_4 (20 mM) at pH 6.5, measurement of $A_{280\ nm}$ (Varian Cary-50 UV Visible Spectrophotometer, Palo Alto, CA, USA), and use of an extinction coefficient of 119,000 $M^{-1}cm^{-1}$, calculated from the predicted amino acid sequence of the mature enzyme.[78] *N*-Terminal sequencing of the band corresponding to the β-chain gave S-N-A-I-A, confirming the expected sequence of the processed enzyme (Protein Facility, University of Texas). For long-term storage, glycerol (10 % v/v) was added and 30 μL aliquots of the resulting mixture were flash frozen and stored at - 80 °C. Typical yields are 4 mg PvdQ / L culture.

Activity and Inhibition Assays

Steady-state kinetic constants were determined for hydrolysis of two substrate classes. PNP-ester hydrolysis was continuously monitored using UV-Vis absorbance spectroscopy (Varian Cary 50) to detect formation of *p*-nitrophenolate; $\varepsilon_{402\ nm}$ = 13,000 $M^{-1}cm^{-1}$. The $\varepsilon_{402\ nm}$ was determined experimentally using the assay buffer. Substrate stock solutions were prepared in methanol, which was determined to be an acceptable assay cosolvent (Figure 2.10). Assays were completed using disposable polystyrene cuvettes (Thermo Fisher), substrate, Na_2HPO_4 (40 mM) at pH 8.0, 25 °C with 20% methanol as a cosolvent, and were initiated with addition of PvdQ (10 nM). Fresh working dilutions of PvdQ (1 μM) were made from more concentrated stocks after each hour of use. Assay Buffer was filtered with a 0.22 μm nitrocellulose membrane (EMD Millipore, Billerica, MA, USA) under house vacuum prior to use to eliminate dust particles. Initial hydrolysis rates (< 10 % substrate consumed) were linear. KaleidaGraph 3.6 (Synergy Software,

Reading, PA, USA) was used to determine k_{cat} and K_M values and associated error by non-linear fitting to the Michaelis-Menten equation. Values determined here are significantly different than previous reported values (e.g. C12-PNP: K_M = 1.4 mM, k_{cat} = 44 min^{-1}).[25] In our hands, the substrates are not sufficiently soluble to use the previously reported assay conditions. Here, inclusion of well-tolerated co-solvent (Figure 2.10) lead to improved kinetic constants (e.g. C12-PNP: K_M = 0.6 μM, k_{cat} 86 min^{-1}) (Table 2.1).

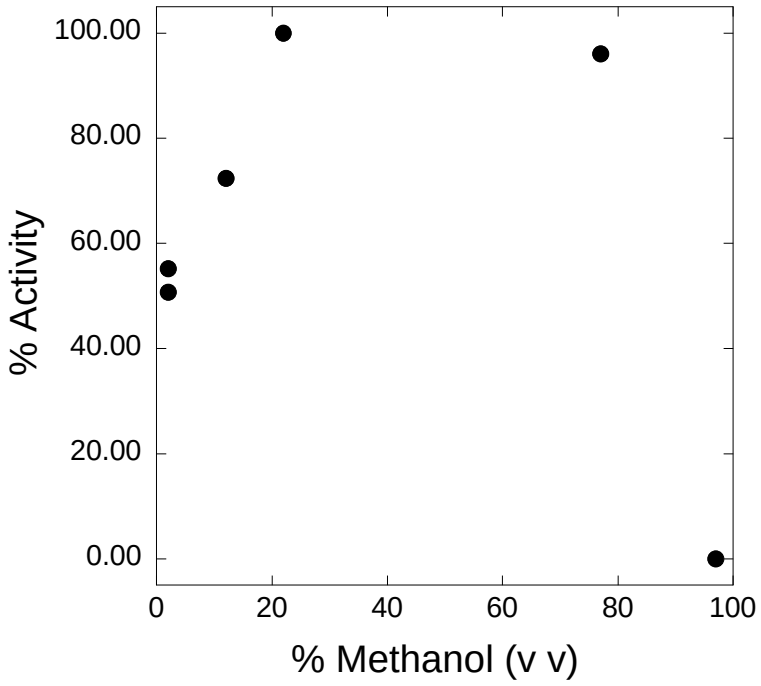

Figure 2.10. Methanol Co-solvent Tolerance.

Hydrolysis rates for C12-PNP (2 μM) in the presence of varying amounts of methanol demonstrate assay tolerance for this co-solvent.

HPLC assay for *N*-acyl-HSL hydrolysis

Briefly, substrate was incubated with PvdQ (conditions as described in Methods) for 5 min and quenched by heat denaturation in boiling water (1 min). We found this

heating step fully inactivates PvdQ activity but does not lead to non-enzymic amide hydrolysis. The reaction mixtures were deproteinized using a 10 kDa molecular weight cut off (MWCO) spin column, filtered, mixed with an equal volume (75 μL) of freshly prepared *o*-phthaldialdehyde (OPA) Reagent (OPA (50 mM) in methanol (1 mL) that is supplemented by 3-mercaptopropionic acid (1.3 mL, 115 mM) and a borate / KCl solution (2.7 mL, 750 mM borate, 700 mM KCl at pH 9.5) and syringe filtered). Samples were incubated for 1 min and then 90 μL was injected onto a 5 μm, 4.6 × 250 mm C18 column (Shimadzu) fitted with a Zorbax XDB-C18 guard column (Phenomenex, Torrance, CA, USA). A Shimadzu Prominence analytical HPLC (Columbia, MD, USA) and two LC-20A pumps were used to run the following solvent program with solvent A being H_2O and solvent B being 70% MeOH. Pumps were initiated with B at 5.0 % and a flow rate of 1 mL / min. From 1 to 14 min, B was increased linearly from 5.0 % to 27.0 %. From 14 to 16 min, B was increased linearly from 27.0 % to 100.0 %. From 18 to 19.5 min, B was linearly decreased from 100.0 % to 5.0 %, with the program ending at 21.5 min. All buffers were filtered and then degassed under house vacuum and treatment by a sonicating bath. An RF10AxL fluorescence detector using 338 nm excitation and 455 nm emission wavelengths was used to detect derivatized product (t_R = 10.6 min), which was quantified by integrating peak area.

Screening and determination of K_i values for alkylboronic acids

Initial screening for PvdQ inhibition by fatty acids and boronic acids was accomplished using a method similar to the PNP-ester assay described above except using

a Wallac Victor^2 plate reader (PerkinElmer, Waltham MA), one concentration of C12-PNP (5 μM) and varying concentrations of fatty acids and boronic acids, diluted from DMSO stock solutions, in triplicate. Final assays did not exceed 1 % DMSO (v/v), which does not inhibit PvdQ.

IC_{50} values for C10-, C14- and C15-$B(OH)_2$ were determined in the same fashion and fit to determine IC_{50} values. The IC_{50} for C8-$B(OH)_2$ was also measured this way, but using a Cary 50 spectrophotometer instead of a plate reader. These IC_{50} values were then converted to K_i values for a competitive inhibition model described elsewhere[64] using the experimentally determined K_M value for the C12-PNP substrate. Because these compounds have IC_{50} values greater than the enzyme concentration, small variations in enzyme concentration have less of an impact on K_i than with the more potent inhibitors below.

K_i values of C12-$B(OH)_2$ and C13-$B(OH)_2$

The K_i values and the mode of inhibition for C12- and C13-$B(OH)_2$ were determined using a modified method to accommodate their high potency. Briefly, PvdQ activity was measured in singlicate assays using disposable polystyrene cuvettes and a Cary-50 UV-Vis spectrophotometer as above to determine IC_{50} values at different concentrations of C12-PNP. The IC_{50} values were plotted against [C12-PNP] / K_M values to determine mode of inhibition and K_i values, as descried elsewhere[64]. Due to the potency of these tight-binding inhibitors, small changes in inhibitor or enzyme concentrations can impact IC_{50} values, so in contrast to the inhibitors above, all kinetic experiments for C12-

and C13-$B(OH)_2$ were performed on the same day using the same enzyme and inhibitor stock solutions.

Crystallography

The crystallization, diffraction, and model building methods used by Professor Dali Liu's group were reported previously in full detail.[31] Briefly, cocrystals of PvdQ and C13-$B(OH)_2$ were grown by hanging drop vapor diffusion at 20 °C and pH 7.5. Crystals appeared in 1 h and grew to maximum size in 5 days. X-ray diffraction data sets were collected at the Advanced Photon Source, beamline 23-ID, Argonne National Laboratory. The wavelength used in monochromatic data collection was 1.0332 Å. The best data set was processed to a resolution of 1.8 Å. The PvdQ–C13-$B(OH)_2$ structure was solved by molecular replacement using the program PHASER with a starting model of a reported structure of PvdQ (PDB ID: 2WYE[16]). The structural solution of the protein was obtained and an extended region of positive difference electron density (F_o-F_c map) was identified (not shown, see Figure 2.6B for a simulated annealing composite omit map). This observed extra density corresponds to the omitted inhibitor moiety at the active site. The expected covalent adduct was fitted into the observed extra electron density using COOT.[31] Structural figures of the protein were created using UCSF Chimera.[69]

***P. aeruginosa* Growth Assays**

The effect of C13-$B(OH)_2$ on cultured cells was monitored using wild type *P. aeruginosa* PA14 or a transposon-disrupted *pvdQ* mutant, *P. aeruginosa* PA14 ID27758 from the PA14 mutant library.[79] This mutant strain has been used previously to study

phenotypes resulting from loss of PvdQ function.[80] Briefly, a 1 mL culture in LB, started from glycerol stocks, was grown with shaking (220 rpm) for approximately 7 h until $Abs_{600\ nm}$ was approximately 0.5. Cells were pelleted (5000 × *g*), washed three times with sterile phosphate-buffered saline (PBS), and resuspended in 250 μL of sterile Iron-Limited MOPS Glucose Medium (25 mM morpholinepropanesulfonic acid at pH 7.2, 93 mM NH_4Cl, 43 mM NaCl, 3.7 mM KH_2PO_4, 1 mM $MgSO_4$, 45 μM diethylene triamine pentaacetic acid (DTPA), 20 mM glucose).[81] DTPA was added to chelate any trace iron, as described elsewhere.[82] Triplicate cultures (1 mL) in the same medium were then inoculated to a starting OD_{600} of 0.01, treated with either vehicle alone (DMSO, 0.1 % v/v) or C13-$B(OH)_2$ (1 μM), and incubated with shaking at 37 °C for up to 70 h. Tests for off-target toxicity were completed in the same manner using the *pvdQ* mutant *P. aeruginosa* strain and the same culture medium, but omitting DTPA and instead supplementing with $FeSO_4$ (3.5 μM)[81] and treating with various inhibitor concentrations (1 nM to 100 μM). When indicated, stock solutions of PAβN (200 mM in DMSO) were diluted into cultures to a final concentration of 40 μM.

Chapter III: PvdQ inhibition by short chain alkylboronic acids reveals substrate exclusion mechanism

INTRODUCTION

Previous studies of PvdQ substrate selectivity using cell-based assays indicated that PvdQ does not process C4-HSL.[13,51] Consistent with these reports, I found that PvdQ does not detectably process *p*-nitrophenyl ester (PNP) substrates with < 8 carbon acyl chains *in vitro*.[31] Exclusion of short chain substrates may be important to the biological function of PvdQ, and would prevent the turnover the *P. aeruginosa* QS molecule, C4-HSL.[13] However, the way that selectivity against short chain substrates is achieved is unclear. Unfortunately, due to the lack of affinity of C4-HSL for PvdQ, there is no obvious strategy to directly study the interaction, or lack thereof, of PvdQ with this substrate or substrates of similar acyl chain length.

Previously, I described studies of PvdQ in complex with, and inhibited by, long chain alkylboronic acids and determined the substrate preference of PvdQ, *in vitro*. These studies revealed the structure of PvdQ in complex with a transition state mimic and helped inform our understanding of the catalytic mechanism of PvdQ, but did little or nothing to improve our understanding of how PvdQ might exclude short chain substrates and also what, if any, role the PvdQ head group site has in substrate recognition and catalysis. The extremely potent affinity of long chain alkylboronic acids (several orders of magnitude more potent than the analogous fatty acids) suggested that the alkylboronic acid family of compounds was worth further investigation and may serve as useful tools for probing PvdQ

mechanisms of ligand preference and exclusion. In order to gain a deeper understanding of how alkylboronic acids achieve their exceptional affinity for PvdQ, as well as to generally study the determinants of PvdQ ligand and substrate selectivity, we undertook the characterization of PvdQ binding and inhibition by short chain alkylboronic acids. In these studies, steady state kinetic measurement of PvdQ inhibition was extended to short chain alkylboronic acids (≤ 4 carbon alkyl chains) and structural studies were extended to both short and medium chain alkylboronic acids (medium chain alkylboronic acids: 5 to 9 carbon alkyl chains). The results of these studies demonstrated the extremely wide range over which alkylboronic acids have potent affinity for PvdQ and suggest a mechanism involving the head group binding site for excluding ligands with chain lengths ≤ 5 atoms, such as C4-$B(OH)_2$ and the quorum sensing signal C4-HSL.

RESULTS AND DISCUSSION

Alkylboronic acids have a broad range of inhibitory affinities

The increased potency of alkylboronic acids for PvdQ, relative to structurally analogous substrates, allowed us to probe a wide range of ligand lengths, which would be inaccessible using substrate due to poor turnover and/or signal (Figure 3.1).[13,31] Determination of K_i values for C2-$B(OH)_2$, C3-$B(OH)_2$, C4-$B(OH)_2$, and C6-$B(OH)_2$ revealed the extremely wide range over which alkylboronic acids can bind to PvdQ with the K_i of the worst ligand (C3-$B(OH)_2$) being about $2.5x10^8$-fold larger than the most potent ligand (C12-$B(OH)_2$) (Table 3.1). These studies also uncovered a linear relationship between PvdQ ligand affinity and ligand alkyl chain length from C6-$B(OH)_2$

to C12-$B(OH)_2$ (Figure 3.1) of 1.07 kcal additional binding energy for each additional methylene. Because PvdQ substrate analogues shorter than C10 become difficult (for HSL substrates) or impossible (for PNP substrates) to characterize by steady state kinetics due to poor affinity for PvdQ, this linear relationship between ligand chain length and PvdQ binding affinity was previously unknown.[25,31] Unsurprisingly, as alkyl chain length extends beyond 13 carbons, affinity for PvdQ gets worse, mirroring the selectivity observed for substrates with alkyl substituents > 14 carbons in length. Consistent with this result, in our previous structure,[31] C13-$B(OH)_2$ appears to occupy almost all of the available space, as does myristate in other structures,[16,25] suggesting a role for steric occlusion in the reduced affinity of alkylboronic acids with *n*-alkylchains longer ≥ 14 carbons.[25] The binding energy observed for each methylene of alkylboronic acid ligands with chain lengths from C6 to C12 of -1.07 kcal/mol is significantly higher than the energy released per methylene for the non-enzymatic transfer of *n*-alkanes from water to *n*-octanol, which is -0.68 kcal/mol.[53,83] This value approaches the experimentally determined upper limit of non-hydrogen atom ligand binding energy of proteins: -1.5 kcal/mol/non-hydrogen atom.[84]

Together, these results suggest that PvdQ has been highly optimized to capitalize on the hydrophobic binding energy of its native substrate's C14 acyl chain and that this interaction dominates the binding energy for ligands ranging from 7 to 13 atoms, as in the case of C6-$B(OH)_2$ and C12-$B(OH)_2$ respectively. This highly optimized binding site may

reflect a biological pressure on the enzyme to process low concentrations of its native substrate.

Notably, the interaction between PvdQ and short chain alkylboronic acids (≤ 4 carbons) produces measurable PvdQ inhibition, however the linear relationship between ligand chain length and binding affinity arguably breaks down in this region (Figure 3.1). It is not known how PvdQ excludes short chain substrates, such as the endogenous quorum sensing signal C4-HSL of *P. aeruginosa*, in the absence of steric hindrance.[13,16] As a major component of *P. aeruginosa's* quorum sensing system, C4-HSL helps control many pathways and activates production of several virulence factors, such as production of elastase and pyocyanin.[50] However, due to a lack of turnover and affinity, interaction (or lack thereof) of PvdQ with short substrates such as C4-HSL is difficult to probe. Therefore, inhibition of PvdQ by C4-$B(OH)_2$ and other short chain alkylboronic acids provides a tool to investigate the interaction of PvdQ with short alkyl chain analogs, which can help reveal mechanisms of ligand exclusion by PvdQ.

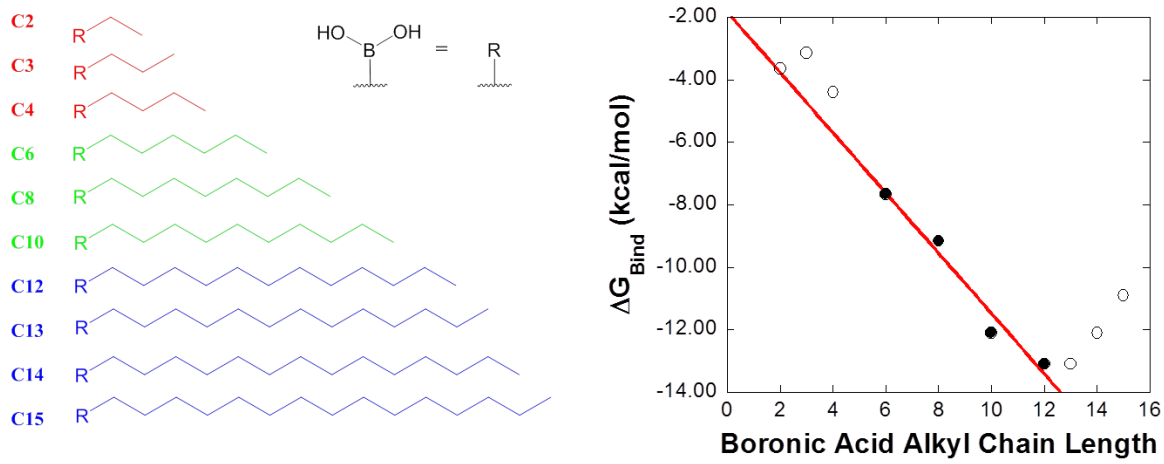

Figure 3.1 ΔG_{bind} for alkylboronic acid binding to PvdQ vs. alkyl chain length.

Left, alkylboronic acid inhibitors of PvdQ are shown. Red = short chain alkylboronates, green = medium chain alkylboronates, blue = long chain alkylboronates. *Right*, plot of ΔG vs. alkyl chain length. Points in black were used to derive linear fit, based on their apparent linear relationship to chain length and their sp^3 covalent mode of binding to PvdQ, as confirmed by X-ray crystallography (Figure 3.2). The slope of the fit line corresponds to the binding energy per methylene for the fitted points and is -1.07 kcal/mol/methylene. The binding energy for boric acid with PvdQ can be extrapolated as -2 kcal/mol ±1 kcal/mol.

Alkylboronic Acid	K_i (M)[a]	ΔG (kcal/mol)[a]
C2-$B(OH)_2$	$2.0 \times 10^{-3} \pm 4 \times 10^{-4}$	-3.6 ± 0.1
C3-$B(OH)_2$	$4.7 \times 10^{-3} \pm 8 \times 10^{-4}$	-3.1 ± 0.1
C4-$B(OH)_2$	$5.5 \times 10^{-4} \pm 9 \times 10^{-5}$	-4.4 ± 0.1
C6-$B(OH)_2$	$2.1 \times 10^{-6} \pm 0.4 \times 10^{-6}$	-7.7 ± 0.1
C8-$B(OH)_2$	$1.61 \times 10^{-7} \pm 3 \times 10^{-9}$	-9.16 ± 0.01
C10-$B(OH)_2$	$1.1 \times 10^{-9} \pm 4 \times 10^{-10}$	-12.1 ± 0.2
C12-$B(OH)_2$	$1.9 \times 10^{-10} \pm 2 \times 10^{-11}$	-13.11 ± 0.06
C13-$B(OH)_2$	$2.0 \times 10^{-10} \pm 4 \times 10^{-11}$	-13.1 ± 0.1
C14-$B(OH)_2$	$1.0 \times 10^{-9} \pm 3 \times 10^{-10}$	-12.1 ± 0.2
C15-$B(OH)_2$	$8.3 \times 10^{-9} \pm 9 \times 10^{-10}$	-10.90 ± 0.06

[a] error values are propagated from fitting errors in IC_{50} determination.

Table 3.1 K_i and ΔG_{bind} values for PvdQ inhibition by alkylboronic acid family

Short chain alkylboronic acids adopt an alternate binding conformation

To investigate the mechanism of short chain substrate exclusion by PvdQ and to better understand the broad range of inhibitor affinities for PvdQ, we determined X-ray crystal structures of PvdQ in complex with C2-$B(OH)_2$, C4-$B(OH)_2$, C6-$B(OH)_2$, and C8-$B(OH)_2$ and compared these results with each other and with our previously determined structure of C13-$B(OH)_2$. Crystals of PvdQ were obtained by previously reported methods and soaked with boronic acid ligands.[31] Structures were solved by Professor Dali Liu's lab to between 1.6 and 2.1 Å resolution by molecular replacement (see Table 3.3 for crystallographic data). The backbones of all structures obtained showed no significant deviation from previously reported structures.[16,25,31,45] As expected, C6-$B(OH)_2$ and C8-$B(OH)_2$ structures form a covalent tetrahedral adduct with the enzyme's Ser β1 side chain

and bind with their alkyl chains in the hydrophobic acyl group binding site, mimicking the proposed reaction transition state, as was found with C13B$(OH)_2$ (Figure 3.2).

Strikingly, however, structures of C2-B$(OH)_2$ and C4-B$(OH)_2$ adopted a different binding mode from the previously reported PvdQ-C13-B$(OH)_2$ structure, forming a planar sp^2 adduct between the boron and seryl oxygens (Figure 3.2), with their alkyl chains bound in the putative head group binding site, instead of the acyl group binding site (See figure 1.4 for PvdQ binding sites). Previously, sp^2 adducts have been reported between boronic acids and other serine hydrolase enzymes,[63,65] so it is significant but not unprecedented that PvdQ can accommodate such an adduct. What is more significant is that this difference in hybridization and chain orientation may help reveal how PvdQ excludes short chain substrates, such as C4-HSL. When bound in this manner, the alkyl chains of C4-B$(OH)_2$ and C2-B$(OH)_2$ reside in a completely different pocket than the alkyl chains of C6-B$(OH)_2$, C8-B$(OH)_2$, and C13-B$(OH)_2$, being flipped outwards into the solvent exposed head group binding site and, crucially, away from the enzyme's oxyanion hole. This effect may be enhanced by the fact that the alkyl chains of C4-B$(OH)_2$ and C2-B$(OH)_2$ both make hydrophobic contacts with the side chains of Val β70 and His β23, which form an isolated hydrophobic patch within the head group binding site, that seems to stabilize the flipped out conformation (Figure 3.3). Furthermore, the entry way of the acyl group binding site, where C2-B$(OH)_2$ and C4-B$(OH)_2$ would be positioned if they bound with the same conformation as longer chain inhibitors like C13-B$(OH)_2$, is more polar than the rest of the acyl group binding site; the pocket's surface in this area is partially built up by an amide

nitrogen and a carbonyl oxygen, which are each less than 4.5 Å from the first four carbons of the alkyl chain of longer ligands. In contrast, there is only one other place in the entire acyl group binding site where a heteroatom is likely to make contact with the bound ligand (Figure 3.4).

A mechanism of short chain substrate exclusion?

Together, analysis of PvdQ bound to short and long chain alkylboronic acids suggests that short substrates are not adequately stabilized in the acyl group binding site of PvdQ, possibly due to the higher polarity of that region and the hydrophobicity of a competing site, to allow sufficient ground and/or transition state stabilization. In contrast, longer ligands (≥ 6 C alkyl chains) extend past the polar heteroatoms at the front of the acyl group binding site and are thus better stabilized. Trade-offs between accuracy and rate are common in the evolution of enzyme selectivity.[85,86] This potential mechanism of excluding short ligands through the action of the polar region at the front of the acyl group binding site may represent such a trade-off: potential ground and transition state hydrophobic binding energy for the cognate ligand of PvdQ (presumably the pyoverdine precursor) have both likely been sacrificed in order to sufficiently limit activity towards short substrates, such as C4-HSL.

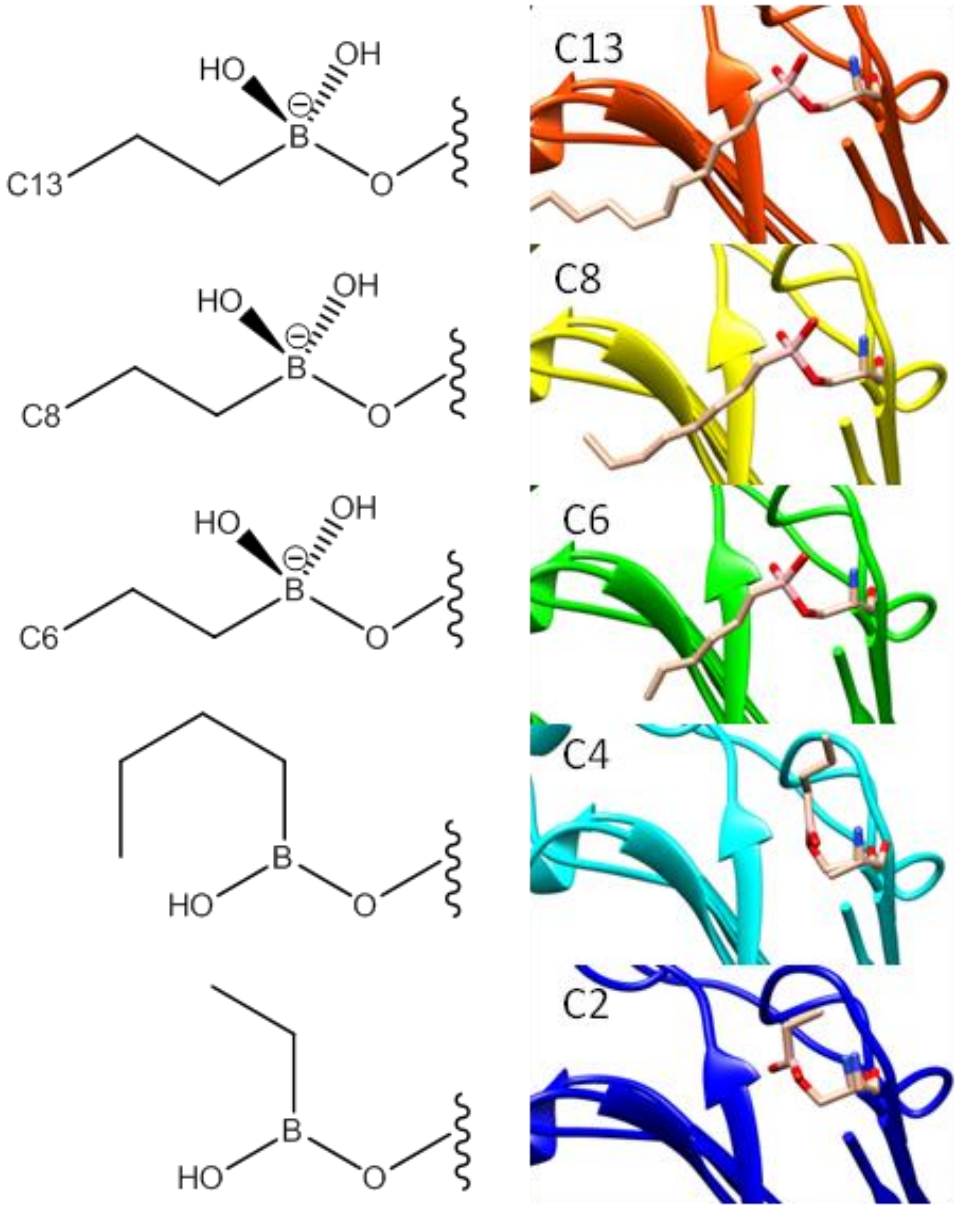

Figure 3.2 Binding conformation of alkylboronic acids and PvdQ

C13-$B(OH)_2$, C8-$B(OH)_2$, and C6-$B(OH)_2$ each adopt sp^3 hybridization with alkyl chains situated in the hydrophobic acyl group binding site. C4-$B(OH)_2$ and C6-$B(OH)_2$ however adopt an alternate conformation with their alkyl substituents pointing away from the acyl group binding site and instead resting in the head group binding site.

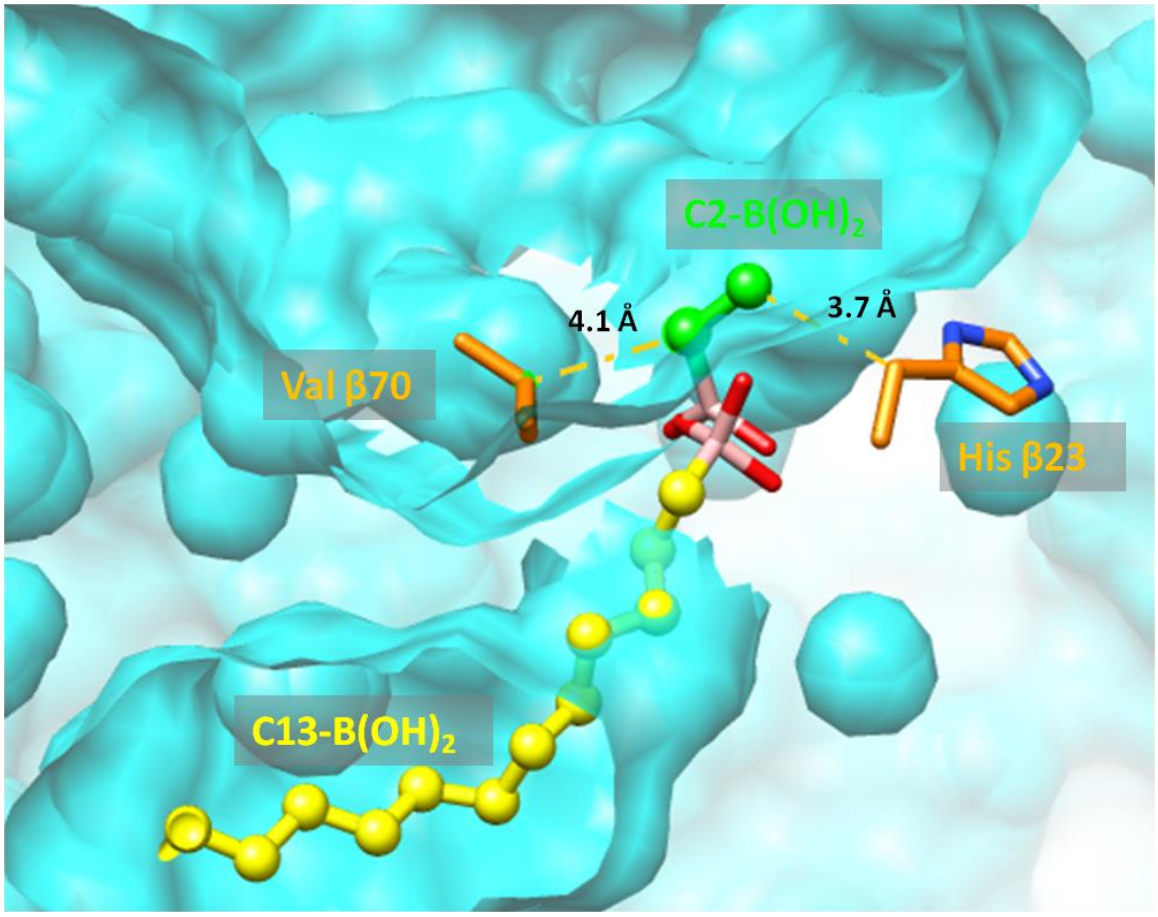

Figure 3.3 Overlay of C2-B(OH)$_2$ and C13-B(OH)$_2$ bound to PvdQ

C2-B(OH)$_2$ (green, with boronic acid shown in pink and red) is shown in its sp^2, flipped out conformation, situated in the hydrophobic patch that is created by His β23 and Val β 70. C13-B(OH)$_2$ (yellow, with boronic acid show in pink and red) is shown for comparison in its sp^3 conformation, mimicking the reaction transition state.

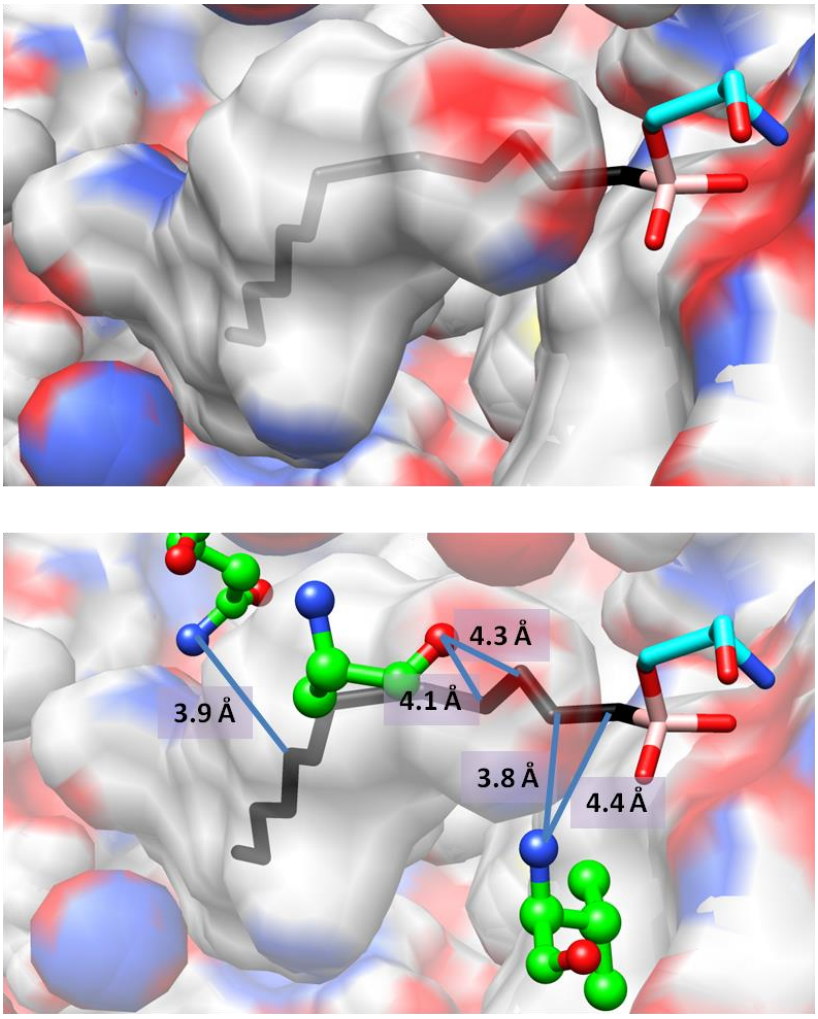

Figure 3.4 The front of the acyl group binding site is more polar than the back

PvdQ surface is shown in gray, colored by heteroatom: red = oxygen, blue = nitrogen. Top, the PvdQ acyl pocket is shown with covalently bound C13-$B(OH)_2$ (black), showing that while most of the pocket surface consists of apolar hydrocarbons, portions in the front, middle, and back include polar heteroatoms. Bottom, the same as the top, however all amino acids with heteroatoms within 4.5 Å from any C13-$B(OH)_2$ alkyl chain atom are shown in green and colored by heteroatom. A total of five such heteroatoms occur, contributed by three amino acid residues. Four of the five occur at the front of the pocket, where the alkyl chains of C2-$B(OH)_2$, C3-$B(OH)_2$, and C4-$B(OH)_2$ would bind. The resultant higher polarity of the front of the pocket may contribute to exclusion of short substrates and ligands, such as C4-HSL and C4-$B(OH)_2$ respectively.

Short chain alkylboronic acids are fragment sized lead compounds that target the PvdQ head group binding site

In addition to shedding light on the mechanism of PvdQ exclusion of short chain substrates, these studies represent a step forward for PvdQ enzymology in that all previously reported X-ray crystal structures of PvdQ have been of apo-enzyme, or enzyme with ligand bound in the tail group binding site of PvdQ.[16,25,31,44,45,45] Our structures of PvdQ bound to C2-$B(OH)_2$ and C4-$B(OH)_2$ are the first ever reported of PvdQ with ligand bound in the putative head group binding site. It is believed that the head group of the pyoverdine precursor consists of a modified non-ribosomal peptide, which starts with a glutamate residue.[87] The C14 acyl tail of the precursor is appended through an amide linkage to the *N*-terminus of this glutamate (Figure 2.1). Therefore, the interaction of PvdQ with the ethyl and butyl groups of C2-$B(OH)_2$ and C4-$B(OH)_2$ (Figure 3.3) may reflect a functional interaction that occurs between PvdQ and the α and β carbons of the native PvdQ substrate's glutamyl residue, suggesting a mechanism by which the native substrate head group is stabilized in complex with PvdQ.

The discovery of alkylboronic acids bound in the head group binding site of PvdQ may also have implications for the effort to develop selective probes and inhibitors that target PvdQ, by showing that boronic acid may be able to be used as a warhead for selectively targeting the head group site. Previously, rational screening by our group and high throughput screening by Professor Andrew Gulick's group (SUNY Buffalo) has lead to the discovery of inhibitors that target the hydrophobic tail group binding site of

PvdQ.[25,31,44,45] Unfortunately, these inhibitors are likely to have poor chemical selectivity given their reliance on non-specific interactions, limited hydrogen-binding, and the available data on activity in cell culture, as discussed above in Chapters 2.[31,44,45] Targeting the head binding group site of PvdQ may therefore be a more effective strategy for developing potent and selective inhibitors because the site is expected to interact with the much more complex pyoverdine precursor of *P. aeruginosa*, giving more opportunity for inhibitors to make selective hydrogen bonding and polar interactions, rather than just non-specific hydrophobic interactions.[16,25,31]

Although C4-$B(OH)_2$ and C2-$B(OH)_2$ have low potencies, they do represent excellent "fragment" sized compounds that specifically target the head group site of PvdQ. Both compounds have very high Ligand Efficiency values of 0.63 and 0.72 kcal/mol/non-hydrogen atom, well above the 0.38 kcal/mol/non-hydrogen atom which is a benchmark for fragments of this size, and meet or surpass the other standards for fragment type leads based on the so called "rule of three".[88,89] (Table 3.2) This supports the idea that boronic acid can be used as a warhead on which to build more specific inhibitors that target the head group binding site of PvdQ.

Property	Fragment lead	C2-$B(OH)_2$	C3-$B(OH)_2$	C4-$B(OH)_2$
Molecular weight	≤300 Da	73.89	87.91	101.91
Ligand Efficiency	≥0.38 kcal/heavy atom	0.72	0.52	0.63
Hydrogen bond donors	≤3	2	2	2
Hydrogen bond acceptors	≤3	2	2	2
c log P	≤3	0.215	0.744	1.27
Rotatable bonds	≤3	1	2	3

Table 3.2 "Rule of three" properties are fulfilled by short chain alkylboronic acids

METHODS

Materials

Unless otherwise noted, all chemicals were from Sigma-Aldrich Chemical Co. (St. Louis, MO, USA). 1-Ethylboronic acid (C2-$B(OH)_2$), 1-propylboronic acid (C3-$B(OH)_2$), 1-butylboronic acid (C4-$B(OH)_2$), 1-hexylboronic acid (C6-$B(OH)_2$), and 1-octylboronic acid (C8-$B(OH)_2$) were from Alfa Aesar (Ward Hill, MA, USA). Graphing and linear curve fitting was performed with KaleidaGraph 3.6 (Synergy Software, Reading, PA, USA). Figures of X-ray crystal structures and analysis of distances, hydrogen bonds, surface hydrophobicity calculation and figure presentation was performed with UCSF Chimera 1.8.[69]

Cloning, Expression and Purification

Recombinant *C*-terminal His_6-affinity tagged PvdQ from *P. aeruginosa* was expressed and purified in Tuner (DE3) pLysS *Escherichia coli* cells (EMD Millipore) and stored in 10% glycerol at -80 ^oC, as described in Chapter 2.

Alkylboronic Acid Inhibition.

Competitive *in vitro* inhibition of PvdQ by C2-, C3-, C4-, and C6-$B(OH)_2$ was measured by a previously reported method by determining IC_{50} values.[31] Briefly, 100-fold stocks of both substrate (dodecyl *p*-nitrophenol) and inhibitor were prepared in MeOH and DMSO, respectively. Samples were prepared by mixing 5 μM substrate, inhibitor of varying concentrations, and Na_2HPO_4 (40 mM) at pH 8.0 with 20% methanol in disposable 1 mL polystyrene cuvettes (Thermo Fisher). Reactions were initiated by addition of PvdQ to a final concentration of 10 nM and absorbance at 402 nm was continuously monitored, corresponding to the release of *p*-nitrophenolate, with a extinction coefficient $\varepsilon_{402\ nm}$ = 13,000 $M^{-1}cm^{-1}$.[31] The $\varepsilon_{402\ nm}$ was determined experimentally using Na_2HPO_4 (40 mM) at pH 8.0 with 20% methanol in disposable 1 mL polystyrene cuvettes. A 2-fold dilution series for each boronic acid was measured, covering an approximate 130-fold concentration range of each boronic acid. A minimum of 9 concentrations were measured for each boronic acid (including 0 mM boronic acid). Concentration-response plots were fit using the Hill equation, solving for both the Hill coefficient and IC_{50}, using KaleidaGraph 3.6 (Synergy Software, Reading, PA, USA). Derived IC_{50} values were used

to calculate K_i based on substrate concentration and the known K_M value, as previously reported for C10-$B(OH)_2$ and other alkylboronic acids.[31,64]

Crystallization and data collection

Crystallization and diffraction of PvdQ with short chain alkylboronic acid ligands, along with model building, were carried out by Professor Dali Liu's lab (Loyola University Chicago) as described previously.[31] Briefly, wild type PvdQ crystals were grown via hanging drop vapor diffusion by mixing 1 μL of PvdQ (10 mg/mL) with 1 μL of the reservoir solution that contains 0.05 M Hepes (pH:7.5); 80 mM RbCl; 10% PEG 4000. The crystals were grown at ambient temperature and displayed good morphology within 5 days. The diffraction quality crystals were soaked in the reservoir solution containing inhibitors and 20 % glycerol as cryo-protectant before flash freezing in liquid nitrogen. Crystallographic data were collected at the Advance Photon Source (APS). Data collection and processing statistics are given in Table 3.3. Phasing was carried out using our model described previously (PDB 4M1J).[31] Ligands were built into the model only in the final stages of refinement. Prior to adding the ligands to the model, the Fo-Fc maps showed well defined electron density for the corresponding ligands.

Ligand	**C2-B(OH)$_2$**	**C4-B(OH)$_2$**	**C6-B(OH)$_2$**	**C8-B(OH)$_2$**
Data Processing				
Space group	C2221	C2221	C2221	C2221
Cell dimension				
α, β, γ (°)	121.9; 167.5; 94.5	121.3; 167.5; 95.0	121.1; 168.2; 94.9	120.7; 166.5; 94.5
a, b, c (Å)	90; 90; 90	90; 90; 90	90; 90; 90	90; 90; 90
Resolution (Å)	42.6 – 1.6	47.5 – 1.8	39.0 – 2.0	47.3 – 2.1
[a]R_{merge} (%)	7.8 (83.4)[b]	15.9 (100)[b]	24.1 (100)[b]	13.4 (81.3)[b]
I/σ (I)	12.7 (1.4)	10.1 (1.2)	5.4(1.6)	13.1(3.1)
Completeness (%)	99.5(100)	99.9(100)	99.2(98.7)	99.9(99.7)
Multiplicity	3.8 (3.7)	5.7 (5.8)	5.1 (5.1)	7.5 (7.6)
No. Reflections	453318	527445	327941	393018
No. Unique Reflections	119528	92191	64713	52338
Refinement				
[c]R_{work}/[d]R_{free} (%)	15.9/19.0	16.5/19.2	18.2/21.5	15.1/19.3
No. of Atoms	6372	6361	6216	6175
Protein	5587	5743	5572	4661
Water	781	650	548	499
B-factors				
Average	29.2	34.7	38.2	31.8
Ligand (Alkyl B(OH)$_2$)	29.7-43.6	17.4-51.9	27.5-83.2	15.1/39.6
[e]RMSD				
Bond length (Å)	0.019	0.013	0.003	0.008
Bond angle (°)	1.707	1.396	0.750	1.03
Ramachandran Statistics				
Most Favored (%)	97.4	97.3	95.8	96.5
Allowed (%)	2.6	2.7	3.9	3.4
Outliers (%)	0.00	0.00	0.3	0.1

[a] $R_{merge} = \Sigma|I_{obs}-I_{avg}|/ \Sigma I_{avg}$

[b] The values for the highest resolution bind are in parentheses.

[c] $R_{work} = \Sigma|F_{obs}-F_{calc}|/ \Sigma F_{obs}$.

[d] Five percent of the reflection data were selected at random as a test set and only these data were used to calculate R_{free}.

[e] RMSD, root mean square deviation

Table 3.3 Crystallographic data

Chapter IV: Uncoupling the self-processing and catalytic activities of PvdQ

INTRODUCTION

The NTN-hydrolase PvdQ is uniquely positioned at the nexus of iron-uptake and virulence-regulating quorum-sensing pathways of the opportunistic pathogen and worldwide health threat, *P. aeruginosa*.[25,31,51] PvdQ structural data,[16,25,31] *in vitro* inhibitors,[25,31,45] and protein engineering[55] has been reported by us and others, but there remains a significant need to better understand how PvdQ interacts with its native siderophore substrate, the pyoverdine precursor. Currently, there is a lack of understanding of what, if any, specific interactions occur between the pyoverdine precursor's NRPS-derived head group[87] and PvdQ.[25] Such interactions might prove invaluable for the development of selective inhibitors and probes, since current inhibitors rely on binding in the predominately hydrophobic acyl-group binding site of PvdQ and are likely to lack target selectivity.[25,31,45] Moreover, an X-ray crystal structure of PvdQ in complex with the unhydrolyzed pyoverdine precursor would represent a significant step forward for the structural biology of pyoverdine biosynthesis in general, since no structures of pyoverdine or any of its precursors in complex with the pyoverdine biosynthetic machinery have yet been attained.[37] However, attempts to trap PvdQ in complex with the pyoverdine precursor at low pH have been unsuccessful, instead yielding product-bound structures which reveal a fatty acid bound in the acyl group binding site, but do not show the NRPS-derived siderophore precursor.[25] Because PvdQ, like all NTN-hydrolases, must undergo a self-

processing reaction to become catalytically active (Figure 4.1), making catalytically impaired mutants of PvdQ to aid in substrate trapping is difficult. Many of the amino acids which are involved in catalysis are also involved in self-processing. In particular, all NTN-hydrolases for which the self-processing reaction has been studied demonstrate involvement of the catalytic nucleophile of the mature enzyme in the self-processing reaction.[17,28,90–99] Therefore, mutations of PvdQ that block catalytic activity are also likely to block self-processing, resulting in an immature propeptide that does not bind substrate and would not be useful for studying ligand binding.

Because of PvdQ's ability to hydrolyze the *N*-acyl homoserine lactone (AHL) quorum sensing molecules of *P. aeruginosa* and other gram-negative species, it is also an attractive target for protein engineering.[31,51,55] Unlike the AHL lactonase class of quorum quenching enzymes, which is not selective for substrate acyl chain length, PvdQ is selective for both *N*-acyl chain length and substitution, which are the features that differentiate the AHL quorum sensing signals of various gram-negative bacteria from one another.[50,100] Therefore, if the substrate selectivity of PvdQ could be engineered without reducing overall catalytic efficiency, PvdQ variants could be useful tools for selectively inhibiting the quorum sensing of specific gram-negative species within polymicrobial settings, aiding the emergent field[6,100–104] of work that studies microbial physiology in mixed bacterial cultures. Moreover, PvdQ derivatives might be developed to block the quorum sensing of specific gram-negative pathogens, such as *P. aeruginosa* (3-oxo-C12-HSL) or *Burkholderia cenocepacia* (C8-HSL), both of which are implicated in infection and poor prognosis for cystic fibrosis and other immunocompromised patients.[55,105] Indeed, such an

engineered PvdQ derivative (PvdQ Lα146W/Fβ24Y), has been reported to have increased activity towards the *B. cenocepacia* signal molecule C8-HSL, relative to WT PvdQ, and to protect *Galleria mellonella* (wax moth) larvae from infection by a *Burkholderia* species.[55] However, this mutant enzyme possesses an overall reduced catalytic efficiency relative to WT PvdQ. PvdQ Lα146W/Fβ24Y, which was specifically engineered to process C8-HSL, hydrolyzes C8-HSL with a catalytic efficiency of 3.4×10^3 $M^{-1}s^{-1}$, while WT PvdQ is able to hydrolyze its best measured HSL substrate, C12-HSL, with an efficiency of 2.2×10^5 $M^{-1}s^{-1}$,[31] which is 65 times better. WT PvdQ also hydrolyzes 3-oxo-C12-HSL, a poor substrate, with an efficiency of 5.8×10^3 $M^{-1}s^{-1}$, which is 1.7 times better than PvdQ Lα146W/Fβ24Y processes C8-HSL. Moreover, this mutant was produced through a laborious rational design method utilizing molecular docking, followed by mutation, expression, and purification of at least 29 distinct PvdQ variants.

Instead of such rational design approaches, one possible approach to PvdQ protein engineering might be to apply directed protein evolution, as has been useful in the engineering of AHL lactonase quorum quenching enzymes.[52,106] Unfortunately, engineering PvdQ is complicated by the need for PvdQ to undergo self-processing.[55] Directed evolution experiments represent a balance between loss and gain of function mutations, with the vast majority of mutations being slightly deleterious or worse and a very small fraction of total possible mutations being beneficial.[86] Therefore, PvdQ self-processing introduces a second functionality of the protein which can suffer loss of function mutations, thus increasing the ratio of potential deleterious to beneficial mutations,

increasing the total library size that would need to be screened and likely decreasing the total number of active mutants that could exist.

One solution to the problems associated with PvdQ self-processing might be to uncouple the catalytic and self-processing activities of PvdQ. This approach has been used with other NTN-hydrolases either by expressing the individual subunits as two distinct peptides and allowing them to associate[107,108] or by production of a circular permutation which allows the protein to be translated as a single catalytically active polypeptide, eliminating the need for self-processing by rearranging the position of the *N* and *C* termini in the protein (Figure 4.1 and described in more detail below).[24] The latter approach has been shown to be a good approach for another wild type NTN-hydrolase and has the added advantage of bypassing any additional incubation time or manipulations that might be needed to make separately expressed subunits correctly fold and associate.[24]

Successful uncoupling of PvdQ's catalytic and self-processing activities would open the door for the rational design of catalytically impaired mutants of PvdQ by site-directed mutagenesis, which would facilitate trapping a substrate-enzyme complex. It would also aid in the directed evolution of PvdQ for engineering the enzyme's substrate selectivity for use as a probe to block specific AHL quorum sensing signals or as a therapeutic protein to disrupt the QS of human pathogens. To address this challenge, I have developed a circular permutation of PvdQ (cpPvdQ) which successfully uncouples its catalytic and self-processing activities. I have also produced catalytically impaired mutants of cpPvdQ, one of which has been used to successfully purify and pull down its substrate, the unhydrolyzed pyoverdine precursor.

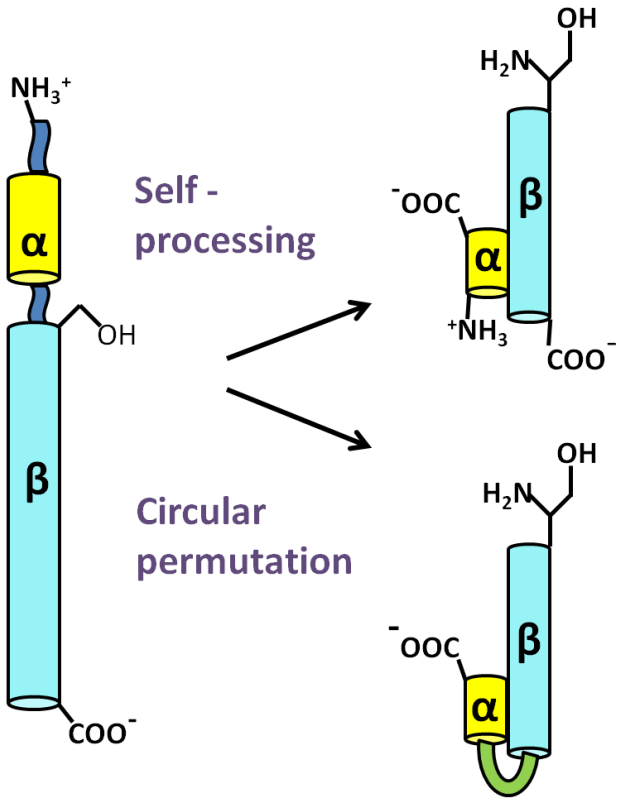

Figure 4.1 Circular permutation of PvdQ

Wild type PvdQ must undergo a self-processing reaction (top pathway) to become catalytically active by creating a new *N*-terminus at the site of the catalytic nucleophile, Ser β1. Circular permutation of PvdQ (bottom pathway) eliminates the need for self-processing by placing the catalytic serine nucleophile on the *N*-terminus of the primary sequence, with the α and β subunits joined by an engineered peptide linker (green), thus uncoupling the self-processing and catalytic activities of PvdQ.

Design of circularly permuted PvdQ

"Circular permutation" rearranges the domain architecture of a protein by connecting its native *N* and *C* termini.[109] In the case of PvdQ, this would eliminate the need for self-processing by placing the β subunit of PvdQ and its *N*-terminal catalytic nucleophile on the *N*-terminus of the permuted polypeptide, followed by the α subunit of PvdQ attached to the *C*-terminus of the β subunit (Figure 4.1).[109] Thus, the protein would be expected to be catalytically active from the time of initial folding, without needing further processing. Construction of a circularly permuted protein requires incorporation of a suitable linker adjoining the two subunits. While a library strategy is sometimes used by screening various linker lengths and amino acid compositions,[109] I instead adopted a rational design approach to design a short, hydrophilic linker based on the existing X-ray crystal structures of PvdQ. The distance between the native *N* and *C* termini of PvdQ is 3.5 Å (Figure 4.2). The small distance between these termini and the large distance of the termini from the active site suggests that PvdQ is an ideal candidate for circular permutation since linking the two termini would be likely to cause minimal perturbation throughout the rest of the enzyme. Given an estimated length of 3.5 Å per amino acid,[24] a three amino acid linker of Gly-Ser-Ser was designed in order to allow sufficient length, conformational flexibility, and hydrophilicity to form a short hydrophilic loop adjoining the two termini. The resulting protein was expressed and isolated to > 95% purity with a 6 × His tag.

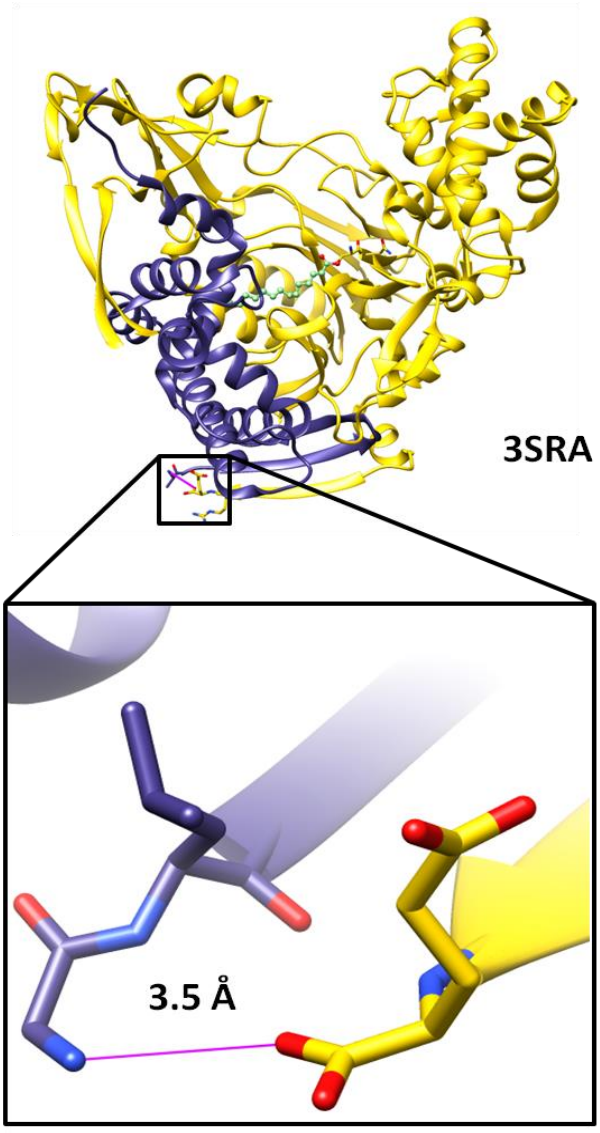

Figure 4.2 Distance between native *N* terminus of α subunit and *C* terminus of β subunit of mature PvdQ

Top, PvdQ (PDB code: 3SRA)[25] acylated with myristic acid is shown with myristic acid in green. The α subunit is shown in blue and β subunit in gold. The termini to be linked in the circular permutation are far (≥ 37 Å) from the active site. *Bottom*, the distance between the terminal α amino group nitrogen of Gly α30 and backbone carbonyl oxygen of Glu β546 is shown.

Expression, Purification, and Steady state kinetics of cpPvdQ

Cytoplasmic expression and purification of cpPvdQ were carried out as described in Methods and Figure 4.9. To compare the catalytic behavior of cpPvdQ with PvdQ in order to determine if cpPvdQ is a good model for PvdQ, steady state kinetic parameters for hydrolysis of a family of acyl-*para*-nitrophenol (PNP) substrates were determined for cpPvdQ and compared to previously measured[31] values for PvdQ (Table 4.1). cpPvdQ was found to prefer myristic-PNP (C14-PNP) based on its catalytic efficiency (k_{cat}/K_M), followed by lauric-PNP (C12-PNP). Capric-PNP (C10-PNP) and palmitic-PNP (C16-PNP) both showed sharp drops in catalytic efficiency relative to C12-PNP and C14-PNP (>20 fold). This overall pattern is consistent with the relationship between substrate chain length and k_{cat}/K_M observed for WT PvdQ, suggesting that cpPvdQ recapitulates the substrate preference of WT PvdQ (Figure 4.3). Catalytic efficiency of cpPvdQ for C12-PNP and C14-PNP substrates was about 50% lower than WT PvdQ for the same substrates, due to moderate decreases in k_{cat} and increases in K_M. For comparison, the maximal catalytic activity of the previously reported variant of PvdQ, PvdQ Lα146W/Fβ24Y, is 99% lower than the maximal activity of WT PvdQ. Therefore, overall efficiency for of cpPvdQ for C14-PNP and C12-PNP substrates is still good ($\geq 5 \times 10^5\ M^{-1}s^{-1}$). Catalytic efficiency for C10-PNP was about the same for cpPvdQ and PvdQ, while efficiency for C16-PNP was actually about four times higher for cpPvdQ relative to PvdQ. The difference with respect to C16-PNP is mostly due to the lower K_M value shown by cpPvdQ for this substrate (1.3 ± 0.2 μM for cpPvdQ, 4 ± 1 μM for WT PvdQ), which is about the same as the K_M values of cpPvdQ for C12-PNP and C14-PNP. This slightly reduced

selectivity by cpPvdQ relative to WT PvdQ suggests that the conformational freedom of the native termini of PvdQ may subtly contribute to substrate recognition and turnover. Despite this small decrease in substrate selectivity, overall these results suggest that cpPvdQ is an excellent model for the catalytic behavior and substrate preference of PvdQ. To further characterize cpPvdQ, X-ray crystallographic studies were undertaken in collaboration with Professor Dali Liu's lab (Loyola University Chicago).

Substrate	K_M **(μM)**	k_{cat} **(min^{-1})**	k_{cat}/K_M **(M^{-1}s^{-1})**
cpPvdQ			
C10-PNP	ND [a]	ND [a]	1.50x10^4 [b]
C12-PNP	1.3 ± 0.2	38 ± 1	4.9x10^5
C14-PNP	1.2 ± 0.2	98 ± 5	1.4Ex10^6
C16-PNP	1.3 ± 0.2	2.5 ± 0.1	3.1x10^4
WT PvdQ			
C10-PNP	60 ± 10	49 ± 5	1.3x10^4
C12-PNP	0.8 ± 0.1	52 ± 3	1.1x10^6
C14-PNP	0.60 ± 0.06	86 ± 3	2.4x10^6
C16-PNP	4 ± 1	1.9 ± 0.1	8x10^3

[a] ND = not determined because substrate K_M was beyond solubility limit.
[b] Fitting error is < 10%

Table 4.1 Comparison of steady state kinetic parameters for cpPvdQ and WT PvdQ with PNP substrates.

Previously measured steady state kinetic constants for hydrolysis of PNP substrates by WT PvdQ (highlighted in red)[31] are compared to the steady state constants of PNP hydrolysis by cpPvdQ, determined in this study (highlighted in blue). cpPvdQ shows similar trends in K_M and k_{cat} as PvdQ for hydrolysis of PNP substrates.

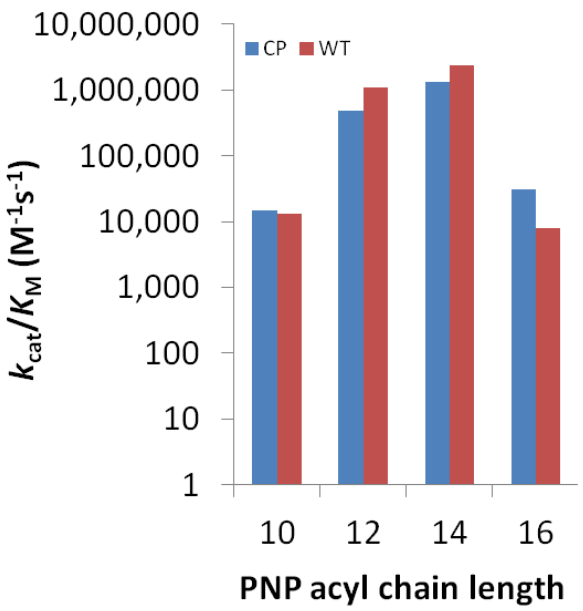

Figure 4.3 Comparison of catalytic efficiency (k_{cat}/K_M) of cpPvdQ and WT PvdQ with PNP substrates.

Catalytic efficiency (k_{cat}/K_M) of cpPvdQ is graphed in blue. Catalytic efficiency of WT PvdQ is graphed in red. cpPvdQ preserves the overall trend of substrate selectivity of WT PvdQ, with slightly decreased catalytic efficiency toward C12-PNP and C14-PNP and slightly increased catalytic efficiency toward C10-PNP and C16-PNP, relative to WT PvdQ.

X-ray crystal structure of cpPvdQ

Crystallization and diffraction of cpPvdQ, along with model building, were carried out by Professor Dali Liu's lab (Loyola University Chicago) as described previously for wild type PvdQ.[31] Briefly, cpPvdQ crystals were grown via hanging drop vapor diffusion by mixing 1 µL of PvdQ (10 mg/mL) with 1 µL of the reservoir solution that contains 0.05 M Hepes (pH:7.5); 80 mM RbCl; 10% PEG 4000. The crystals were grown at ambient temperature and displayed good morphology within 5 days. The diffraction quality crystals were soaked in the reservoir solution containing inhibitors and 20 % glycerol as cryo-

protectant before flash freezing in liquid nitrogen. Crystallographic data were collected at the Advance Photon Source (APS). Phasing was carried out using our model described previously (PDB 4M1J).[31] The overall model was found to align well with our previously reported model for PvdQ[31] and with the PvdQ models reported by other groups.[16,25] The RMSD of cpPvdQ relative to our previous model of PvdQ is 0.3 Å (Figure 4.4). Electron density for the Gly-Ser-Ser linker is weak, suggesting that it is poorly structured. However, density for the linker is clearly present (Figure 4.5). This lack of a rigid structure is unsurprising, given that the *N* and *C* termini of the native protein which are linked by the Gly-Ser-Ser linker in cpPvdQ are often poorly structured in prior X-ray crystal structures of PvdQ[25,31] and given that the linker of cpPvdQ was designed to be flexible in order to allow conformational freedom. A structural overlay of cpPvdQ and PvdQ (Figure 4.3) shows the closeness of alignment, especially within the active site. The positions of the cpPvdQ catalytic amino acids Ser1, Val69, and Asn268 are highly conserved with PvdQ. The close match between the X-ray crystal structures of PvdQ and cpPvdQ supports the use of cpPvdQ as a model for PvdQ.

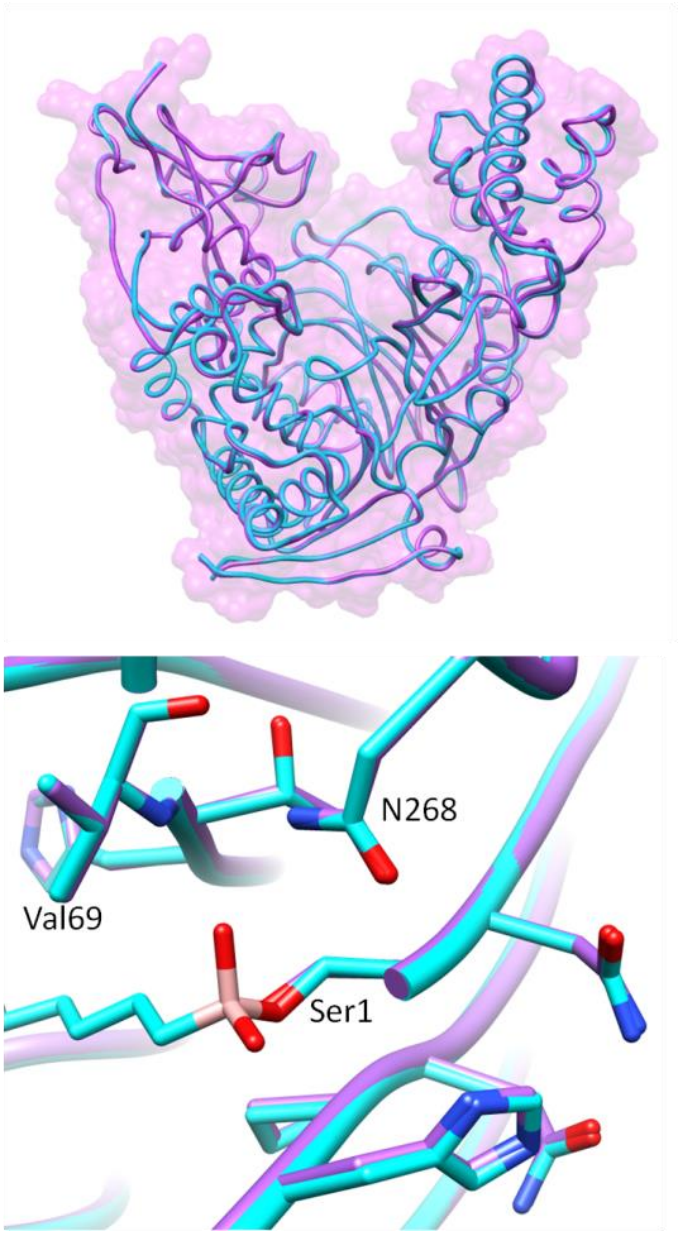

Figure 4.4 Structure of cpPvdQ

The X-ray crystal structure of cpPvdQ (purple) is overlaid with our prior structure of WT PvdQ covalently bound to C13-$B(OH)_2$ (blue, PDB: 4M1J). *Top*, the overall alignment of the backbones of cpPvdQ with WT PvdQ is apparent and has an RMSD of 0.3 Å. *Bottom,* close alignment of the cpPvdQ catalytic machinery with PvdQ is apparent, demonstrating that cpPvdQ is a good model for PvdQ.

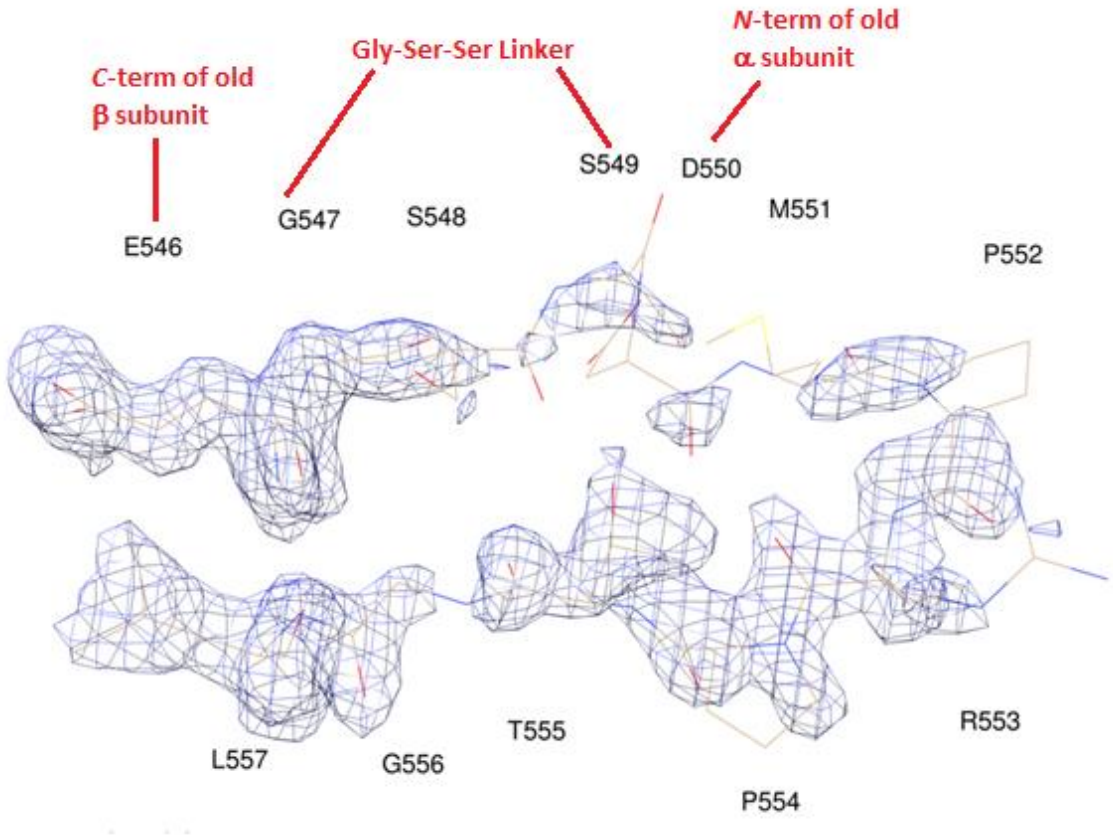

Figure 4.5 Electron density of engineered cpPvdQ Gly-Ser-Ser linker and connected termini

The termini joined by the Gly-Ser-Ser (annotated as G547-S548-S549) linker in cpPvdQ are poorly structured, but display electron density that is consistent with the proposed model for cpPvdQ. Figure prepared by, and used with permission of, Professor Dali Liu (Loyola University Chicago).

Engineering of cpPvdQ-Link for investigation of self-processing

In addition to determining a structure of PvdQ in complex with the pyoverdine precursor, it would also be useful to study how the PvdQ propeptide interacts with its linker peptide prior to cleavage. Determination of the pre-cleavage structure could lead

to the identification of alternate sites on PvdQ to target for inhibitor development. Therefore, to investigate how PvdQ interacts with the native linker of the PvdQ propeptide, and to possibly discover useful binding sites on the surface of PvdQ, a cpPvdQ mutant was designed as a mimic of the pre-cleavage structure (Figure 4.6). A construct of cpPvdQ was prepared where the native amino acid linker of the PvdQ propeptide which adjoins the α and β subunits prior to PvdQ self-processing (Figure 4.6) was appended to the *N*-terminus of cpPvdQ (cpPvdQ-Link). cpPvdQ-Link should imitate the 3-dimensional structure of the PvdQ propeptide, prior to self-processing of the peptide bond between the catalytic serine and the linker, assuming that the bond at the other end of the linker is cleaved first in WT PvdQ. cpPvdQ-Link was purified by the same procedure as cpPvdQ and gave a single band on an SDS-PAGE gel that was indistinguishable from cpPvdQ (not shown). This was not surprising, since the difference in MW between the two proteins is expected to be ≈ 2.5 kDa, and below the resolving power of a typical SDS-PAGE gel in that size range. Activity for cpPvdQ-Link was measured and cpPvdQ-Link was found to have a K_M for hydrolysis of C14-PNP that is nearly identical to that for cpPvdQ, but a k_{cat} that is ≈ 70 % lower than for cpPvdQ. However, unprocessed cpPvdQ-Link would be expected to be catalytically inactive. Therefore, the combination of a near identical K_M value to cpPvdQ with a 70% decreased k_{cat} value suggested that a portion of cpPvdQ-Link had undergone self-processing. cpPvdQ-Link was incubated at 4, 22, and 37 ^oC for a week to allow further self-processing, however this did not affect hydrolytic activity toward C14-PNP (data not shown), suggesting further self-processing does not occur outside of the cell.

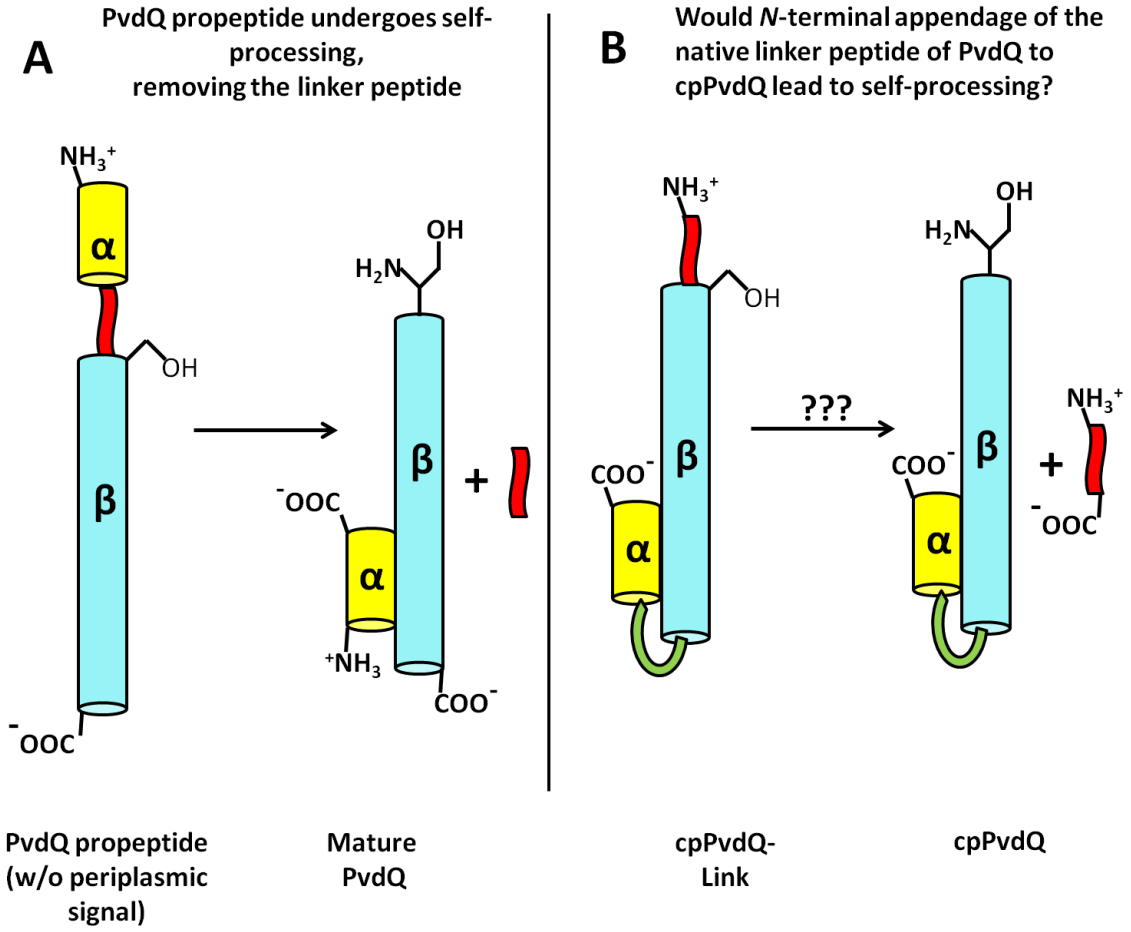

Figure 4.6 Design of cpPvdQ-Link mutant

The native linker peptide of PvdQ is shown in red. A) The PvdQ propeptide undergoes self-processing to form mature PvdQ and release the native linker peptide. B) cpPvdQ-Link is shown, which may be a useful tool for studying PvdQ interaction with the linker peptide, if cpPvdQ-Link is capable of carrying out the self-processing reaction to produce active cpPvdQ and release the linker peptide.

To determine if the linker had been removed from some or all of cpPvdQ-Link, purified cpPvdQ-Link and cpPvdQ were subjected to protein electrospray ionization-mass spectrometry (protein ESI-MS) by the Proteomics Facility (University of Texas, Austin) using an AB SCIEX Q-Trap 400 (Framingham, MA, USA). cpPvdQ was found to have one major peak after deconvolution at 80,922 ± 1 Da, consistent with its predicted molecular weight of 80,917 Da (Figure 4.7). In contrast, two major peaks for cpPvdQ-Link were observed, one at 80,922 Da and a smaller peak at 83,394 Da. The difference between these peaks of 2,470 Da corresponds roughly with the expected MW of 2,716 Da for the linker portion of cpPvdQ-Link, suggesting that a portion of cpPvdQ-Link underwent processing, while the rest retained the linker peptide. That the observed difference in mass is smaller than expected for the linker peptide may be a result of partial proteolytic degradation of the linker region of cpPvdQ-link.

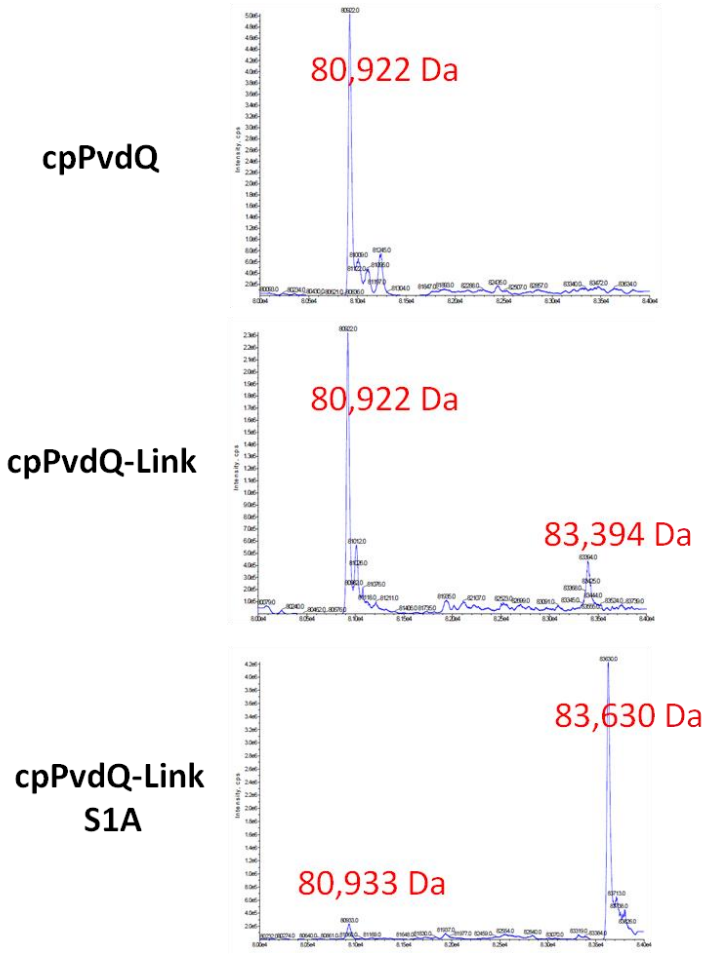

Figure 4.7 cpPvdQ-Link and cpPvdQ-Link S1A self-processing

Top, ESI-MS of cpPvdQ shows a single family of deconvoluted peaks centered around 80,922 Da, close to the predicted MW of 80,917 Da. *Middle,* ESI-MS of cpPvdQ-Link gives two distinct families of deconvoluted peaks, at 80,922 Da (likely corresponding to cpPvdQ-Link after the linker is removed) and at 83,394 Da, close to the predicted MW of 83,633 Da for cpPvdQ-Link with the linker still attached. The slightly low mass for the second peak relative to the predicted mass of cpPvdQ-Link may be due to partial proteolytic degradation of the linker region. The presence of the peak at 80,922 Da demonstrates that cpPvdQ-Link undergoes self-processing and may be a useful tool for studying PvdQ self-processing. *Bottom,* ESI-MS of cpPvdQ-Link S1A again shows two distinct families of peaks with one very low abundance family of peaks at 80,933 Da that likely represents processed cpPvdQ-Link S1A and a second, predominate family at 83,630 Da, which is close to the expected mass of 83,617 Da for unprocessed cpPvdQ-Link S1A and indicates that the S1A mutation largely blocks self-processing.

Next, I redesigned the construct to block all self-processing. Based on the self-processing mechanisms of other NTN-hydrolases, PvdQ self-processing is expected to occur through an *N* to *O* acyl shift of the peptide backbone (from the α amino group of Ser β1 to the seryl oxygen of Ser β1), driven by a strained peptide bond between Ser β1 and the Gly residue immediately to its *N*-terminus.[24,92,93] In order to produce a mutant of cpPvdQ-Link that maintains its linker therefore, the catalytic amino acid Ser1 was mutated to produce cpPvdQ-Link S1A (numbering based on cpPvdQ numbering, where the *N*-terminal catalytic nucleophile is Ser1). Steady state kinetic analysis of cpPvdQ S1A showed no activity above background for hydrolysis of C14-PNP. Protein ESI-MS of cpPvdQ S1A revealed two families of peaks, however the vast majority was centered at 83,633 Da, nearly identical to the predicted MW of 83,616.71 Da for cpPvdQ-Link S1A with the linker attached (Figure 4.7), demonstrating that the linker peptide remains attached to this mutant and that the S1A mutation blocks self-processing. Co-crystallization studies are now under way to determine the structure of cpPvdQ-Link S1A to see if the retained linker protein reveals any binding interactions with the head group binding site.

Catalytic attenuation of cpPvdQ

In order to achieve the overarching goal of acquiring an X-ray crystal structure of a PvdQ variant in complex with its substrate, the pyoverdine precursor, catalytically impaired mutants are needed in order to facilitate trapping a substrate-enzyme complex. To achieve this, mutations were introduced into cpPvdQ at the catalytic nucleophile (Ser1)

and the oxyanion hole (Asn268). These single and double mutants (cpPvdQ S1A, N268D, S1A/N268D, and S1A/N268A) were each found to have reduced catalytic activity toward C14-PNP, as expected. The k_{cat}/K_M value for the single mutant cpPvdQ S1A was found to be 3.5×10^3 $M^{-1}s^{-1}$, about a 400-fold decrease relative to cpPvdQ. The residual level of catalysis observed for cpPvdQ S1A suggests that the catalytic serine nucleophile is not absolutely necessary for substrate turnover by cpPvdQ. Instead, the role of the catalytic nucleophile in this mutant might be fulfilled by a water molecule, a different amino acid, or perhaps the *N*-terminal α amino group of the mutated residue, Ala1. Turnover of C14-PNP by the oxyanion hole deficient single mutant, cpPvdQ N268D, was observable, but was too slow to reliably quantify. This result demonstrates that stabilization of the oxyanion reaction intermediate is crucial for catalysis and that PvdQ may be more sensitive to perturbation of its oxyanion-stabilizing amino acids than it is to perturbation of its catalytic nucleophile. Turnover of C14-PNP by cpPvdQ S1A/N268D and S1A/N268A could not be detected above background hydrolysis rates.

Pull down of the pyoverdine precursor

To demonstrate the utility of catalytically impaired cpPvdQ mutants for future structural studies and demonstrate their affinity for the pyoverdine precursor, the double mutant cpPvdQ S1A/N268D was used to bind the pyoverdine precursor that is produced by a *pvdQ* transposon insertion mutant of the *P. aeruginosa* strain PA14 (Δ*pvdQ* PA14). Briefly, purified cpPvdQ S1A/N268D was incubated with raw cell free *pvdQ* transposon insertion *P. aeruginosa* supernatant, containing the pyoverdine precursor. The resulting

complex of pyoverdine precursor with catalytically impaired cpPvdQ was washed (first bound to NiNTA resin, then in a concentrator tube with a 10,000 Da molecular weight cutoff membrane). Finally, the pyoverdine precursor was released from the catalytically impaired enzyme by lowering the pH to ≈ 2, which causes PvdQ to denature (data not shown) and was expected to have the same effect on cpPvdQ and its mutants. Fractions from this binding and enrichment experiment were monitored by absorbance at 355 nm on a Shimadzu Prominence analytical HPLC (Columbia, MD, USA) and by matrix-assisted laser desorption/ionization-time of flight-mass spectrometry (MALDI-TOF-MS) on an AB SCIEX Voyager DE-PRO with a molecular weight gate of 500 Da and a scanning range of 500 to 2000 Da in negative ionization mode.

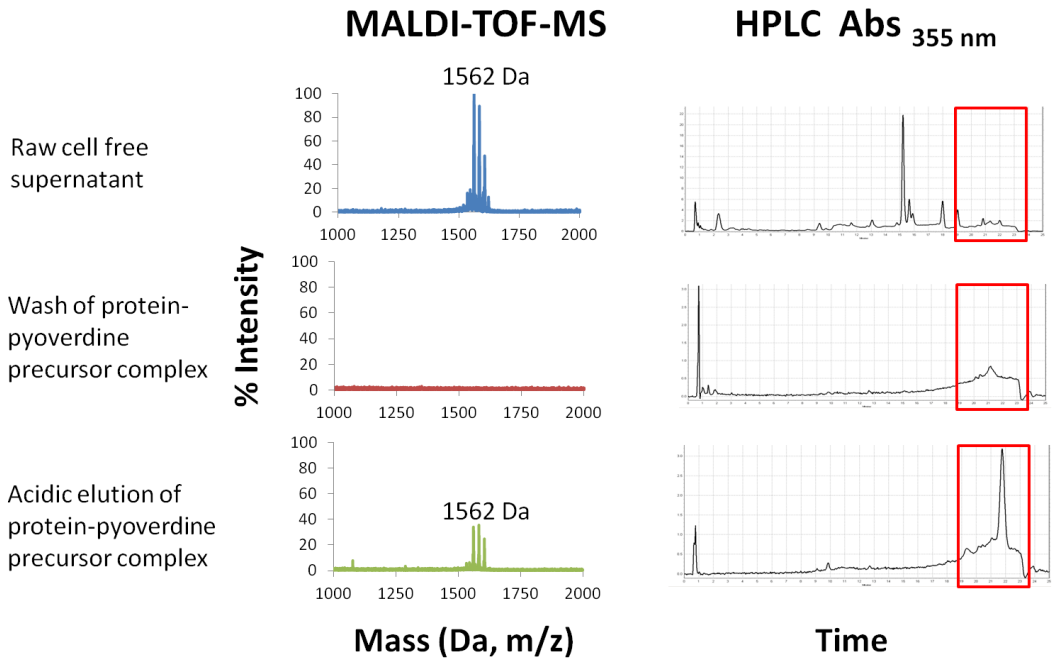

Figure 4.8 Pull down of pyoverdine precursor by cpPvdQ S1A/N268D

Each row shows MALDI-TOF-MS spectra from 1000 Da to 2000 Da and an HPLC chromatogram at Abs $_{355nm}$ for a 25 minute, 0% to 70% binary methanol gradient of the respective sample. MS intensities were normalized relative to the highest MS signal for a given sample from 500 Da to 2000 Da. The region of the HPLC chromatograms where pyoverdine precursor is expected to elute based on previous reports[25] and our own experience collecting HPLC fractions and analyzing them by MALDI-TOF-MS (data not shown) is boxed in red. *Top*, the cell free supernatant of *pvdQ* transposon insertion PA14 produced a strong MS signal at 1562 Da, corresponding with the expected value of 1560.75 Da for the pyoverdine precursor.[25] The numerous peaks in the HPLC chromatogram demonstrate the complexity of the raw cell free supernatant and that many impurities cannot be seen by MALDI-TOF-MS. *Middle,* concentrator tube flow-through from washing the cpPvdQ S1A/N268D-pyoverdine precursor complex with 50 mM phosphate, pH 8.0, has a flat MS and the HPLC chromatogram shows only a small, poorly resolved family of peaks at the end of the gradient. The absence of a clear MS signal suggests the peaks observed by HPLC do not correspond to the pyoverdine precursor and that the wash did not release the pyoverdine precursor. *Bottom*, concentrator tube flow-through from washing the cpPvdQ S1A/N268D-pyoverdine precursor complex with 50 mM phosphate, adjusted to pH ≈ 2 with 0.5 M HCl yields a MS with a clear family of peaks with the strongest peak at 1562 Da and a well defined peak in the HPLC trace in the area where the pyoverdine precursor is expected to elute, showing that the pyoverdine precursor was both pulled down and purified by cpPvdQ S1A/N268D.

HPLC of the cell free supernatant containing the pyoverdine precursor yielded a chromatogram with several peaks (Figure 4.8), including small peaks in the area where the precursor is expected to elute (t_R = 19 to 23 min). The MALDI-TOF-MS trace for the cell free supernatant showed one predominant family of peaks centered around 1562 ± 1 Da, consistent with the predicted mass of the pyoverdine precursor of 1560.75 Da.[25] After washing the protein-precursor complex with 50 mM phosphate buffer, pH 8.0, in a 10,000 MWCO concentrator which was expected to retain the protein-pyoverdine precursor complex, the HPLC chromatogram of the flow-through became flat, except at the end of the run, where a poorly resolved family of small peaks is visible, indicating that most material had been washed away. The MALDI-TOF-MS from the same wash gave no appreciable signal. Finally, after acidifying the protein-precursor mixture in order to denature the cpPvdQ mutant and release any bound ligands, the HPLC chromatogram of the concentrator tube flow-through contained a defined peak where the precursor is expected to elute. The MALDI-TOF-MS trace showed a family of peaks centered around 1562 Da, consistent with the mass of the pyoverdine precursor, indicating that the pyoverdine precursor was successfully pulled down from a complex mixture using the affinity of the catalytically impaired cpPvdQ S1A/N268D. Notably, no MALDI-TOF-MS peak is visible at 1353 Da, the expected molecular weight for pyoverdine precursor that has been deacylated by PvdQ. This indicates that although cpPvdQ S1A/N268D maintains affinity for the pyoverdine precursor, it does not readily catalyze its hydrolysis, and suggests that cpPvdQ S1A/N268D is a good tool for future co-crystallization studies that trap a PvdQ variant in complex with unhydrolyzed pyoverdine precursor (Figure 4.8).

CONCLUSION

The protein engineering technique of circular permutation was successfully used to uncouple the self-processing and catalytic activities of PvdQ. The resulting protein, cpPvdQ, was found to recapitulate the catalytic and structural properties of the wild type enzyme, suggesting it is a good model for PvdQ. A mutant of cpPvdQ with an appended *N*-terminal linker peptide (cpPvdQ-Link) designed to imitate the WT PvdQ propeptide's linker region was found to undergo processing, suggesting that cpPvdQ may be a viable model for studying PvdQ self-processing. The processing of cpPvdQ-Link was successfully blocked by creating a cpPvdQ-Link S1A mutant, and structural studies of this variant protein are underway to identify how the linker peptide interacts with PvdQ, possibly revealing a new binding site on the surface of PvdQ. Finally, catalytically impaired single and double mutants of cpPvdQ were produced with the goal of facilitating trapping the native substrate of PvdQ, the pyoverdine precursor, and getting an X-ray crystal structure, which would be a significant step forward in the structural biology of pyoverdine biosynthesis. Toward this end, the double mutant cpPvdQ S1A/N268D was demonstrated by HPLC and MALDI-TOF-MS to successfully pull down and purify the pyoverdine precursor out of a crude mixture, demonstrating that the mutant possesses binding affinity for the precursor and is sufficiently catalytically impaired to allow pull down without deacylating the precursor. Co-crystallization studies are now underway to characterize cpPvdQ S1A/N268D in complex with the pyoverdine precursor, which would represent a significant step forward both in the enzymology of PvdQ and in the general structural biology of pyoverdine biosynthesis.

METHODS

Materials

Unless otherwise noted, all chemicals and primers were from Sigma-Aldrich Chemical Co. (St. Louis, MO, USA). All restriction enzymes and dNTPs were from New England BioLabs (Beverly, MA, USA). *p*-Nitrophenyl esters of capric (C10-PNP), lauric (C12-PNP), myristic (C14-PNP) and palmitic (C16-PNP) acids were from Research Organics, Cleveland, OH. Phusion DNA polymerase and PCR buffer was from Thermo Fisher Scientific (Waltham, MA, USA). Graphing and linear curve fitting was performed with KaleidaGraph 3.6 (Synergy Software, Reading, PA, USA). Figures of X-ray crystal structures, analysis of distances, and figure presentation were performed with UCSF Chimera 1.8.[69]

Design and Cloning of cpPvdQ

To determine the appropriate linker length to create cpPvdQ, the distance between the α amino group of the α subunit's Gly α7 (the most *N*-terminal amino acid to show electron density in the α subunit of structure 3SRA) and the backbone carbonyl oxygen of the β subunit's *C*-terminal Glu β546 was measured to be 3.5 Å (Figure 4.2) using UCSF Chimera. To allow sufficient conformational freedom, a linker with 3 amino acids was designed, assuming approximately 3.5 Å per amino acid. Small, hydrophilic amino acids were chosen to allow flexibility and solubility for the solvent exposed loop, the sequence of the linker was Gly-Ser-Ser. WT PvdQ has a periplasmic signal sequence (residues 1-23 of the propeptide), which is removed from the *N*-terminus of the PvdQ propeptide after

transport to the periplasm. This was omitted from cpPvdQ since I thought it was possible that incomplete cleavage of the periplasmic signal would occur and lead to inactive enzyme. Initial attempts at expression gave very low yields of purified cpPvdQ (< 0.25 mg/L cell culture), so a codon-optimized version of the coding sequence for the above construct was obtained from GenScript (Piscataway, NJ, USA) in a pUC57 cloning vector. The coding sequence of codon-optimized cpPvdQ is:

ATATGTCGAACGCTATCGCTGTCGGCTCAGAACGCTCCGCAGATGGTAAAGG
CATGCTGCTGGCAAACCCGCACTTCCCGTGGAATGGTGCGAT
GCGCTTTTATCAGATGCATCTGACCATTCCGGGCCGTCTGGATGTGATGGGTG
CGAGTCTGCCGGGTCTGCCGGTGGTTAACATCGGTTTCTCCCGTCAT
CTGGCATGGACCCACACGGTCGATACCAGCTCTCACTTTACGCTGTATCGCCT
GGCACTGGACCCGAAAGACCCGCGTCGCTACCTGGTGGATGGCCGTA
GCCTGCCGCTGGAAGAAAAATCTGTCGCTATTGAAGTGCGCGGCGCGGATGG
TAAACTGTCACGTGTTGAACATAAAGTCTATCAGTCGATCTACGGTCC
GCTGGTCGTGTGGCCGGGCAAACTGGATTGGAATCGCAGCGAAGCGTATGCG
CTGCGTGACGCCAACCTGGAAAATACCCGTGTTCTGCAGCAATGGTAC
AGTATTAACCAGGCCTCCGATGTGGCAGACCTGCGTCGTCGTGTTGAAGCGC
TGCAGGGCATCCCGTGGGTCAATACCCTGGCGGCCGATGAACAGGGTA
ACGCCCTGTATATGAATCAATCCGTTGTCCCGTACCTGAAACCGGAACTGATT
CCGGCATGCGCAATCCCGCAGCTGGTGGCTGAAGGTCTGCCGGCACT
GCAGGGCCAAGATTCACGCTGTGCGTGGTCGCGTGACCCGGCAGCTGCACAG
GCAGGTATTACCCCGGCAGCACAACTGCCGGTCCTGCTGCGCCGTGAT

TTCGTGCAGAACTCAAATGACTCGGCATGGCTGACGAACCCGGCATCTCCGC

TGCAGGGTTTTAGCCCGCTGGTTTCTCAAGAAAAACCGATCGGTCCGC

GTGCACGTTATGCACTGAGTCGCCTGCAGGGTAAACAACCGCTGGAAGCGAA

AACCCTGGAAGAAATGGTTACGGCTAACCACGTCTTCTCAGCAGATCA

GGTGCTGCCGGACCTGCTGCGTCTGTGCCGTGATAATCAGGGCGAAAAATCG

CTGGCTCGCGCATGTGCTGCACTGGCACAGTGGGATCGTGGTGCAAAT

CTGGACAGTGGCTCCGGTTTTGTTTACTTCCAGCGCTTTATGCAACGTTTCGC

CGAACTGGATGGCGCATGGAAAGAACCGTTTGATGCACAGCGTCCGC

TGGACACCCCGCAAGGTATTGCTCTGGATCGTCCGCAGGTGGCGACGCAGGT

TCGTCAAGCCCTGGCAGACGCCGCAGCTGAAGTGGAAAAAAGCGGCAT

CCCGGATGGTGCACGTTGGGGTGACCTGCAGGTTTCTACCCGCGGCCAAGAA

CGTATTGCCATCCCGGGCGGTGATGGTCATTTTGGTGTTTATAACGCA

ATTCAGAGTGTCCGCAAAGGTGACCACCTGGAAGTGGTTGGCGGTACCTCCT

ACATCCAGCTGGTGACGTTCCCGGAAGAAGGTCCGAAAGCTCGTGGCC

TGCTGGCGTTTAGTCAGAGTTCCGATCCGCGCTCCCCGCATTATCGTGACCAA

ACCGAACTGTTCAGCCGCCAGCAATGGCAGACGCTGCCGTTTTCTGA

TCGTCAAATTGATGCGGACCCGCAGCTGCAACGCCTGTCTATCCGTGAAGGTT

CATCGGATATGCCGCGTCCGACCGGTCTGGCAGCAGACATTCGTTGG

ACGGCCTATGGCGTGCCGCACATCCGTGCAAAAGATGAACGTGGCCTGGGTT

ACGGCATTGGTTATGCTTACGCGCGTGACAACGCTTGCCTGCTGGCAG

AAGAAATCGTTACCGCCCGTGGTGAACGCGCACGTTATTTCGGCTCAGAAGG

TAAAAGCTCTGCAGAACTGGATAACCTGCCGTCGGACATTTTCTACGC

GTGGCTGAATCAGCCGGAAGCTCTGCAAGCGTTTTGGCAGGCACAAACCCCG
GCAGTGCGTCAGCTGCTGGAAGGTTATGCAGCTGGCTTCAATCGCTTT
CTGCGTGAAGCGGATGGTAAAACCACGAGCTGTCTGGGCCAGCCGTGGCTGC
GTGCAATTGCAACCGATGACCTGCTGCGTCTGACGCGTCGTCTGCTGG
TCGAAGGTGGTGTGGGCCAGTTTGCTGATGCGCTGGTTGCGGCCGCACCGCC
GGGTGCTGAAAAAGTTGAAAATCTGTACTTCCAATCACATCATCATCA
TCATCACTAAGAATTC.

cpPvdQ was cut from pUC57 using NdeI and EcoRI restriction enzymes and directly ligated into similarly digested pET24a(+), so that a 6× His tag would be encoded on the *C*-terminus. The insert and flanking regions in this expression vector, pET24-cpPvdQ, were verified by DNA sequencing (DNA Facility, University of Texas, Austin).

Production of cpPvdQ mutant expression constructs

Single and double mutants of cpPvdQ were produced based on a modified version of the QuickChange™ method[110] using Phusion® polymerase by introducing the desired mutation into the 5' end of the sense primer and using pET24a-cpPvdQ as template (all primers are listed in Table 4.2). Single mutations were first introduced into cpPvdQ, and then used as template for creating double mutants. cpPvdQ-Link was used as template for cpPvdQ-Link S1A. Site-directed mutagenesis Primers and PCR conditions were designed based on the Phusion® Site-Directed Mutagenesis Kit manual. Briefly, a 150 µL PCR reaction was prepared containing 100 ng of template DNA, 200 nmoles of each dNTP, 3 units of Phusion® polymerase (1.5 µL), made 0.5 µM in each primer (one mutagenic sense

primer and one non-mutagenic anti-sense primer) and Phusion® "5 × HF buffer" was added so as to be diluted 5-fold to a final concentration of 1 ×. The reaction mixture was aliquoted into 6 tubes and subjected to a melting temperature gradient from 55 ºC to 72 ºC in a MJ Research PTC-200 gradient thermocycler (St. Bruno, Quebec, Canada). The thermocycler program was as follows: 98 ºC for 30 s, followed by 25 repeated cycles of 98 ºC for 10 s, 55 ºC to 72 ºC T_m gradient for 30 s, and 72 ºC for 90 s, followed by a final extension step of 72 ºC for 10 min. Alternately, for primers with predicted T_m values ≥ 70 ºC, a two step PCR program was used, where the melting step was omitted. T_m values were calculated using the online tool for Phusion® T_m calculation from Thermo Fisher.[111] The resulting PCR product was incubated with DPN-1 for 1 h at 37 ºC to digest template DNA, subjected to ethanol precipitation by standard methods,[112] and transformed into the appropriate *E. coli* strain for down-stream applications (DH5α for sequencing or SHuffle (DE3) pLysS (SHuffle, New England BioLabs) for protein expression).

Production of cpPvdQ-Link was achieved by splicing-overlap-extension of the native linker region of WT *pvdQ* from pET24A-PvdQ with the 5' region of the cpPvdQ coding sequence in pET24a-cpPvdQ, using standard methods.[113] Briefly, end and internal primers were designed to amplify each fragment. Primers were first used to amplify each individual fragment with 50 µL reaction mixtures containing: 50 ng template, 0.5 µL of 10 mM dNTPs, 2.5 µL of 10 µM of each primer, 0.5 µL of Phusion® polymerase, and 10 µL of "5 × Phusion® HF buffer". The first PCR step used the following program: 98 ºC for 30s, (98 ºC for 10 s, 69.3 ºC for 30 s, 72 ºC for 40 s), repeated 25 times and followed by 72 ºC for 10 min. The resulting PCR products were purified using Qiagen PCR Cleanup

Kit. In the second PCR step, the same reaction mixture was prepared, however using equimolar amounts of both PCR products from step 1 as template (100 ng total template) and using the two end primers for amplification. The encoded amino acid sequence of the appended *N*-terminal peptide is ALSGEQAFQVAEQRRQRFRLERG. cpPvdQ-Link S1A was produced by using cpPvdQ-Link as the template for QuickChange™. Primers for all mutants are listed in Table 4.2. DNA sequences of all mutants were confirmed by DNA sequencing of the insert and flanking regions (DNA Facility, University of Texas, Austin).

PCR reaction	Primer sequences (5' to 3')
cpPvdQ S1A QuickChange™	*Sense*: TATACATATGGCGAACGCTATCGC *Antisense*: TATATCTCCTTCTTAAAGTTAAACAAAATTATTTC
cpPvdQN268D QuickChange™	*Sense*: GCAGAACTCAGATGACTCGGCAT *Antisense*: ACGAAATCACGGCGCAGC
cpPvdQN268A QuickChange™	*Sense*: GCAGAACTCAGCTGACTCGGCAT *Antisense*: ACGAAATCACGGCGCAGC
PvdQ linker amplification for SOE step 1	*Sense* (outside primer): ACTGACATATGGCCTTGAGCGGCGAGCA *Antinsense* (inside primer): ATAGCGTTCGAGCCGCGCTCCAGGC
cpPvdQ amplification for SOE step 1	*Sense* (inside primer): GAGCGCGGCTCGAACGCTATCGCTGTCGG *Antinsense* (outside primer): CTCGAGAATTCTTAGTGATGATGATGATGATGTGATT
SOE step 2	*Sense* (outside primer): ACTGACATATGGCCTTGAGCGGCGAGCA *Antinsense* (outside primer): CTCGAGAATTCTTAGTGATGATGATGATGATGTGATT
cpPvdQ-Link S1A	*Sense:* GAGCGCGGCGCTAACGCTAT *Antisense:* CAGGCGGAAGCGCTGGC

Table 4.2 PCR primers used in this study, with mutated codons underlined.

Expression, Purification, and Steady State Kinetic Characterization of cpPvdQ and cpPvdQ mutants

Recombinant *C*-terminal His_6-affinity tagged cpPvdQ and cpPvdQ mutants were unable to be expressed in the Tuner cells previously used for WT PvdQ,[31] likely due to the lack of a periplasmic signal and the necessity of surface disulfide bond formation on PvdQ and cpPvdQ, which cannot form in the cytoplasm.[16] Instead, pET24a-cpPvdQ and its mutants were transformed, expressed, and purified in SHuffle cells, which feature an oxidizing cytoplasmic environment, allowing disulfide bond formation in the cytosol and enhancing cytoplasmic expression of cpPvdQ.

An overnight starter culture of SHuffle cells carrying pET24a-cpPvdQ or one of its mutants was grown at 30 ^{o}C in Luria Bertani-Kanamycin (LB-Kan) medium, shaking at 200 rpm, and then diluted 50-fold into LB-Kan. Inoculated cultures were shaken at 200 rpm and 30 ^{o}C for about two h until $OD_{600} \approx 0.5$, at which time the culture was chilled on ice, made 0.5 mM in IPTG (using a freshly prepared 1000× stock from dry powder), and shaken at 15 ^{o}C for 48 h. As described in Chapter 2 for WT PvdQ, cells were pelleted, lysed, and subjected to a two-step purification by incubating batchwise first with NiNTA resin and then second with Q-sepharose anion exchange resin, followed by concentration. cpPvdQ and cpPvdQ mutants in 50 mM phosphate, pH 8.0, were made 10% in glycerol, flash frozen, and stored at -80 ^{o}C for future use.

SDS-PAGE analysis of purified cpPvdQ and its mutants following the above expression and purification procedure was carried out using a discontinuous gel with a 12% acrylamide resolving layer and stained with GelCode ^{TM} Blue Safe Protein Stain (Thermo Fisher), as described in Chapter 2. The resulting gel showed that cpPvdQ was ≥ 90% homogenous, with a single major band at 80 kDa (Figure 4.9). Typical yields of purified cpPvdQ and its mutants were ≈1.3 mg of purified protein per L of cell culture, compared to 2 mg of purified protein per L of cell culture for WT PvdQ. The decrease in overall yield may be a consequence of cytoplasmic expression, or other factors. Steady state kinetic analyses of hydrolysis of acyl-PNP substrates by cpPvdQ and cpPvdQ mutants were carried out as described in Chapter 2, by continuously monitoring the release of free PNP anion at 400 nm until ≤ 10% of total substrate had been hydrolyzed, based on the extinction coefficient of 13,000 $M^{-1}cm^{-1}$.[31]

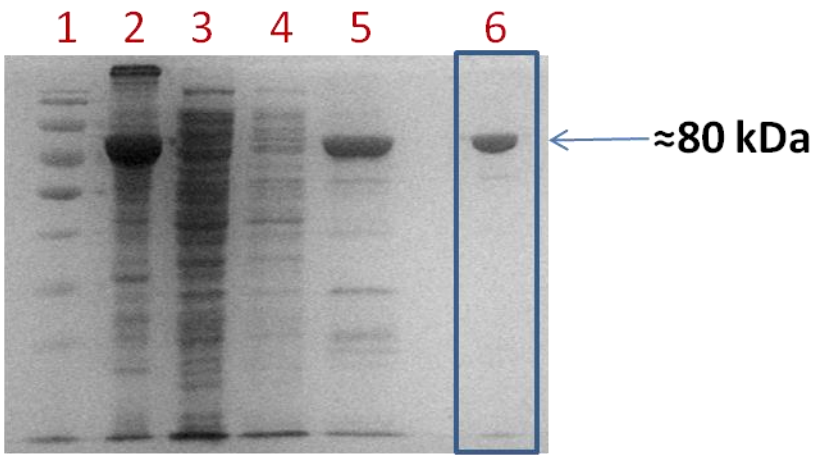

Figure 4.9 SDS-PAGE analysis of cpPvdQ expression and purification

cpPvdQ was analyzed by 12% SDS-PAGE as described for WT PvdQ in chapter 2. Lane 1: Fisher EZ Run MW Ladder (Thermo Fisher), lane 2: insoluble cell lysate from pellet, lane 3: soluble cell lysate from supernatant, lane 4: NiNTA wash, lane 5: NiNTA eluant, lane 6: pooled Q-sepharose anion exchange flow-through and wash (washed with 50 mM NaCl, 50 mM NaH_2PO_4, pH 8.0).

Binding and Enrichment of the Pyoverdine Precursor

To produce the pyoverdine precursor, a glycerol stock of transposon- disrupted *pvdQ* transposon insertion PA14 was used to innoculate 20 mL sterile LB culture at 37 ^oC and 200 rpm in the dark for 12 to 16 h. The culture was then pelleted and washed twice with sterile phosphate buffered saline, then once with MOPS-Glucose minimal media (see Chapter 1), with iron excluded from the recipe but no chelator added. The washed cells were then diluted 1000-fold into 400 mL of MOPS-Glucose minimal media without iron or chelator in a 4 L baffled flask and shaken for approximately 24 hours at 37 ^oC, 200 rpm,

in the dark. After 24 h the culture turned light green and the cells were pelleted by centrifugation (7000 × *g*; Beckman Coulter Avanti JE Centrifuge (Brea, CA, USA)). The resulting cell free supernatant was then filtered using a sterile 0.22 μm, GP Millipore Express PLUS Membrane with a 1 L reservoir, made 20 mM in imidazole by addition of solid imidazole, adjusted to pH 8 with 1 M NaOH, and stored in the dark at 4 ^{o}C until needed.

The variant cpPvdQ S1A/N268D was chosen to test the ability of a catalytically impaired mutant of cpPvdQ to bind the pyoverdine precursor. Purified cpPvdQ S1A/N268D (0.35 mg of 10 mg/mL glycerol stock) was incubated batchwise with 170 μL settled NiNTA resin at 4 ^{o}C with gentle shaking for 25 minutes. The suspension was then added to 20 mL of cell free supernatant and batch-bound for another 25 min as before. The mixture was pelleted by centrifugation and the supernatant set aside for later analysis. The remaining resin was transferred to a 1.5 mL microfuge tube and washed 3 times with 850 μL of Binding Buffer (Chapter 2: 20 mM imidazole, 50 mM NaH_2PO_4, 600 mM NaCl, pH 8.0) by repeated centrifugation in a tabletop microfuge, followed by removal of the supernatant and resuspension in fresh Binding Buffer. Following these washes, the cpPvdQ S1A/N268D-pyoverdine precursor complex was eluted from the NiNTA resin 2 times using 350 μL of Precursor Elution Buffer (Binding Buffer made 125 mM in imidazole). The resulting eluant was then applied to a mini centricon tube with a 10,000 Da molecular weight cutoff membrane and spun for 10 min at 18,000 × g in a tabletop centrifuge to concentrate. Following this, the material retained in the spin column was washed twice by applying 100 μL of 50 mM NaH_2PO_4, pH 8.0, and spinning for 10 minutes

at 18,000 × *g*. Finally, the material retained in the spin column was washed with 350 µL of 50 mM NaH_2PO_4 at a pH of approximately 2, and spun for 10 min at 18,000 × *g* in order to denature cpPvdQ S1A/N268D and allow any bound pyoverdine precursor to flow through. The flow-through of each wash step throughout the procedure was collected and analyzed by HPLC and MALD-TOF-MS.

For HPLC analysis, 50 µL of the appropriate sample was injected onto a 5 µm, 4.6 × 250 mm, C18 column (Shimadzu) fitted with a Zorbax XDB-C18 guard column (Phenomenex, Torrance, CA, USA). A Shimadzu Prominence analytical HPLC (Columbia, MD, USA) and two LC-20A pumps were used with the following program with a binary solvent system flowing at 1 mL/min. The column was washed for 1 min with 5 % solvent B, followed by a linear gradient from 5 % to 100 % solvent B for 19 min, followed by 2 min at 100 % solvent B, followed by a linear gradient from 100 % to 5 % solvent B over 1 min, followed by 2 min at 5 % solvent B, for a total program length of 25 min. Solvent A was H_2O with 0.1% formic acid and solvent B was 70% MeOH with 0.1% formic acid. A SPD-20A Prominence UV/Vis detector (Shimadzu) was used to detect absorbance at 355 nm. All buffers were filtered and then degassed under house vacuum and treatment in a sonicating bath, prior to use each day.

For MALDI-MS-TOF analysis, 0.5 µL of each sample was spotted on a MALDI plate, along with 0.5 µL of α-cyano-4-hydroxycinnamic acid (CHCA) matrix (8 mg solid CHCA mixed with 1 mL of 50% acetonitrile, 0.3% trifluoroacetic acid) and allowed to air dry until crystals formed. Plates were loaded into an AB SCIEX Voyager DE-PRO MALDI-TOF-MS, and calibrated with Calibration Mix 1 from the Sequazyme Peptide

Mass Standards Kit (Thermo Fisher) by matching of monoisotopic peaks. Samples were subjected to 200 shots, with laser intensity set to give an energy score of approximately 10,000 with a positive ionization mode and the detector set to reflector mode. A 500 Da molecular weight gate was used.

Bibliography

(1) Stover, C. K., Pham, X. Q., Erwin, A. L., Mizoguchi, S. D., Warrener, P., Hickey, M. J., Brinkman, F. S. L., Hufnagle, W. O., Kowalik, D. J., Lagrou, M., and others. (2000) Complete genome sequence of *Pseudomonas aeruginosa* PAO1, an opportunistic pathogen. *Nature 406*, 959–964.

(2) Navon-Venezia, S., Ben-Ami, R., and Carmeli, Y. (2005) Update on *Pseudomonas aeruginosa* and *Acinetobacter baumannii* infections in the healthcare setting. *Curr. Opin. Infect. Dis. 18*, 306–313.

(3) Cornelis, P., and Dingemans, J. (2013) *Pseudomonas aeruginosa* adapts its iron uptake strategies in function of the type of infections. *Front. Cell. Infect. Microbiol. 3*, 1–7.

(4) Høiby, N. (1993) Antibiotic therapy for chronic infection of *Pseudomonas* in the lung. *Annu. Rev. Med. 44*, 1–10.

(5) Singh, P. K., Schaefer, A. L., Parsek, M. R., Moninger, T. O., Welsh, M. J., and Greenberg, E. P. (2000) Quorum-sensing signals indicate that cystic fibrosis lungs are infected with bacterial biofilms. *Nature 407*, 762–764.

(6) Warren, L. M. (2008) Quinolone trafficking via outer membrane vesicles in *Pseudomonas aeruginosa*. Doctoral Dissertation, The University of Texas in Austin, Austin, TX.

(7) D'Agata, E. M. C. (2004) Rapidly Rising Prevalence of Nosocomial Multidrug-Resistant, Gram-Negative Bacilli: A 9-Year Surveillance Study. *Infect. Control Hosp. Epidemiol. 25*, 842–846.

(8) Livermore, D. M. (2009) Has the era of untreatable infections arrived? *J. Antimicrob. Chemother. 64*, i29–i36.

(9) Frederick, R. E., Mayfield, J. A., and DuBois, J. L. (2009) Iron trafficking as an antimicrobial target. *BioMetals 22*, 583–593.

(10) Romero, M., Acuna, L., and Otero, A. (2012) Patents on Quorum Quenching: Interfering with Bacterial Communication as a Strategy to Fight Infections. *Recent Pat. Biotechnol. 6*, 2–12.

(11) *N*-Terminal nucleophile aminohydrolases (Ntn hydrolases) superfamily. http://supfam.cs.bris.ac.uk/SUPERFAMILY/cgi-bin/scop.cgi?sunid=56235

(12) Acyl-homoserine lactone acylase PvdQ precursor - pvdQ - *Pseudomonas aeruginosa* (strain ATCC 15692 / PAO1 / 1C / PRS 101 / LMG 12228). *UniProt Protein Knowledgebase*. http://www.uniprot.org/uniprot/Q9I194

(13) Huang, J. J., Han, J.-I., Zhang, L.-H., and Leadbetter, J. R. (2003) Utilization of Acyl-Homoserine Lactone Quorum Signals for Growth by a Soil Pseudomonad and *Pseudomonas aeruginosa* PAO1. *Appl. Environ. Microbiol. 69*, 5941–5949.

(14) Hannauer, M., Schäfer, M., Hoegy, F., Gizzi, P., Wehrung, P., Mislin, G. L. A., Budzikiewicz, H., and Schalk, I. J. (2012) Biosynthesis of the pyoverdine siderophore of *Pseudomonas aeruginosa* involves precursors with a myristic or a myristoleic acid chain. *FEBS Lett. 586*, 96–101.

(15) Furnham, N., Sillitoe, I., Holliday, G. L., Cuff, A. L., Laskowski, R. A., Orengo, C. A., and Thornton, J. M. (2012) Exploring the Evolution of Novel Enzyme Functions within Structurally Defined Protein Superfamilies. *PLoS Comput. Biol. 8*, e1002403.

(16) Bokhove, M., Jimenez, P. N., Quax, W. J., and Dijkstra, B. W. (2010) The quorum-quenching *N*-acyl homoserine lactone acylase PvdQ is an Ntn-hydrolase with an unusual substrate-binding pocket. *Proc. Natl. Acad. Sci. U. S. A. 107*, 686–691.

(17) Brannigan, J. A., Dodson, G., Duggleby, H. J., Moody, P. C. E., Smith, J. L., Tomchick, D. R., and Murzin, A. G. (1995) A protein catalytic framework with an N-terminal nucleophile is capable of self-activation. *Nature 378*, 416–419.

(18) Duggleby, H. J., Tolley, S. P., Hill, C. P., Dodson, E. J., Dodson, G., and Moody, P. C. E. (1995) Penicillin acylase has a single-amino-acid catalytic centre. *Nature 373*, 264–268.

(19) Oinonen, C., and Rouvinen, J. (2000) Structural comparison of Ntn-hydrolases. *Protein Sci. 9*, 2329–2337.

(20) (2004) Voet D, and Voet J. Zymogens, in *Biochemistry* 3rd ed., John Wiley & Sons, Hoboken NJ, pp 527–528.

(21) Zhiryakova, D., Ivanov, I., Ilieva, S., Guncheva, M., Galunsky, B., and Stambolieva, N. (2009) Do N-terminal nucleophile hydrolases indeed have a single amino acid catalytic center? *FEBS J. 276*, 2589–2598.

(22) Smith, J. L., Zaluzec, E. J., Wery, J. P., Niu, L., Switzer, R. L., Zalkin, H., and Satow, Y. (1994) Structure of the allosteric regulatory enzyme of purine biosynthesis. *Science 264*, 1427–1433.

(23) Lowe, J., Stock, D., Jap, B., Zwickl, P., Baumeister, W., and Huber, R. (1995) Crystal structure of the 20S proteasome from the archaeon *T. acidophilum* at 3.4 Å resolution. *Science 268*, 533–539.

(24) Li, W., Cantor, J. R., Yogesha, S. D., Yang, S., Chantranupong, L., Liu, J. Q., Agnello, G., Georgiou, G., Stone, E. M., and Zhang, Y. (2012) Uncoupling Intramolecular Processing and Substrate Hydrolysis in the *N*-Terminal Nucleophile Hydrolase hASRGL1 by Circular Permutation. *ACS Chem. Biol. 7*, 1840–1847.

(25) Drake, E. J., and Gulick, A. M. (2011) Structural Characterization and High-Throughput Screening of Inhibitors of PvdQ, an NTN Hydrolase Involved in Pyoverdine Synthesis. *ACS Chem. Biol. 6*, 1277–1286.

(26) Suresh, C. G., Pundle, A. V., SivaRaman, H., Rao, K. N., Brannigan, J. A., McVey, C. E., Verma, C. S., Dauter, Z., Dodson, E. J., and Dodson, G. G. (1999) Penicillin V acylase crystal structure reveals new Ntn-hydrolase family members. *Nat. Struct. Biol. 6*, 414–416.

(27) Kim, Y., Yoon, K., Khang, Y., Turley, S., and Hol, W. G. (2000) The 2.0 Å crystal structure of cephalosporin acylase. *Struct. Lond. Engl. 1993 8*, 1059–1068.

(28) Hewitt, L., Kasche, V., Lummer, K., Lewis, R. J., Murshudov, G. N., Verma, C. S., Dodson, G. G., and Wilson, K. S. (2000) Structure of a slow processing precursor penicillin acylase from *Escherichia coli* reveals the linker peptide blocking the active-site cleft. *J. Mol. Biol. 302*, 887–898.

(29) Groll, M., Ditzel, L., Löwe, J., Stock, D., Bochtler, M., Bartunik, H. D., and Huber, R. (1997) Structure of 20S proteasome from yeast at 2.4Å resolution. *Nature 386*, 463–471.

(30) Jimenez, P. N., Koch, G., Papaioannou, E., Wahjudi, M., Krzeslak, J., Coenye, T., Cool, R. H., and Quax, W. J. (2010) Role of PvdQ in *Pseudomonas aeruginosa* virulence under iron-limiting conditions. *Microbiology 156*, 49–59.

(31) Clevenger, K. D., Wu, R., Er, J. A. V., Liu, D., and Fast, W. (2013) Rational Design of a Transition State Analogue with Picomolar Affinity for *Pseudomonas aeruginosa* PvdQ, a Siderophore Biosynthetic Enzyme. *ACS Chem. Biol. 8*, 2192–2200.

(32) Ratledge, C., and Dover, L. (2000) Iron metabolism in Pathogenic Bacteria. *Annu Rev Microbiol. 54*, 881–941.

(33) Andrews, S. C., Robinson, A. K., and Rodriguez-Quinones, F. (2003) Bacterial iron homeostasis. *FEMS Microbiol. Rev. 27*, 215–237.

(34) Otto, B. R., Verweij-van Vught, A. M. J. J., and Maclaren, D. M. (1992) Transferrins and Heme-Compounds as Iron Sources for Pathogenic Bacteria. *Crit. Rev. Microbiol. 18*, 217–233.

(35) Cox, C. D., Rinehart, K. L., Moore, M. L., and Cook, J. C. (1981) Pyochelin: novel structure of an iron-chelating growth promoter for *Pseudomonas aeruginosa*. *Proc. Natl. Acad. Sci. U. S. A. 78*, 4256–4260.

(36) Dumas, Z., Ross-Gillespie, A., and Kummerli, R. (2013) Switching between apparently redundant iron-uptake mechanisms benefits bacteria in changeable environments. *Proc. R. Soc. Biol. 280*, 20131055.

(37) Krewulak, K. D., and Vogel, H. J. (2008) Structural biology of bacterial iron uptake. *Biochim. Biophys. Acta. 1778*, 1781–1804.

(38) Schalk, I. J., and Guillon, L. (2013) Pyoverdine biosynthesis and secretion in *Pseudomonas aeruginosa* : implications for metal homeostasis: Pyoverdine biosynthesis. *Environ. Microbiol. 15*, 1661–1673.

(39) Brillet, K., Ruffenach, F., Adams, H., Journet, L., Gasser, V., Hoegy, F., Guillon, L., Hannauer, M., Page, A., and Schalk, I. J. (2012) An ABC Transporter with Two Periplasmic Binding Proteins Involved in Iron Acquisition in *Pseudomonas aeruginosa*. *ACS Chem. Biol. 7*, 2036–2045.

(40) Takase, H., Nitanai, H., Hoshino, K., and Otani, T. (2000) Impact of Siderophore Production on *Pseudomonas aeruginosa* Infections in Immunosuppressed Mice. *Infect. Immun. 68*, 1834–1839.

(41) Schalk, I. J. (2008) Metal trafficking via siderophores in Gram-negative bacteria: Specificities and characteristics of the pyoverdine pathway. *J. Inorg. Biochem. 102*, 1159–1169.

(42) Guillon, L., El Mecherki, M., Altenburger, S., Graumann, P. L., and Schalk, I. J. (2012) High cellular organization of pyoverdine biosynthesis in *Pseudomonas aeruginosa*: clustering of PvdA at the old cell pole: Pyoverdin biosynthesis at the old cell pole. *Environ. Microbiol. 14*, 1982–1994.

(43) Neres, J., Wilson, D. J., Celia, L., Beck, B. J., and Aldrich, C. C. (2008) Aryl Acid Adenylating Enzymes Involved in Siderophore Biosynthesis: Fluorescence Polarization Assay, Ligand Specificity, and Discovery of Non-nucleoside Inhibitors via High-Throughput Screening. *Biochemistry 47*, 11735–11749.

(44) Theriault, J. R., Wurst, J., Jewett, I., Verplank, L., Perez, J. R., Gulick, A. M., Drake, E. J., Palmer, M., Moskowitz, S., Dasgupta, N., Brannon, M. K., Dandapani, S., Munoz, B., and Schreiber, S. (2013) Identification of a small molecule inhibitor of Pseudomonas aeruginosa PvdQ acylase, an enzyme involved in siderophore pyoverdine synthesis. *NIH Probe Rep.* PMID: 23658940

(45) Wurst, J. M., Drake, E. J., Theriault, J. R., Jewett, I. T., VerPlank, L., Perez, J. R., Dandapani, S., Palmer, M., Moskowitz, S. M., Schreiber, S. L., Munoz, B., and Gulick, A. M. (2014) Identification of Inhibitors of PvdQ, an Enzyme Involved in the Synthesis of the Siderophore Pyoverdine. *ACS Chem. Biol.* 1536–44.

(46) Somu, R. V., Boshoff, H., Qiao, C., Bennett, E. M., Barry, C. E., and Aldrich, C. C. (2006) Rationally Designed Nucleoside Antibiotics That Inhibit Siderophore Biosynthesis of *Mycobacterium tuberculosis*. *J. Med. Chem. 49*, 31–34.

(47) Imperi, F., Massai, F., Facchini, M., Frangipani, E., Visaggio, D., Leoni, L., Bragonzi, A., and Visca, P. (2013) Repurposing the antimycotic drug flucytosine for suppression of *Pseudomonas aeruginosa* pathogenicity. *Proc. Natl. Acad. Sci. 110*, 7458–7463.

(48) Yeterian, E., Martin, L. W., Guillon, L., Journet, L., Lamont, I. L., and Schalk, I. J. (2010) Synthesis of the siderophore pyoverdine in *Pseudomonas aeruginosa* involves a periplasmic maturation. *Amino Acids 38*, 1447–1459.

(49) Papaioannou, E., Wahjudi, M., Nadal-Jimenez, P., Koch, G., Setroikromo, R., and Quax, W. J. (2009) Quorum-Quenching Acylase Reduces the Virulence of *Pseudomonas aeruginosa* in a *Caenorhabditis elegans* Infection Model. *Antimicrob. Agents Chemother. 53*, 4891–4897.

(50) Rutherford, S. T., and Bassler, B. L. (2012) Bacterial Quorum Sensing: Its Role in Virulence and Possibilities for Its Control. *Cold Spring Harb. Perspect. Med.* PMID:23125205

(51) Sio, C. F., Otten, L. G., Cool, R. H., Diggle, S. P., Braun, P. G., Bos, R., Daykin, M., Camara, M., Williams, P., and Quax, W. J. (2006) Quorum Quenching by an *N*-Acyl-Homoserine Lactone Acylase from *Pseudomonas aeruginosa* PAO1. *Infect. Immun. 74*, 1673–1682.

(52) Chow, J. Y., Wu, L., and Yew, W. S. (2009) Directed Evolution of a Quorum-Quenching Lactonase from *Mycobacterium avium* subsp. *paratuberculosis* K-10 in the Amidohydrolase Superfamily. *Biochemistry 48*, 4344–4353.

(53) Momb, J., Wang, C., Liu, D., Thomas, P. W., Petsko, G. A., Guo, H., Ringe, D., and Fast, W. (2008) Mechanism of the Quorum-Quenching Lactonase (AiiA) from *Bacillus thuringiensis* . 2. Substrate Modeling and Active Site Mutations. *Biochemistry 47*, 7715–7725.

(54) Thomas, P. W., Stone, E. M., Costello, A. L., Tierney, D. L., and Fast, W. (2005) The Quorum-Quenching Lactonase from *Bacillus thuringiensis* Is a Metalloprotein. *Biochemistry 44*, 7559–7569.

(55) Koch, G., Nadal-Jimenez, P., Reis, C. R., Muntendam, R., Bokhove, M., Melillo, E., Dijkstra, B. W., Cool, R. H., and Quax, W. J. (2014) Reducing virulence of the human pathogen *Burkholderia* by altering the substrate specificity of the quorum-quenching acylase PvdQ. *Proc. Natl. Acad. Sci. U. S. A. 111*, 1568–1573.

(56) Wahjudi, M., Murugappan, S., van Merkerk, R., Eissens, A. C., Visser, M. R., Hinrichs, W. L. J., and Quax, W. J. (2013) Development of a dry, stable and inhalable acyl–homoserine–lactone–acylase powder formulation for the treatment of pulmonary *Pseudomonas aeruginosa* infections. *Eur. J. Pharm. Sci. 48*, 637–643.

(57) Ochsner, U. A., Wilderman, P. J., Vasil, A. I., and Vasil, M. L. (2002) GeneChip® expression analysis of the iron starvation response in *Pseudomonas aeruginosa*: identification of novel pyoverdine biosynthesis genes. *Mol. Microbiol. 45*, 1277–1287.

(58) Koch, G., Jimenez, P. N., Muntendam, R., Chen, Y., Papaioannou, E., Heeb, S., Cámara, M., Williams, P., Cool, R. H., and Quax, W. J. (2010) The acylase PvdQ has a conserved function among fluorescent *Pseudomonas* spp.: PvdQ in fluorescent Pseudomonads. *Environ. Microbiol. Rep. 2*, 433–439.

(59) Huang, J. J., Petersen, A., Whiteley, M., and Leadbetter, J. R. (2006) Identification of QuiP, the Product of Gene PA1032, as the Second Acyl-Homoserine Lactone Acylase of Pseudomonas aeruginosa PAO1. *Appl. Environ. Microbiol. 72*, 1190–1197.

(60) Shaner, N. C., Campbell, R. E., Steinbach, P. A., Giepmans, B. N. G., Palmer, A. E., and Tsien, R. Y. (2004) Improved monomeric red, orange and yellow fluorescent proteins derived from *Discosoma* sp. red fluorescent protein. *Nat. Biotechnol. 22*, 1567–1572.

(61) Copley, S. D. (2012) Moonlighting is mainstream: Paradigm adjustment required. *BioEssays 34*, 578–588.

(62) Baker, S. J., Ding, C. Z., Zhang, Y.-K., Hernandez, V., and Xia, Y. (2009) Therapeutic potential of boron-containing compounds. *Future Med. Chem. 1*, 1275–1288.

(63) Smoum, R., Rubinstein, A., Dembitsky, V. M., and Srebnik, M. (2012) Boron Containing Compounds as Protease Inhibitors. *Chem. Rev. 112*, 4156–4220.

(64) Copeland, R. A. (2005) Evaluation of enzyme inhibitors in drug discovery. A guide for medicinal chemists and pharmacologists. *Methods Biochem. Anal. 46*, 1–265.

(65) Philipp, M., and Bender, M. L. (1971) Inhibition of serine proteases by arylboronic acids. *Proc. Natl. Acad. Sci. U. S. A. 68*, 478–480.

(66) Zervosen, A., Herman, R., Kerff, F., Herman, A., Bouillez, A., Prati, F., Pratt, R. F., Frère, J.-M., Joris, B., Luxen, A., Charlier, P., and Sauvage, E. (2011) Unexpected Tricovalent Binding Mode of Boronic Acids within the Active Site of a Penicillin-Binding Protein. *J. Am. Chem. Soc. 133*, 10839–10848.

(67) Transue, T. R., Krahn, J. M., Gabel, S. A., DeRose, E. F., and London, R. E. (2004) X-ray and NMR Characterization of Covalent Complexes of Trypsin, Borate, and Alcohols. *Biochemistry 43*, 2829–2839.

(68) Katz, B. A., Finer-Moore, J., Mortezaei, R., Rich, D. H., and Stroud, R. M. (1995) Episelection: novel Ki. apprx. nanomolar inhibitors of serine proteases selected by binding or chemistry on an enzyme surface. *Biochemistry 34*, 8264–8280.

(69) Pettersen, E. F., Goddard, T. D., Huang, C. C., Couch, G. S., Greenblatt, D. M., Meng, E. C., and Ferrin, T. E. (2004) UCSF Chimera: A visualization system for exploratory research and analysis. *J. Comput. Chem. 25*, 1605–1612.

(70) Wallace, A. C., Laskowski, R. A., and Thornton, J. M. (1995) LIGPLOT: a program to generate schematic diagrams of protein-ligand interactions. *Protein Eng. Des. Sel. 8*, 127–134.

(71) Ferrerass, J., Ryu, J.-S., Lello, F. D., Tan, D. S., and Quadri, L. E. N. (2005) Small-molecule inhibition of siderophore biosynthesis in Mycobacterium tuberculosis and *Yersinia pestis*. *Nat. Chem. Biol. 1*, 29–32.

(72) Pearson, J. P., Van Delden, C., and Iglewski, B. H. (1999) Active efflux and diffusion are involved in transport of *Pseudomonas aeruginosa* cell-to-cell signals. *J. Bacteriol. 181*, 1203–1210.

(73) Srikumar, R., Kon, T., Gotoh, N., and Poole, K. (1998) Expression of *Pseduomonas aeruginosa* Multidrug Effluc Pumps MexA-MexB-OprM and MexC-MexD-OprJ in a Multidrug-Sensitive *Escherichia coli* Strain. *Antimicrob. Agents Chemother. 42*, 65–71.

(74) Hernandez, V., Crepin, T., Palencia, A., Cusack, S., Akama, T., Baker, S. J., Bu, W., Feng, L., Freund, Y. R., Liu, L., Meewan, M., Mohan, M., Mao, W., Rock, F. L., Sexton, H., Sheoran, A., Zhang, Y., Zhang, Y.-K., Zhou, Y., Nieman, J. A., Anugula, M. R., Keramane, E. M., Savariraj, K., Reddy, D. S., Sharma, R., Subedi, R., Singh, R., O'Leary, A., Simon, N. L., De Marsh, P. L., Mushtaq, S., Warner, M., Livermore, D. M., Alley, M. R. K., and Plattner, J. J. (2013) Discovery of a Novel Class of Boron-Based Antibacterials with Activity against Gram-Negative Bacteria. *Antimicrob. Agents Chemother. 57*, 1394–1403.

(75) Lomovskaya, O., Warren, M. S., Lee, A., Galazzo, J., Fronko, R., Lee, M., Blais, J., Cho, D., Chamberland, S., Renau, T., Leger, R., Hecker, S., Watkins, W., Hoshino, K., Ishida, H., and Lee, V. J. (2001) Identification and Characterization of Inhibitors of Multidrug Resistance Efflux Pumps in *Pseudomonas aeruginosa*: Novel Agents for Combination Therapy. *Antimicrob. Agents Chemother. 45*, 105–116.

(76) Kaufmann, G. F., Sartorio, R., Lee, S.-H., Rogers, C. J., Meijler, M. M., Moss, J. A., Clapham, B., Brogan, A. P., Dickerson, T. J., and Janda, K. D. (2005) Revisiting quorum sensing: discovery of additional chemical and biological functions for 3-oxo-*N*-acylhomoserine lactones. *Proc. Natl. Acad. Sci. U. S. A. 102*, 309–314.

(77) Thomas, P. W., and Fast, W. (2011) Heterologous overexpression, purification, and *in vitro* characterization of AHL lactonases. In *Quorum Sensing Methods and Protocols.* Rumbaugh K, *Methods in Molecular Biology 692*.

(78) Biology WorkBench 3.2. http://seqtool.sdsc.edu/CGI/BW.cgi.

(79) Liberati, N. T., Urbach, J. M., Miyata, S., Lee, D. G., Drenkard, E., Wu, G., Villanueva, J., Wei, T., and Ausubel, F. M. (2006) An ordered, nonredundant library of *Pseudomonas aeruginosa* strain PA14 transposon insertion mutants. *Proc. Natl. Acad. Sci. U. S. A. 103*, 2833–2838.

(80) Overhage, J., Bains, M., Brazas, M. D., and Hancock, R. E. W. (2008) Swarming of *Pseudomonas aeruginosa* Is a Complex Adaptation Leading to Increased Production of Virulence Factors and Antibiotic Resistance. *J. Bacteriol. 190*, 2671–2679.

(81) Korgaonkar, A. K., and Whiteley, M. (2011) *Pseudomonas aeruginosa* Enhances Production of an Antimicrobial in Response to *N*-Acetylglucosamine and Peptidoglycan. *J. Bacteriol. 193*, 909–917.

(82) Fung, C., Naughton, S., Turnbull, L., Tingpej, P., Rose, B., Arthur, J., Hu, H., Harmer, C., Harbour, C., Hassett, D. J., Whitchurch, C. B., and Manos, J. (2010) Gene expression of *Pseudomonas aeruginosa* in a mucin-containing synthetic growth medium mimicking cystic fibrosis lung sputum. *J. Med. Microbiol. 59*, 1089–1100.

(83) Allen Fersht. (1999) Structure and mechanism in protein science: A guide to enzyme catalysis and protein folding. W.H. Freeman, New York.

(84) Kuntz, I. D., Chen, K., Sharp, K. A., and Kollman, P. A. (1999) The maximal affinity of ligands. *Proc. Natl. Acad. Sci. U. S. A. 96*, 9997–10002.

(85) Tawfik, D. S. (2014) Accuracy-rate tradeoffs: how do enzymes meet demands of selectivity and catalytic efficiency? *Curr. Opin. Chem. Biol. 21*, 73–80.

(86) Tokuriki, N., Jackson, C. J., Afriat-Jurnou, L., Wyganowski, K. T., Tang, R., and Tawfik, D. S. (2012) Diminishing returns and tradeoffs constrain the laboratory optimization of an enzyme. *Nat. Commun. 3*, 1257.

(87) Visca, P., Imperi, F., and Lamont, I. L. (2007) Pyoverdine siderophores: from biogenesis to biosignificance. *Trends Microbiol. 15*, 22–30.

(88) Congreve, M., Carr, R., Murray, C., and Jhoti, H. (2003) A “rule of three”for fragment-based lead discovery? *Drug Discov. Today 8*, 876–877.

(89) Jhoti, H., Williams, G., Rees, D. C., and Murray, C. W. (2013) The “rule of three” for fragment-based drug discovery: where are we now? *Nat. Rev. Drug Discov. 12*, 644–644.

(90) Lee, Y. S., and Park, S. S. (1998) Two-step autocatalytic processing of the glutaryl 7-aminocephalosporanic acid acylase from *Pseudomonas* sp. strain GK16. *J. Bacteriol. 180*, 4576–4582.

(91) Yin, J., Deng, Z., Zhao, G., and Huang, X. (2011) The N-terminal Nucleophile Serine of Cephalosporin Acylase Executes the Second Autoproteolytic Cleavage and Acylpeptide Hydrolysis. *J. Biol. Chem. 286*, 24476–24486.

(92) Kim, J. K., Yang, I. S., Shin, H. J., Cho, K. J., Ryu, E. K., Kim, S. H., Park, S. S., and Kim, K. H. (2006) Insight into autoproteolytic activation from the structure of cephalosporin acylase: a protein with two proteolytic chemistries. *Proc. Natl. Acad. Sci. U. S. A. 103*, 1732–1737.

(93) Lee, Y. S., Kim, H. W., and Park, S. S. (2000) The Role of alpha-Amino Group of the *N*-terminal Serine of beta Subunit for Enzyme Catalysis and Autoproteolytic

Activation of Glutaryl 7-Aminocephalosporanic Acid Acylase. *J. Biol. Chem. 275*, 39200–39206.

(94) Kim, Y. (2002) Precursor Structure of Cephalosporin Acylase. INSIGHTS INTO AUTOPROTEOLYTIC ACTIVATION IN A NEW *N*-TERMINAL HYDROLASE FAMILY. *J. Biol. Chem. 277*, 2823–2829.

(95) Kim, J. K., Yang, I. S., Rhee, S., Dauter, Z., Lee, Y. S., Park, S. S., and Kim, K. H. (2003) Crystal Structures of Glutaryl 7-Aminocephalosporanic Acid Acylase: Insight into Autoproteolytic Activation. *Biochemistry 42*, 4084–4093.

(96) Yoon, J., Oh, B., Kim, K., Park, J., Han, D., Kim, K. K., Cha, S.-S., Lee, D., and Kim, Y. (2004) A Bound Water Molecule Is Crucial in Initiating Autocatalytic Precursor Activation in an *N*-terminal Hydrolase. *J. Biol. Chem. 279*, 341–347.

(97) Saarela, J., Oinonen, C., Jalanko, A., Rouvinen, J., and Peltonen, L. (2004) Autoproteolytic activation of human aspartylglucosaminidase. *Biochem J 378*, 363–371.

(98) Cho, K. J., Kim, J. K., Lee, J.-H., Shin, H. J., Park, S. S., and Kim, K. H. (2009) Structural features of cephalosporin acylase reveal the basis of autocatalytic activation. *Biochem. Biophys. Res. Commun. 390*, 342–348.

(99) Bokhove, M., Yoshida, H., Hensgens, C. M. H., Metske van der Laan, J., Sutherland, J. D., and Dijkstra, B. W. (2010) Structures of an Isopenicillin N Converting Ntn-Hydrolase Reveal Different Catalytic Roles for the Active Site Residues of Precursor and Mature Enzyme. *Structure 18*, 301–308.

(100) Fast, W., and Tipton, P. A. (2012) The enzymes of bacterial census and censorship. *Trends Biochem. Sci. 37*, 7–14.

(101) Korgaonkar, A., Trivedi, U., Rumbaugh, K. P., and Whiteley, M. (2013) Community surveillance enhances *Pseudomonas aeruginosa* virulence during polymicrobial infection. *Proc. Natl. Acad. Sci. U. S. A. 110*, 1059–1064.

(102) Ramsey, M. M., and Whiteley, M. (2009) Polymicrobial interactions stimulate resistance to host innate immunity through metabolite perception. *Proc. Natl. Acad. Sci. U. S. A. 106*, 1578–1583.

(103) Moree, W. J., McConnell, O. J., Nguyen, D. D., Sanchez, L. M., Yang, Y.-L., Zhao, X., Liu, W.-T., Boudreau, P. D., Srinivasan, J., Atencio, L., Ballesteros, J., Gavilán, R. G., Torres-Mendoza, D., Guzmán, H. M., Gerwick, W. H., Gutierrez, M., and Dorrestein, P. C. (2014) Microbiota of Healthy Corals are Active Against Fungi in a Light Dependent Manner. *ACS Chem. Biol.* epub ahead of print, PMID: 25058318

(104) Moree, W. J., Phelan, V. V., Wu, C.-H., Bandeira, N., Cornett, D. S., Duggan, B. M., and Dorrestein, P. C. (2012) Interkingdom metabolic transformations captured by microbial imaging mass spectrometry. *Proc. Natl. Acad. Sci. U. S. A. 109*, 13811–13816.

(105) Korgaonkar, A. K. (2012) A mechanism for interspecies competition and virulence in Pseudomonas aeruginosa-containing polymicrobial infections. Doctoral Dissertation, The University of Texas in Austin, Austin, TX.

(106) Chow, J. Y., Xue, B., Lee, K. H., Tung, A., Wu, L., Robinson, R. C., and Yew, W. S. (2010) Directed Evolution of a Thermostable Quorum-quenching Lactonase from the Amidohydrolase Superfamily. *J. Biol. Chem. 285*, 40911–40920.

(107) Li, Y., Chen, J., Jiang, W., Mao, X., Zhao, G., and Wang, E. (1999) In vivo post-translational processing and subunit reconstitution of cephalosporin acylase from *Pseudomonas* sp. 130. *Eur. J. Biochem. 262*, 713–719.

(108) Boanca, G. (2006) Uncoupling the Enzymatic and Autoprocessing Activities of *Helicobacter pylori* -Glutamyltranspeptidase. *J. Biol. Chem. 281*, 19029–19037.

(109) Yu, Y., and Lutz, S. (2011) Circular permutation: a different way to engineer enzyme structure and function. *Trends Biotechnol. 29*, 18–25.

(110) Liu, C. F., Liu, D., Momb, J., Thomas, P. W., Lajoie, A., Petsko, G. A., Fast, W., and Ringe, D. (2013) A Phenylalanine Clamp Controls Substrate Specificity in the Quorum-Quenching Metallo-γ-lactonase from *Bacillus thuringiensis*. *Biochemistry 52*, 1603–1610.

(111) Tm Calculator | Thermo Scientific. http://www.thermoscientificbio.com/webtools/tmc/

(112) Sambrook, J. (2001) Concentrating Nucleic Acids, in *Molecular cloning: a laboratory manual* 3rd ed., pp A8.12–A8.13. Cold Spring Harbor Laboratory Press, Cold Spring Harbor, N.Y.

(113) McPherson, M. J., and Møller, S. G. (2000) Introducing mutations by splicing overlap extension (SOEing), in *PCR*, pp 143–148. *The Basics*; Springer, New York, NY.

Vita

Kenneth David Clevenger grew up and went to primary and secondary school in a suburb of Indianapolis, IN. Following high school graduation, he enrolled at Butler University in Indianapolis where he was a member of Phi Kappa Psi fraternity, and received a Bachelor of Science in Chemistry while carrying out undergraduate research investigating the surface behavior of the protein cytochrome *c* using plane-polarized light, under the direction of Professor Geoff Hoops and Professor Todd Hopkins. Following graduation, he moved to Austin, Texas in order to pursue a Doctor of Philosophy in Biochemistry and joined the lab of Professor Walter Fast in the spring of 2009. Following completion of his Ph.D., he has accepted a postdoctoral fellowship at Northwestern University in the lab of Neil Kelleher, where he expects to work on natural product discovery and systems approaches to biochemistry, using mass spectrometry based metabolomics and proteomics platforms.

Permanent Email Address: kdclevenger at gmail dot com

This dissertation was typed by Kenneth David Clevenger